On functional equations leading to analytical solutions of internal waves

Felix Beckebanze

Master thesis, March 2015

Abstract

This master thesis deals with the construction of analytical solutions to small-amplitude internal gravity waves. In the first part analytical solutions to internal waves in inviscid and uniformly stratified fluids confined to a two-dimensional trapezoid are constructed. The new method by which these exact solutions are constructed gives new insight into the complex self-similar structure of the velocity field. In the second part the generation of internal waves in a uniformly stratified ocean by barotropic flow over irregular topography is described. Exact solutions to the internal wave field derived from solutions to Abel's functional equation are presented for a finite support bottom topography which lacks tidal conversion for a specific barotropic tidal frequency.

Contents

1 General Introduction

Internal waves can arise in stratified and rotating fluids, such as oceans and interiors of (fluid) stars. These fluids exhibit a motionless stable state, called hydrostatic or cyclostrophic equilibrium, in which the pressure gradient force is balanced by gravity or centrifugal forces. Small perturbations in the direction of the pressure gradient on this equilibrium lead to oscillation of the fluid particles around their stable motionless state. In the absence of viscosity the kinetic energy added by the perturbation cannot be lost, which means that there is no return to the hydrostatic equilibrium. Instead the perturbation, here after called internal wave, propagates through the interior of the fluid. An outstanding property of internal waves in a uniformly-stratified fluids is that their propagation direction has a fixed angle with respect to the pressure gradient in the fluid (dependent on the frequency associated with the internal wave). A direct consequence of this property is the abnormal "rule of reflection" for internal waves: the angle of reflection equals the incident angle with respect to the pressure gradient - independent of the orientation of the surface where the internal wave is reflected. This is contrary to the familiar reflection rule for surface waves, where the angle of the incoming wave equals the angle of the reflected wave with respect to the reflecting boundary.
Depending on the slope of the reflecting boundary with respect to the propagation direction of the internal wave the amplitude of the internal wave perturbation can be intensified or weakened upon reflection. Repeated intensification - called focusing - of the small amplitude internal waves upon reflection leads to spatially localized large amplitude internal waves in the fluid.
While a viscous fluid in a state of sufficiently small perturbations on hydrostatic equilibrium is well approximated by an ideal fluid (frictionless), this is certainly not the case when velocity gradients become large. The amplification of a small amplitude internal wave by focusing is well described by the linearised, incompressible, inviscid Navier-Stokes equations under Boussinesq approximation close to hydrostatic equilibrium. Upon infinite repeated focusing the internal waves can accumulate on a one-dimensional subspace inside the two-dimensional domain. Such a subspace of the domain is called attractor. As the attractor is approached the kinetic energy of the internal waves goes to infinity. This leads to a state in which both friction and non-linear terms do play a significant role, making the small-amplitude assumption invalid. The large amplitude internal wave can lead to mixing of the fluid through wave breaking and Stokes drift, among other processes.

In the stratified oceans internal waves are generated by barotropic tidal oscillation over irregular bottom topographies. A barotropic velocity field is by definition vertically uniform in its horizontal components and the barotropic tidal flow is excited by the gravitational force exerted by the moon on the oceans. Approximately 30 % of the total tidal energy dissipation goes into the generation of internal waves [6], referred to as tidal conversion. Most of this energy is eventually turned into mixing of the ocean. Mixing is observed to take place above steep topographies (see [16] and [6]) where the internal waves are generated. Propagation of the internal waves can also lead to mixing far away from the location of tidal conversion. Tidal conversion is far from uniformly distributed over the ocean and the shape of the bottom topography plays a crucial role in the generation of internal waves.
Deep water formation at high latitudes has to be compensated by upwelling some-

where else in the ocean. This requires a process which stirs the abyssal ocean [14]. Mixing of internal waves is potentially important in facilitating upwelling of deep water. In [15] it is estimated that more than 40 % of the energy needed to explain the upwelling comes from tidal energy. The contribution of radiated internal tides is approximately 10 %. The uncertainties in these numbers are large due to sparse observations of the abyssal sea as well as due to the spatially localized internal waves. It is this role of internal waves in the deep ocean circulation which has put research on internal waves back onto the scientific agenda in the last two decades.

This master thesis is concerned with finding exact solutions for internal waves in a closed trapezoidal domain (section 2) and internal waves generated by barotropic flow over irregular topography (section 3).
Constructing and analysing exact solutions to internal wave problems is useful for the general understanding of internal waves in a number of ways.
Solving the governing equations analytically is the only way to resolve the velocity field on all spatial scales. This is of interest especially for closed domains with repeated focusing, as the steady state velocity fields for such domains exhibit complex fractal structures.
The method by which the internal waves are constructed gives insight into the solution itself. This turns out to be useful for the understanding the fractal structure. The construction procedure can also be incorporated in numerical solvers for internal wave problems. This can potentially lead to a numerical solver which conserves more properties of the internal waves than standard numerical solvers.
Last but not least exact internal wave solutions are essential in testing the performance of numerical internal wave models.

In section 2 of this thesis analytical solutions for small-amplitude internal waves in a frictionless uniformly-stratified two-dimensional fluid constrained to a trapezoidal basin are constructed. All standing internal wave solutions inside trapezoidal domains exhibiting a so-called (1,1) attractor are constructed analytically. A (1,1) attractor reflects on all four boundaries (surface, bottom and two sides, one of which is sloping) exactly once. 'Standing' means that the system is in steady state without external forcing. This turns out to be an ill-posed problem as the solution space is infinite-dimensional. A solution is unique once it is prescribe on a so-called fundamental interval [13]. For all non-trivial prescriptions on the fundamental intervals the solution exhibits complex self-similarities around the attractor.
The presented exact solutions are a generalization of an exact self-similar solution for a special case of the class of trapezoids with (1,1) attractors presented in [11].
The analytical solutions are constructed independently using two methods: first the method also used in [11] is applied. This method reduces the governing equations, introduced in section (1.1), to a functional equation known as Schröder's functional equation. This functional equation is solved in Fourier space, which results in exact expressions for all Fourier coefficients of the internal wave solution.
As an alternative, the exact standing internal wave solutions are constructed using a new method, which finds solutions to the Abel functional equation. This method is developed within this master project in collaboration with Grant Keady and presented in theorem 6 in Beckebanze and Keady, 2014. This article is added as an appendix to this thesis. The construction procedure gives new insight into the self-similarity of the standing internal wave solution. The new method can also be used

for the construction of internal waves generated by tidal flow over irregular bottom topography.

Section 3 describes the generation of internal waves in uniformly stratified fluid due to oscillation of barotropic flow over weakly sloping bottom topographies. An interesting feature of this process, called tidal conversion, is the existence of topographies lacking tidal conversion [10]. In section (3.1) tidal conversion is put into context with solutions to Abel's functional equation. This makes it possible to give a measure-theoretic probability to encounter a topography lacking tidal conversion in the space of all topographies with finite support. It is conjectured that in Lebesgue measure this probability is zero.
Certainly there exist infinitely many topographies that can lack tidal conversion. In section (3.3.1) exact solutions by Law [8] are used to construct infinitely many topographies which lack tidal conversion for a specific forcing frequency.
For a family of piecewise quadratic ridges the baroclinic internal wave fields generated through tidal conversion are constructed analytically in section (3.4). This is done for a range of barotropic tide frequency, which includes a frequency for which no tidal conversion takes place. Streamfunction solutions are also computed exactly for different relative heights of the ridge, varying from 0 to 50% of the entire ocean depth.
The baroclinic streamfunction at some fixed time can be derived from solutions to Abel's functional equation, similar to the method applied in section 2. This method is not capable of constructing exact time-dependent streamfunctions. Above the flat part of the bottom this can be achieved by adding a complex component to the exact streamfunction in Fourier space. For the part of the domain above the irregular bottom the extension to a full time-dependent streamfunction is done by a numerical method, verifying the correctness of the analytical streamfunction solution above the flat part of the bottom.
The analytical baroclinic wave fields at some fixed time are used to calculate the barotropic tide energy dissipation (averaged over one tidal period). This is done in section (3.4.6) and reveals interesting dependencies of the energy dissipation of the frequency of the barotropic tide and the relative height of the irregular part of the bottom.

Conclusions are drawn in section 4.

1.1 Derivation of governing equation

The Navier-Stokes momentum equations in a co-rotating frame, referred to as an f-plane, with gravity $\mathbf{g} = -g\hat{z}$ working in the vertical direction z only, are given by

$$\rho \frac{d\mathbf{u}}{dt} = -\rho\ \mathbf{f} \times \mathbf{u} - \boldsymbol{\nabla} p + \rho\ \mathbf{g}. \tag{1}$$

Here $\mathbf{u} = (u, v, w)^T$ is the three dimensional velocity vector in Cartesian coordinates (x, y, z), ρ is the density, p is the pressure and $\mathbf{f} = 2\boldsymbol{\Omega}$ is the Coriolis parameter. See chapters 3 and 4 in [3] for a detailed derivation of (1).
The continuity equation is given by

$$\frac{\partial \rho}{\partial t} + \boldsymbol{\nabla} \cdot (\rho \mathbf{u}) = 0.$$

The system is closed by adding an equation of state for the density ρ if this equation does not introduce new unknowns. Here it is assumed that the density is conserved, which means that

$$\frac{d\rho}{dt} = 0, \qquad \text{hence} \qquad \frac{\partial \rho}{\partial t} + \mathbf{u} \cdot \boldsymbol{\nabla} \rho = 0, \tag{2}$$

leading to the incompressibility equation

$$\boldsymbol{\nabla} \cdot \mathbf{u} = 0.$$

Internal waves have co-dimension two. This means that any internal wave in a three-dimensional fluid can (locally) be confined to a two-dimensional subspace. This subspace always includes the vertical direction. It is therefore appropriate to neglect all dependency on one of the horizontal directions, here chosen to be the y-direction.
The density perturbations $\rho'(t, x, z)$ on the height-dependent average $\rho_0 + \rho_*(z)$ are assumed to be small and the height-dependency in turn is assumed to be small compared to the overall average ρ_0. These assumptions are usually appropriate for the abyssal ocean where the density varies in the order of permil over kilometres height. It allows to apply the Boussinesq approximation, which means that $\rho(t, x, z) = \rho_0 + \rho_*(z) + \rho'(t, x, z)$ is replaced by ρ_0 in all terms except for the gravity term.
Under these assumptions the linearised momentum equations become

$$\begin{aligned} \rho_0 \partial_t u &= +\rho_0 f v - \partial_x p \\ \partial_t v &= -f u \\ \rho_0 \partial_t w &= \qquad\quad \partial_z p - \rho g. \end{aligned} \tag{3}$$

and the equation of state (2) becomes

$$\partial_t \rho = -w\Gamma, \tag{4}$$

where $\Gamma = \partial_z \rho_*$ is a constant (for uniform stratification). Here ∂_s denotes the derivative with respect to some variable s.
Taking the time derivative of the first and third equations in (3) and dividing them by ρ_0, removing $\partial_t v$ by substituting the second equation for it and removing $\partial_t \rho$ by using (4) results in

$$\begin{aligned} \partial_{tt} u &= -f^2 u - \partial_{xt} p \\ \partial_{tt} w &= \qquad -\partial_{zt} p + \frac{\Gamma g}{\rho_0} w. \end{aligned} \tag{5}$$

The pressure term is removed by subtracting the x-derivative of the second equation in (5) from to the z-derivative of the first equation, giving

$$\partial_{ztt} u - \partial_{xtt} w = -f^2 \partial_z u + N^2 \partial_x w \tag{6}$$

where $N^2 = -\frac{g\Gamma}{\rho_0}$ and N is known as the Brunt-Väisälä frequency. For a stable stratification the density must increases with depth, so $\Gamma < 0$, which corresponds to $N^2 > 0$.
Notice that the continuity equation $\partial_x u + \partial_z w = 0$ is implicitly satisfied if one

introduces streamfunction $\hat{\Psi}$ with $u = \partial_z \hat{\Psi}$ and $w = -\partial_x \hat{\Psi}$. Expressing (6) in terms of the streamfunction Ψ gives

$$\partial_{zztt}\hat{\Psi} + \partial_{xxtt}\hat{\Psi} = -f^2\partial_{zz}\hat{\Psi} - N^2\partial_{xx}\hat{\Psi}.$$

This linear equation can be solved by superimposing solutions for monochromatic waves, $\hat{\Psi} = e^{-i\omega t}\Psi(x,z)$. For a given frequency ω the spatial dependency $\Psi(x,z)$ has to satisfy

$$\frac{\partial^2\Psi}{\partial x^2} - \vartheta^2\frac{\partial^2\Psi}{\partial z^2} = 0, \tag{7}$$

where $\vartheta = \sqrt{\frac{\omega^2 - f^2}{N^2 - \omega^2}}$. In the following it is $\Psi(x,z)$ which is referred to as the streamfunction. In section (2) only real-valued streamfunctions (corresponding to standing internal waves) are considered. In section 3 the spatial dependence of the streamfunction is extended with an imaginary part, which is emphasized by adding a bar on the streamfunction: $\bar{\Psi}$.
In this study only the hyperbolic case, in which $\vartheta > 0$, is considered. In that case scaling and stretching of the spatial coordinates (x,z) leads to

$$\frac{\partial^2\Psi}{\partial x^2} - \frac{\partial^2\Psi}{\partial z^2} = 0. \tag{8}$$

This is the equation which is central in section 2.
In the subsequent part on tidal conversion, section 3, the fluid is assumed to be non-rotating, $f = 0$. Adding the assumption that $N >> \omega$ (very close to hydrostatic equilibrium) leads to $\vartheta = \frac{\omega}{N}$.
In section 3 the interest lies on the dependence of the velocity field above irregular topography on the forcing frequency ω for fixed Brunt-Väisälä frequency N. Rather than scaling the vertical coordinate with $\vartheta = \frac{\omega}{N}$, which depends on ω and N, it is more appropriate to scale the vertical coordinate in the governing equations (7) with $1/N$, leading to

$$\frac{\partial^2\Psi}{\partial x^2} - \omega^2\frac{\partial^2\Psi}{\partial z^2} = 0. \tag{9}$$

Scaling the time t makes it possible to consider ω of magnitude 1. The forcing frequency ω for which no tidal conversion takes place is in all cases chosen to be $\omega = 1$.

Boundary condition

Every fluid is confined to some domain. It is an elementary constraint to assume no flow through the boundary of the domain. For the frictionless fluid considered in this thesis this results in the so-called free slip boundary condition, which means that at the boundary the velocity field is parallel to the boundary. As the velocity is along constant lines of the streamfunction Ψ this means that the streamfunction must be constant on the boundary of the domain.
For the closed domains considered in section 2 the streamfunction is chosen to take the value zero on the boundary. The slightly different boundary condition for barotropic tides in horizontally infinitely wide domains is introduced in the beginning of section 3.

2 Standing internal waves in trapezoid

In this section analytical streamfunction solutions confined to trapezoidal domains and exhibiting (1,1) attractors are constructed and analysed. The construction is done by two different methods. The first method finds solutions by first translating the boundary condition to Fourier space. This method is presented in subsection (2.1).
In subsection (2.2) the second method leading to exact streamfunction solutions is presented. The method reduces the boundary condition to a so-called Abel's functional equation first. This functional equation is then solved by a method presented in [1], which is inspired by a group action algorithm presented in [9]. The calculations are much shorter and the resulting exact streamfunction solutions give new insight into the fractal structure of the streamfunction. This fractal structure is discussed in section (2.3). In section (2.4) the two methods leading to exact internal wave solutions are compared and discussed.
The kinetic energy of the internal wave velocity field integrated over the trapezoidal domains is infinite. Distributing the kinetic energy over the Fourier modes of the velocity field leads to a well-defined series. In appendix A it is shown that for the trapezoidal domain considered in [11] this series has $\log_5$-periodicity as the Fourier mode approaches infinity.
Appendix B, section (5.2), discusses a set of countable-infinite linear equations. This set of equations, referred to as Γ-equation, appears in the derivation of the exact streamfunction solutions in [11]. In (5.2.1) its derivation is presented in detail, (5.2.2) shows that the countable-infinite matrix Γ in the Γ-equation is a well-defined operator on the Hilbert space ℓ^2 and (5.2.3) shows that Γ is unter-determined, implying that it is not invertible.
Constraints on solutions to the functional equation derived in (2.1.1) are discussed in appendix C, section (5.3). Appendix D, section (5.4), presents a proof that any non-trivial internal wave solution in a domain exhibiting an attractor is a weak solution.

2.1 Method 1: constructing exact solution in Fourier space

In [11] an analytical internal wave streamfunction solution for a trapezoidal domainis constructed by transforming the boundary condition into Fourier space and finding exact expressions for the Fourier coefficients of the streamfunction. This streamfunction solution has previously also been calculated numerically [17].
Here the method used in [11] is applied to construct exact streamfunction solutions for a much larger class of trapezoidal domains. This is divided in the derivation of a functional equation, which guarantees the vanishing of the streamfunction on all boundaries, in subsection (2.1.1) and how it can be used to derive the Fourier coefficients of the streamfunction (subsection (2.1.2)). Subsection (2.1.2) also presents a series of plots from the family of trapezoidal domains for which streamfunctions are constructed.

2.1.1 Derivation of functional equation

Here exact streamfunction solutions Ψ for standing internal waves are constructed for the trapezoidal domain

$$D_\tau := \{(x,z) \in \mathbb{R}^2 : z \in (-\tau, 0) \text{ if } x \in (-1,0) \text{ and } z \in (\tau(x-1), 0) \text{ if } x \in (0,1)\}$$

with $\tau \in (1,2)$. The streamfunction Ψ must satisfy (8) and 'standing' means that Ψ is real-valued. On the boundary ∂D_τ of the domain D_τ the streamfunction Ψ has to be constant, as discussed in section (1.1) and it is chosen to take $\Psi = 0$ on ∂D_τ. The streamfunction Ψ is constructed by determining its Fourier coefficients. In order to satisfy (8) one has to restrict the general Fourier expansion of Ψ to the sum over products of the form $a_n e^{i\omega_n x} e^{i\omega_n z}$ for arbitrary constants ω_n. All boundary conditions except the sloping wall boundary condition $z = \tau(x-1)$ are already satisfied when taking

$$\Psi(x,z) = \sum_{n=1}^{\infty} a_n \sin\left(n\pi \frac{x+1}{\tau}\right) \sin\left(n\pi \frac{z}{\tau}\right). \tag{10}$$

In the coordinates $\zeta^{\pm} = x + 1 \pm z$ (10) takes the form

$$\Psi = \frac{1}{2} \sum_{n=1}^{\infty} a_n \left(\cos\left(n\pi \frac{\zeta^-}{\tau}\right) - \cos\left(n\pi \frac{\zeta^+}{\tau}\right)\right).$$

Since we require the streamfunction Ψ to vanish at the sloping boundary $z = \tau(x-1)$ for $x \in [0,1]$:

$$\Psi(x, \tau(x-1)) = \frac{1}{2} \sum_{n=1}^{\infty} a_n \left(\cos(n\pi(\frac{x+1}{\tau} - x + 1)) - \cos(n\pi(\frac{x+1}{\tau} + x - 1))\right) = 0.$$

To derive a functional equation as in [11] it is necessary that the constant terms of the arguments of both cosines terms are equal. This is achieved by the coordinate transformation $x = \frac{\xi}{2} + \tau - 1$, which leads to

$$\sum_{n=1}^{\infty} a_n \left(\cos(n\pi \left(\frac{\tau-1}{2\tau}\xi + \tau - 1\right)) - \cos(n\pi \left(\frac{\tau+1}{2\tau}\xi + \tau - 1\right))\right) = 0. \tag{11}$$

Defining $F(\xi) := \sum_{n=1}^{\infty} a_n \cos(n\pi(\frac{\tau-1}{2\tau}\xi + \tau - 1))$ and forcing power $p := \frac{\tau+1}{\tau-1} > 1$ the condition (11) is equivalent to the functional equation, known as Schröder's functional equation

$$F(\xi) = F(p\xi). \tag{12}$$

Notice that the transformation $x = \frac{\xi}{2} + \tau - 1$ projects $x \in [0,1]$ onto $\xi \in [2(1-\tau), 2(2-\tau)]$. For $\tau \in (1,2)$ we have that $1 - \tau < 0 < 2 - \tau$, so ξ can be positive as well as negative. So if $F(\xi)$ is prescribed on the intervals $I_- := [2(1-\tau), 2(1-\tau)p^{-1}]$ and $I_+ := [2(2-\tau)p^{-1}, 2(2-\tau)]$, then $F(\xi)$ is known for all $\xi \in [2(1-\tau), 2(2-\tau)]$ due to the functional equation (12). Intervals with this property are referred to as *fundamental intervals* [13]: once a choice for a solution F on some fundamental interval is made, then F is uniquely defined by the functional equation on all of its domain. A fundamental interval is in general not unique and does not have to be

connected.
Notice that any solution $F(\xi)$ to (12) can be split into symmetric and antisymmetric part. It turns out that $F(\xi)$ must be purely symmetric around the centres $c_- := (1-\tau)(1+p^{-1})$ and $c_+ := (2-\tau)(1+p^{-1})$ of the intervals I_- and I_+. In order to prove this for I_+ assume that $F(\xi)$ is antisymmetric on I_+. Any function $F(\xi)$ for $\xi \in I_+$ which is antisymmetric around c_+ can be written as

$$F(\xi) = \sum_{l=1}^{\infty} \alpha_l \sin\left(l\pi\left(\frac{\xi}{(2-\tau)(1-p^{-1})} - \frac{1+p^{-1}}{1-p^{-1}}\right)\right) = \sum_{l=1}^{\infty} \alpha_l \sin(l\pi\zeta_+) \tag{13}$$

for some sequence $(\alpha_l)_{l\in\mathbb{N}} \in \ell^2$ and $\zeta_+ \in [-1,1]$ because $\zeta_+(\xi) := \frac{\xi}{(2-\tau)(1-p^{-1})} - \frac{1+p^{-1}}{1-p^{-1}}$ maps I_+ onto $[-1,1]$. Inserting now the inverse relation $\xi = (2-\tau)\frac{p-1}{p}\zeta_+ + (2-\tau)\frac{p+1}{p}$ into the definition of $F(\xi)$ and using the functional equation (12) we get

$$\begin{aligned} F_\tau(\xi) &= F_\tau(p\xi) = \sum_{n=1}^{\infty} a_n \cos\left(n\pi\left(\frac{\tau-1}{2\tau}p\xi + \tau - 1\right)\right) \\ &= \sum_{n=1}^{\infty} a_n \cos\left(n\pi\left(\frac{\tau-1}{2\tau}((2-\tau)(p-1)\zeta_+ + (2-\tau)(p+1)) + \tau - 1\right)\right) \\ &= \sum_{n=1}^{\infty} a_n (-1)^n \cos\left(n\pi\left(\frac{2-\tau}{\tau}\zeta_+\right)\right). \end{aligned} \tag{14}$$

Notice that the assumption that $F(\xi)$ is antisymmetric on I_+ leads to a contradiction because $F(\xi)$ cannot simultaneously be antisymmetric (by (13)) and symmetric (by (14)). So $F(\xi)$ must be symmetric on I_+. The proof that $F(\xi)$ must be symmetric on I_- is analogous.

2.1.2 Calculating Fourier coefficients a_n for general $(1,1)$-attractor

The idea is to derive the Fourier coefficients a_n by integrating $F(\xi)$ times $\cos(n\pi(\frac{\tau-1}{\tau}\xi + \tau - 1))$ over an interval for ξ of length $\frac{4\tau}{\tau-1}$, which of course requires $F(\xi)$ to be prescribed on an interval of length $\frac{4\tau}{\tau-1}$. To show this, assume that $F(\xi)$ is known for $\xi \in I_s := [s, s+\frac{4\tau}{\tau-1}]$ for some $s \in \mathbb{R}$. The m^{th} Fourier coefficient F_m for $m \in \mathbb{N}$ of $F(\xi)$ over this interval I_s is then given by

$$\begin{aligned} F_m &= \int_s^{s+\frac{4\tau}{\tau-1}} \cos\left(m\pi\left(\frac{\tau-1}{2\tau}\xi + \tau - 1\right)\right) F(\xi) d\xi \\ &= \int_s^{s+\frac{4\tau}{\tau-1}} \sum_{n=1}^{\infty} \cos\left(m\pi\left(\frac{\tau-1}{2\tau}\xi + \tau - 1\right)\right) a_n \cos\left(n\pi\left(\frac{\tau-1}{2\tau}\xi + \tau - 1\right)\right) d\xi \\ &= \frac{2\tau}{\tau-1}\delta_{nm}a_n = 2\frac{\tau}{\tau-1}a_m. \end{aligned} \tag{15}$$

From this it is clear that we can extract the Fourier coefficients a_n of the stream-function Ψ once we are able to calculate the Fourier coefficients F_m over an interval some interval I_s.
The interval $[2(1-\tau), 2(2-\tau)]$, on which $F(\xi)$ is defined once $F(\xi)$ is prescribed

on the two fundamental intervals I_+ and I_-, is not sufficiently large to derive the Fourier coefficients a_n as suggested by (15).
A natural extension of $F(\xi)$ for $\xi \notin [2(1-\tau), 2(2-\tau)]$ is to use the functional equation $F(p\xi) = F(\xi)$. It turns out that expanding $F(\xi)$ to $\xi \in I_c := [pc_-, pc_+]$ and then require $F(\xi)$ to be periodic with period $T_\tau = p(c_+ - c_-) = p((1+p^{-1})(2-\tau-1+\tau)) = p\frac{p+1}{p} = p+1 = \frac{\tau+1}{\tau-1} + \frac{\tau-1}{\tau-1} = \frac{2\tau}{\tau-1}$ leads to non-trivial analytical streamfunction solutions for D_τ. Notice that the length of I_c is exactly half the length of I_s. So we can for example choose $s = pc_-$ and then integrate $F(\xi)\cdot\cos(m\pi(\frac{\tau-1}{2\tau}\xi+\tau-1)$ from pc_- to $pc_- + \frac{4\tau}{\tau-1}$.
It turns out that it is sufficient to integrate $F(\xi)\cdot\cos(m\pi(\frac{\tau-1}{2\tau}\xi+\tau-1)$ from pc_- to $pc_+ = pc_- + \frac{2\tau}{\tau-1}$, so only over half of the interval $[pc_-, pc_- + \frac{4\tau}{\tau-1}]$. This is the case because

$$\begin{aligned} F_m &= \int_{pc_-}^{pc_+} \cos(m\pi(\frac{\tau-1}{2\tau}\xi+\tau-1))F(\xi)d\xi \\ &= \int_{pc_-}^{pc_+} \sum_{n=1}^{\infty} \cos(m\pi(\frac{\tau-1}{2\tau}\xi+\tau-1))a_n\cos(n\pi(\frac{\tau-1}{2\tau}\xi+\tau-1))d\xi \\ &= \sum_{n=1}^{\infty} \frac{\tau}{\tau-1}\delta_{nm}a_n = \frac{\tau}{\tau-1}a_m. \end{aligned}$$

One is free to choose $F(\xi)$ on the fundamental intervals I_+ and I_-. If one maps both fundamental intervals I_+ and I_- onto $[-1,1]$ with the coordinate transformations $\zeta_+ = \frac{\xi}{(2-\tau)(1-p^{-1})} - \frac{1-p^{-1}}{1+p^{-1}}$ (inverse map: $\xi = (2-\tau)\frac{p-1}{p}\zeta_+ + (2-\tau)\frac{p+1}{p}$) and $\zeta_- = \frac{\xi}{(1-\tau)(p^{-1}-1)} + \frac{1-p^{-1}}{1+p^{-1}}$ (inverse map: $\xi = (1-\tau)\frac{1-p}{p}\zeta_- + (1-\tau)\frac{p+1}{p}$) then choosing $F(\xi)$ freely on the fundamental intervals is equivalent to choosing $\alpha_i^+, \alpha_j^- \in \mathbb{R}$ for all $i,j \in \mathbb{N}$ arbitrarily for $F(\zeta_+) = \sum_{i=1}^{\infty}\alpha_i^+\cos(\pi i\zeta_+)$ and $F(\zeta_-) = \sum_{i=1}^{\infty}\alpha_i^-\cos(\pi i\zeta_-)$. In [11] the analytical streamfunction solution for $\tau = \frac{3}{2}$ is calculated for the choice $\alpha_1^+ = \alpha_1^- = 1$ and all other coefficients zero. This is the motivation to plot analytical streamfunction solutions for this choice of $F(\xi)$ on the fundamental intervals, as done in the following.

Analytical streamfunction solution

The choice $\alpha_1^+ = \alpha_1^- = 1$ leads to

$$a_m = \frac{\tau-1}{\tau}(S_1^+ + S_1^- + S_2^+ + S_2^-) \tag{16}$$

with

$$S_1^+ = \sum_{n=0}^{\infty}\int_{2(2-\tau)p^{-n}}^{2(2-\tau)p^{-(n+1)}} \cos\left(m\pi\left(\frac{\tau-1}{2\tau}\xi+\tau-1\right)\right)\cos\left(\pi\left(\frac{\xi p^n}{(2-\tau)(1-p^{-1})} - \frac{1+p^{-1}}{1-p^{-1}}\right)\right)d\xi,$$

$$S_1^- = \sum_{n=0}^{\infty}\int_{2(1-\tau)p^{-(n+1)}}^{2(1-\tau)p^{-n}} \cos\left(m\pi\left(\frac{\tau-1}{2\tau}\xi+\tau-1\right)\right)\cos\left(\pi\left(\frac{\xi p^n}{(1-\tau)(p^{-1}-1)} + \frac{1+p^{-1}}{1-p^{-1}}\right)\right)d\xi,$$

$$S_2^+ = \int_{2(2-\tau)}^{pc_+} \cos\left(m\pi\left(\frac{\tau-1}{2\tau}\xi+\tau-1\right)\right)\cos\left(\pi\left(\frac{\xi}{(2-\tau)(1-p^{-1})} - \frac{1+p^{-1}}{1-p^{-1}}\right)\right)d\xi$$

and

$$S_2^- = \int_{pc_-}^{2(1-\tau)} \cos\left(m\pi\left(\frac{\tau-1}{2\tau}\xi+\tau-1\right)\right)\cos\left(\pi\left(\frac{\xi}{(1-\tau)(p^{-1}-1)}+\frac{1+p^{-1}}{1-p^{-1}}\right)\right)d\xi.$$

The plots of the streamfunction and the kinetic energy of the internal waves shown below are achieved by first integrating $S_1^{\pm}$, $S_2^{\pm}$ in *Mathematica* and then calculating the streamfunction $\Psi(x,z)$ as given in (10) on a grid with 1000×1000 grid points in MATLAB. This has been performed for a number of values of τ[1].
The kinetic energy is defined by $E = \frac{1}{2}(u^2+w^2)$ with $u = \partial_z\hat{\Psi}$ and $w = -\partial_x\hat{\Psi}$. This definition for the kinetic energy is independent of density ρ because ρ is assumed to be (approximately) constant and can therefore be scaled out.

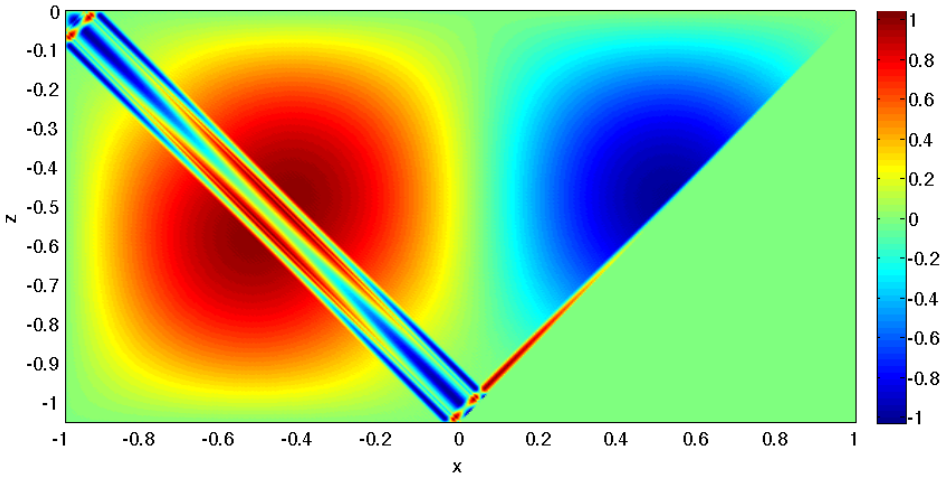

Figure 1: *This figure shows the analytical streamfunction solution for* $\tau = 1.0501$. *The solution is generated on* 1000×1000 *grid points (everything below sloping boundary is zero). Colours towards red indicate at positive streamfunction value while negative streamfunction are in blue.*

[1]It turns out *Mathematica* does not give the correct integrals for $S_1^{\pm}$ and $S_2^{\pm}$ for a number of values of $\tau \in (1,2)$ because inserting for example $\tau = \frac{3}{2}$ gives Inf in MATLAB, indicating (in this case) that one divides by zero. It is not correct to get infinite values because the integrals are all bounded for $\tau \in (1,2)$. This issue can easily be solved by treating cases like $\tau = \frac{3}{2}$ separately. In the following plots this computational issue is avoided by adding 0.0001 to values τ. No analytical expressions of a_m is given due to this issue.

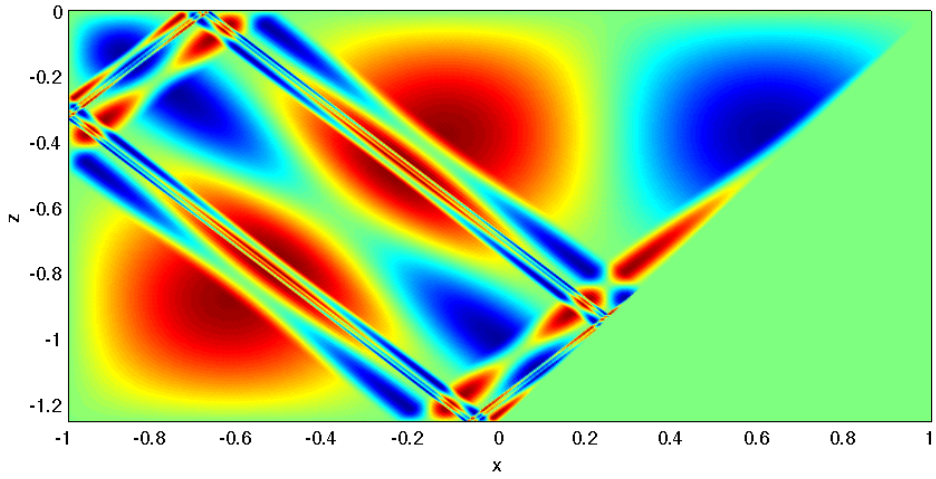

Figure 2: *This figure shows the analytical streamfunction solution for* $\tau = 1.2501$.

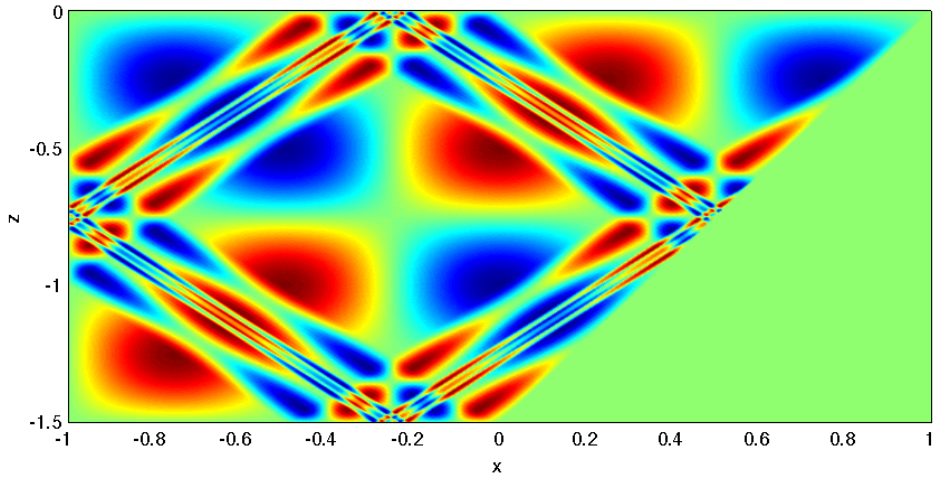

Figure 3: *This figure shows the analytical streamfunction solution for* $\tau = 1.5001$. *Neglecting the unnoticeable perturbation due to the fourth decimal in* τ *this is equal to the streamfunction solution in* [11] *for* $\tau = 1.5$.

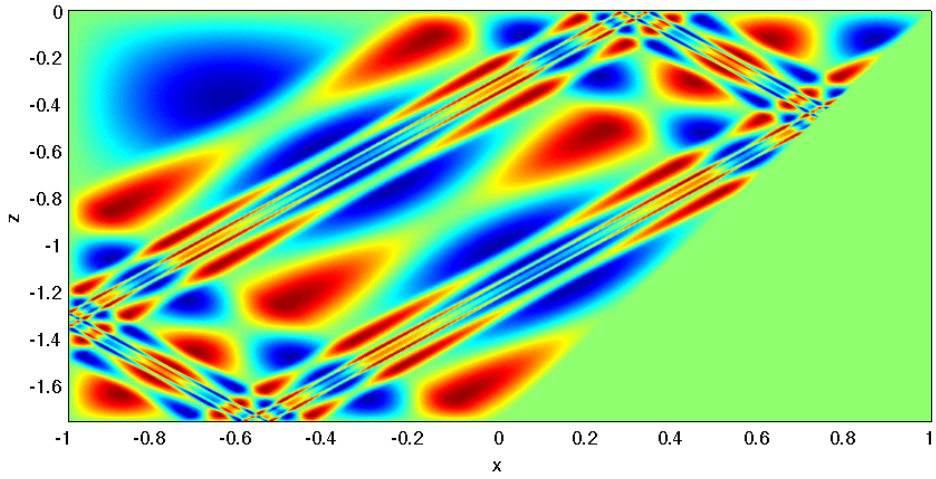

Figure 4: *This figure shows the analytical streamfunction solution for* $\tau = 1.7501$.

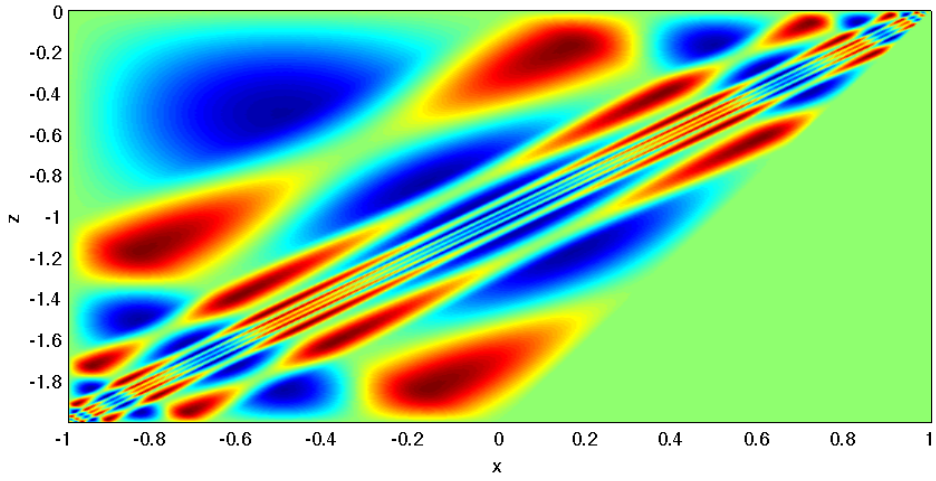

Figure 5: *This figure shows the analytical streamfunction solution for* $\tau = 1.9999$.

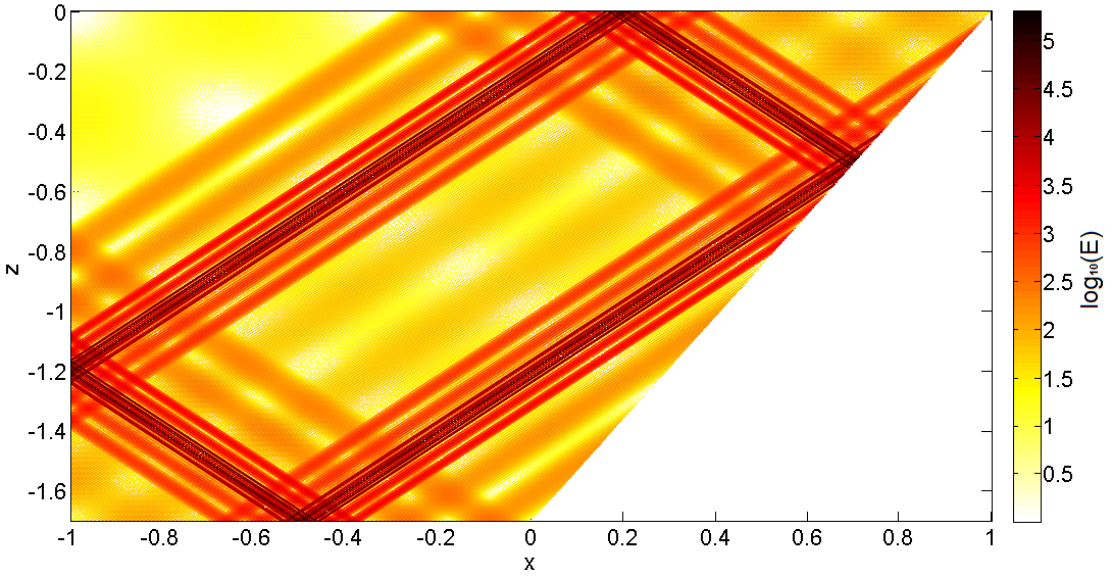

Figure 6: *This figure shows the kinetic energy* $E = \frac{1}{2}(u^2 + w^2)$ *for* $\tau = 1.701$ *on a* $\log_{10}$ *scale. It shows that the kinetic energy increases by several orders of magnitude as one approaches the attractor. In fact the kinetic energy goes to infinity as one takes the limit to the attractor. The kinetic energy integrated over the entire domain is also infinite. The presented kinetic energy is evaluated on a grid with 1500 times 1500 grid points and all values below* 1 *(on the* $\log_{10}$ *scale this is below* 0*) are shown white.*

2.2 Method 2: construction by solving Abel's functional equation

A general real-valued solution to the governing equation (7) is given by $\Psi(x, z) = f(x-z)+g(x+z)$ for arbitrary functions $f, g : \mathbb{R} \to \mathbb{R}$. Vanishing of the streamfunction Ψ at the surface $z = 0$ gives that $g = -f$. The task in finding all streamfunction solutions to (7) which vanishes at the boundary ∂D is therefore to find functions f with the property

$$f(x - z) = f(x + z) \quad \text{for all } (x, z) \in \partial D, z < 0. \tag{17}$$

In [9] an algorithm is presented which solves the Abel functional equation. This has been the inspiration for the solution procedure presented in [1] and applied in the following to the trapezoidal domains. In order to apply the method to internal waves confined to the trapezoidal domain D_τ the boundary condition (17) has to be reformulated to Abel's functional equation.

2.2.1 Reduction to Abel's functional equation

Here the boundary condition for an internal wave field in the trapezoidal domain

$$D_\tau := \{(x, z) \in \mathbb{R}^2 | -\tau \leq z \leq 0 \text{ for } -1 \leq x \leq 0 \text{ and } \tau(x-1) \leq z \leq 0 \text{ for } 0 < x \leq 1\}$$

is reformulated to Abel's functional equation. This is done by tracing so-called characteristics through the domain. A characteristic is a inclined line through the domain of interest, which has a fixed angle with respect to the vertical (same angle as internal wave propagation, here this is 45 degrees). Physically characteristics are meaningful as the kinetic energy of internal waves is propagated along characteristics. A web is a trajectory along characteristics through the domain, such that changes between characteristics only occur on the boundary. See figure (7) for an illustration of some characteristics and webs. Notice that either $-f(x-z)$ or $f(x+z)$ is conserved along a characteristic. Upon reflection at the boundary the web changes direction, following another characteristic and the other component of the streamfunction $\Psi(x,z)$ is thus conserved. If x is one reflection point of a web at the surface $z=0$ and x' is another reflection point at the surface of the same web, then $f(x)=f(x')$. A comprehensive discussion of characteristics and webs in the context of internal waves can be found in [13].
Let $(x_0,0)$ for $x_0 \in [-1,1]$ be some point on the surface $z=0$. In the following it is determined where the web passing through $(x_0,0)$ along the characteristic downwards to the right next reflects at the surface (after being reflected once at the sloping wall, the bottom $z=-\tau$ and the vertical wall $x=-1$). The positions of these reflections are denoted by (x_i,z_i), $i=1,2,3$ and the next reflection at the surface $z=0$ is at x_4.
The interest lies in the the map $T(x_1)=x_4=x_4(x_1)$, which captures the relevant properties of the two-dimensional topography by following interection points of webs from one surface point to the next surface point. See also figure (7) for an illustration of the map T. From the topography D_τ it is immediately clear that $z_2=-\tau$ and $x_3=-1$. The web through surface point x_0, parametrized by the characteristic $c_0(x)=-x+x_0$ for the first section, intersects the sloping wall $z=\tau(x-1)$ at

$$c_0(x_1) = -x_1 + x_0 = z_1 = \tau(x_1 - 1),$$

which gives $x_1 = \frac{x_0+\tau}{\tau+1}$. The web continues along the characteristic $c_1(x) = x+z_1-x_1$ with $z_1 = \tau(x_1-1) = \tau\frac{x_0+\tau}{\tau+1} - \tau$ and intersects the bottom $z=-\tau$ at

$$c_1(x_2) = x_2 + (\tau-1)\frac{x_0+\tau}{\tau+1} - \tau = -\tau.$$

So $x_2 = -\frac{\tau-1}{\tau+1}(x_0+\tau)$, leading the web to follow the characteristic $c_2(x) = -x + x_2 + z_2$, which intersects the vertical wall $x_3=-1$ at

$$c_2(-1) = 1 - \frac{\tau-1}{\tau+1}(x_0+\tau) - \tau = z_3.$$

The characteristic $c_3(x) = x - x_3 + z_3$ intersects the surface $z=0$ at

$$c_3(x_4) = x_4 - (-1) + 1 - \tau - \frac{\tau-1}{\tau+1}(x_0+\tau) = 0,$$

giving

$$T(x_0) = x_4(x_0) = \frac{\tau-1}{\tau+1}(x_0+\tau) - 2 + \tau = p^{-1}(x_0+r)$$

where $p = \frac{\tau+1}{\tau-1} > 1$ and $r = 2\frac{\tau^2-\tau-1}{\tau-1}$. This leads to the Schröder functional equation

$$f(T(x)) = f(x) \qquad \text{for } x \in [-1,1] \tag{18}$$

to be solved, as f is conserved along webs for $\Psi(x,z) = f(x-z) - f(x+z)$. The constraint

$$f(-1-z) = f(-1+z) \qquad \text{for } z \in [-\tau, 0], \tag{19}$$

given by the wall at $x = -1$, means that f has to be defined over a larger range than $[-1, 1]$, namely over $[-1-\tau, -1+\tau]$. This interval is extended to $\mathbb{R}$ by the constraint

$$f(x-\tau) = f(x+\tau) \qquad \text{for } x \in [-1, 0], \tag{20}$$

which requires the vanishing of $\Psi(x,z)$ at the flat bottom $z = -\tau$ for $x \in [-1, 0]$. So $f(x)$ has period 2τ and is symmetric around $x = -1 + \tau n$ for all $n \in \mathbb{Z}$ (this follows from symmetry around $x = -1$ and 2τ-periodicity).

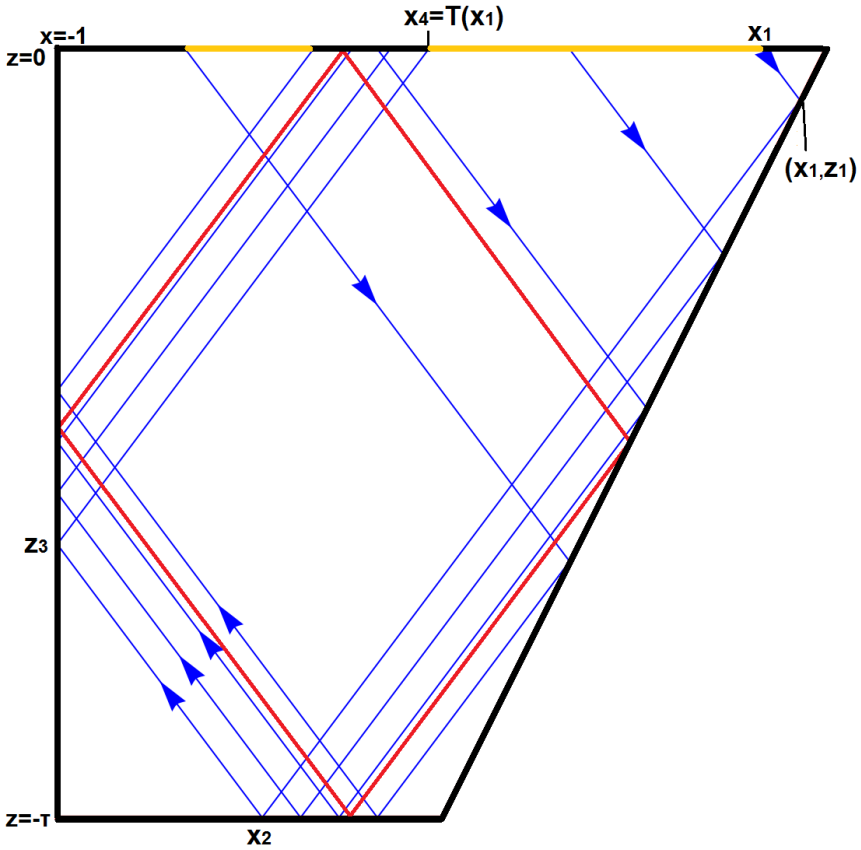

Figure 7: *This figure gives an illustration of the four characteristics (blue lines) along one loop through the trapezoidal domain (from surface to surface). The attractor for this trapezoidal domain with* $\tau = \frac{3}{2}$ *is shown in red, which is the limit cycle for all characteristics. The characteristics starting at* x_0 *reflects at* (x_1, z_y), $(x_2, -\tau)$, $(-1, z_3)$ *and reaches the surface at* x_4. *The map* T *is defined such that it projects* x_1 *onto* x_4. *The yellow intersections of the surface* $z = 0$ *show two possible fundamental intervals.*

The map T has a fixed point in $s_{0,-} = -1+\tau^2-\tau \in (-1,1)$, which follows by solving $T(s_{0,-}) = p^{-1}(s_{0,-}+r) = s_{0,-}$ for $s_{0,-}$. The meaning of the zero and the minus sign in the subscript will become clear in the following. The fixed point $s_{0,-} = -1+\tau^2-\tau$ of T is projected onto $s_{0,+} = -1-\tau^2+\tau \in (-3,-1)$ by symmetry of $f(x)$ around $x=-1$. The sign subscript therefore indicates that $s_{0,-}$ and $s_{0,+}$ indicates that these two fixed points are related by symmetry around $x=-1$. The periodicity with period 2τ projects the two points $s_{0,\pm}$ onto $s_{n,\pm} = -1+2\tau n \mp (\tau^2-\tau)$ for all $n \in \mathbb{Z}$. Notice that $s_{n+1,+} \in [-1+2\tau n, -1+2\tau(n+1)]$ and $s_{n,-} \in [-1+2\tau n, -1+2\tau(n+1)]$ for each $n \in \mathbb{Z}$. This means that each interval $J_n = [-1+2\tau n, -1+2\tau(n+1)]$ contains exactly two fixed points for T, namely $s_{n+1,+}$ and $s_{n,-}$. Due to the periodicity one can also define f on the circle $S = 2\tau S^1$, where S^1 denotes the unit circle. The fixed points $s_{n,-}$ and $s_{n,+}$ split this circle S into two regions.
The Schröder functional equation (18) has to be solved on both regions separately because non-trivial continuous solutions to (18) can only be attained if one excludes fixed points of T. See Appendix D (5.4) and Theorem 3 in Beckebanze and Keady, (2014) for the solvability of the Schröder's functional equation, which is closely related to fixed point of the map T. A comprehensive analysis of the solvability of the Schröder's functional equation can be found in [7].
Lets focus on the subintervals $S_1 = (s_{0,+}, s_{0,-})$ and $S_2 = (s_{0,-}, s_{1,+})$ of S. These two subintervals span S excluding its fixed points because $s_{1,+} = s_{0,+} + 2\tau$. The center of these subregions are respectively -1 and $-1+\tau$, so any solution f on S_i, $i = 1,2$, has to be symmetric around the center of the interval (this to satisfy constraints (19) and (20)).
One way to find all solutions f to Schröder's functional equation (18) is to find injective solutions a_1 on S_1 and a_2 on S_2 to the Abel's functional equation

$$a(T(x)) = a(x) + 1$$

and compose the injective solutions a_i with all continuous period-1 functions P_i, e.g.

$$f = P_i \circ a_i \qquad \text{on } S_i.$$

2.2.2 Solving Abel's functional equation

The implication of theorem 5 in [1] is that the composition $f = P \circ a$ gives all possible solutions to (18).
The solution f being symmetric around the centres of the intervals S_1 and S_2 can be guaranteed by taking P_1 and P_2 even functions and a_1 and a_2 antisymmetric around the centres -1 and $-1+\tau$, respectively. Clever choices for the fundamental intervals of a_i on S_i, $i = 1,2$ are the intervals $I_i^{[0]}$, $i = 1,2$ which are centred around -1 and $-1+\tau$. The index [0] indicates that these are fundamental intervals and the use of this index will become clear in the following.

Lets determine the bounds of these fundamental intervals centred around -1 and $-1+\tau$:
For $I_1^{[0]} = [\gamma_1, T(\gamma_1))$ solve

$$T(\gamma_1) - (-1) = |\gamma_1 - (-1)|$$

to get $\gamma_1 = -\tau$. Similarly solve

$$|T(\gamma_2) - (-1+\tau)| = \gamma_2 - (-1+\tau)$$

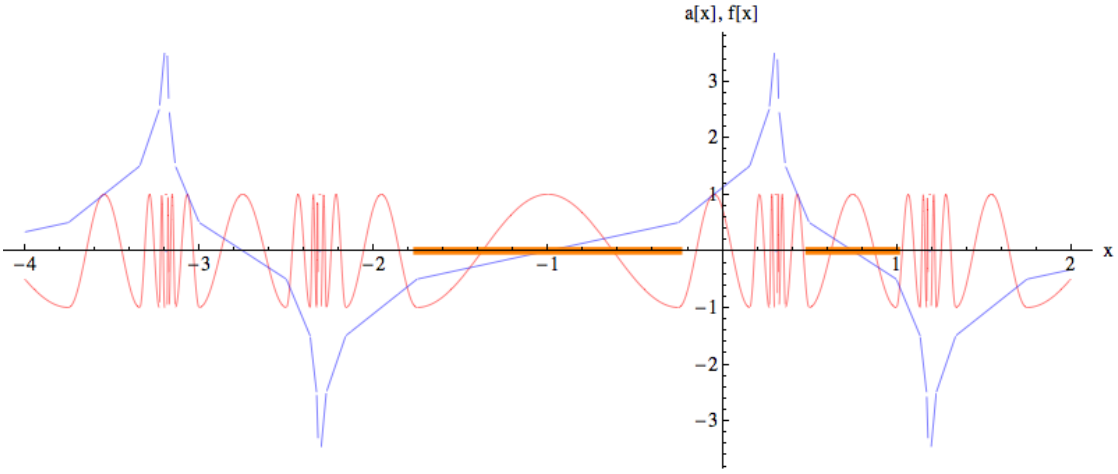

Figure 8: *This figure shows a (blue) as defined in (21) and $f = P \circ a$ (red) for $\tau = 1.75$, where $P(x) = \cos(2\pi x)$. The fundamental intervals $I_1^{[0]}$ and $I_2^{[0]}$ are indicated by the orange ranges on the x-axis. Apparent discontinuities in a are due to numerical errors made by the plotting algorithm in Mathematica.*

for γ_2 to get $I_2^{[0]} = [T(\gamma_2), \gamma_2) = [T(1), 1) = [-3+2\tau, 1)$. The easiest injective choices for a_i which are antisymmetric around the center of the intervals I_1 and I_2 are linear functions $a_i^{[0]} = \frac{x-T(\gamma_i)}{\gamma_i - T(\gamma_i)} - \frac{1}{2}$. Here the superscript $[n]$ for functions a denotes that a is valid on the interval $I^{[n]} := T^n(I^{[0]})$ for $n \in \mathbb{Z}$. Iteratively prescribing $a_i^{[n]}$ on intervals $I_i^{[n]} = [T^n(\gamma_i), T^{n+1}(\gamma_i))$ gives

$$a_i^{[n]}(x) = \frac{x - T^n(\gamma_i)}{T^{n+1}(\gamma_i) - T^n(\gamma_i)} + n - \frac{1}{2} \qquad \text{for } x \in I_i^{[n]}. \tag{21}$$

In figure (8) the solution $a(x)$ from (21) as well as $f(x) = P(a(x))$ with $P(x) = \cos(2\pi x)$ and $\tau = 1.75$ is shown. For this choice of P the streamfunction $\Psi(x, z) = P(a(x-z)) - P(a(x+z))$ is identical to the streamfunctions plotted in figures (1)-(5).

2.3 Fractal structure

In the figures in section (2.1.2) one can see that the streamfunction features many self-similarities. The analytical description of the streamfunction by method 2 makes it possible to analyse the fractal structure in the streamfunction in more detail.
In the previous section it has been shown that $\Psi(x, z) = f(x - z) - f(x + z)$ where $f = P \circ a$ for arbitrary period-1 function P and a satisfying $a(T(x)) = a(x) + 1$. It is the map T which is crucial in understanding the self-similarities of the internal waves in the trapezoidal domains.
Consider some point (x_∞, z_∞) on the attractor. Without loss of generality we assume that (x_∞, z_∞) lies on part of the attractor which can be parametrized by $z = -x + c$ for some constant c. In the following it is shown that

$$\Psi(\zeta + x_\infty, \zeta + z_\infty) = \Psi(p^{-1}\zeta + x_\infty, p^{-1}\zeta + z_\infty)$$

for $p = \frac{\tau+1}{\tau-1} > 1$ and ζ sufficiently close to the attractor[2]. This means that the fractal structure on the cascade $\{(x_i, z_i) = (p^{-i}\zeta + x_\infty, p^{-i}\zeta + z_\infty)\}_{i\in\mathbb{N}}$ onto the attractor point (x_∞, z_∞) is exact with focusing power p for any starting points (x_0, z_0) sufficiently close to the attractor (of course inside the domain and closest to the part of the attractor of interest).
As the attractor corresponds to fixed points of the map T it must hold that $T(x_\infty + z_\infty) = x_\infty + z_\infty$. Writing out $\Psi(\zeta + x_\infty, \zeta + z_\infty)$ and using the linearity of $T(x) = p^{-1}(x + r)$ gives

$$\begin{aligned}
&\Psi(\zeta + x_\infty, \zeta + z_\infty) = f(x_\infty - z_\infty) - f(2\zeta + x_\infty + z_\infty) \\
&= f(x_\infty - z_\infty) - f(T(2\zeta + x_\infty + z_\infty)) \\
&= f(p^{-1}\zeta + x_\infty - p^{-1}\zeta - z_\infty) - f(p^{-1}(2\zeta) + x_\infty + z_\infty) \\
&= \Psi(p^{-1}\zeta + x_\infty, p^{-1}\zeta + z_\infty).
\end{aligned}$$

2.4 Discussion

Here advantages and disadvantages of the two methods that lead to exact streamfunctions are discussed. Method 1 (subsection(2.1)) is referred as the Fourier method and method 2 (subsection (2.2.2) as the functional equation method.
When using this Fourier method for practical purposes, e.g. plotting the streamfunction Ψ, then the Fourier series has to be truncated at some $n = N_{max}$. This results in an approximation of the exact solution which is defined on all of D_τ, but which is only an approximation.
The description of Ψ by the functional equation method also has to be truncated after a finite number of iterative prescriptions. The resulting streamfunction is not defined on all of D_τ: an area around the attractor is left unspecified, but it is exact wherever it is defined.
For any point in $(x_0, z_0) \in D_\tau$, which does not lie on the attractor, finitely many steps are sufficient to determine the exact value of $\Psi(x_0, z_0)$ with the functional equation method. For the Fourier method all countable infinite many Fourier coefficients a_n have to be computed to determine $\Psi(x_0, z_0)$ exactly.
The theoretically exact computation of $\Psi(x_0, z_0)$ is in practice limited by the fact that numerical errors are made in each function composition. This means that the errors in $\Psi(x_0, z_0)$ can build up considerably if a large number of function compositions T^n have to be computed numerically. For the trapezoidal domain the map T happens to be linear, making its superposition easy to calculate.
It depends on the specific practical purposes whether the Fourier method or the functional equation method is more appropriate. For the analysis of the fractal structure of the streamfunction the functional equation method is certainly more useful.

It is suggested that the functional equation method can also be used to build numerical schemes which solve the Schröder functional equation and can thereby numerically calculate the internal wave streamfunction. To give a possible structure of such a numerical scheme consider some domain with an irregular bottom such that the

[2]The variable ζ has to be sufficiently small such that $(\zeta + x_\infty, \zeta + z_\infty) \in D_\tau$ and such that (x_∞, z_∞) is the closest part of the attractor. This means that there is not other part of the attractor which is closer to $(\zeta + x_\infty, \zeta + z_\infty)$.

map T cannot be calculated analytically. If however the map T can be calculated numerically by tracing characteristics and numerically calculating intersections with the boundary of the domain (in many cases this can be done efficiently with bounded numerical errors) then one can construct an exact piecewise linear solution a to the Abel's functional equation with this numerically approximated map T. An advantage is that once the solution a is calculated one can find all solutions to Schröder's functional equation by superposition with arbitrary periodic functions.
If experimental data of standing internal waves are given then one can also use the freedom in the periodic function P and the given function a to find the best fit of a standing internal wave solution to the data. As P is periodic one could use sinusoidal functions as the basis for the function space of P.

3 Tidal conversion

It is estimated that approximately 30% of the tidal energy in the oceans is lost to internal waves. This process is called tidal conversion. The dissipation of tidal energy to internal waves is far from uniformly distributed over the oceans, as illustrated in figure (9), where the estimated rate of energy loss of the barotropic M_2 tide is shown. The regions of intense energy dissipation correspond to regions of irregular bottom topography (compare the M_2 dissipation rate with the ocean's bottom topography in figure (10)). There are also regions with ridges and shelfs where the energy dissipation of the M_2 is not significantly intensified. This qualitative comparison shows that tidal conversion is linked to bottom topography in a complicated manner.
In this section the response of two-dimensional monochromatic barotropic flow over irregular bottom topography is analysed It is assumed that the barotropic mode is sufficiently weak such that non-linear responses and changes in the surface elevation can be neglected. Throughout the section it is also assumed that the fluid is uniformly stratified, not rotating and frictionless. In [10] it is shown that for a fluid satisfying these assumptions there exist irregular bottom topographies which lack tidal conversion. The exact streamfunction solutions for a specific monochromatic barotropic flow over smooth bottom topography and its response presented in [10] show that there are internal waves trapped to the region of irregular bottom topography, but no internal waves propagate away from this region. This is a remarkable result as it is known that barotropic tides over bottom topographies other than a flat bottom generally lead to the generation of propagating internal waves. In a steady state the kinetic energy of the trapped internal waves is constant over time, so the irregular bottom topography does not lead to any dissipation of tidal energy. In this section the emphasis lies on constructing exact solutions for topographies which lack tidal conversion for a specific frequency of the barotropic tide.
The Abel functional equation and the solution method presented in [1] is put into context with tidal conversion in subsection (3.1). In subsection (3.3) the analytical solution presented in [8] is revised to put it into context with tidal conversion. A more sophisticated bottom topography which lacks tidal conversion for one specific parameter value is constructed in section (3.4). The construction of the solution consists of several steps and makes the main part of this section.

3.1 Mathematical description of tidal conversion

In the following the baroclinic response due to barotropic flow over irregular bottom is analysed Here barotropic flow is by definition a velocity field whose horizontal components are vertically uniform. Be aware that there are different definitions of barotropic flow in literature. The assumptions on the fluid are identical to those proposed in section (1.1). This means that the velocity field (u, w) can be described by superposition of (possibly infinitely many) monochromatic waves $u(x, z, t) = \frac{\partial \Psi}{\partial z} e^{-i\omega t}$, $w(x, z, t) = \frac{\partial \Psi}{\partial x} e^{-i\omega t}$ with the streamfunction Ψ satisfying

$$\Psi_{xx} - \omega^2 \Psi_{zz} = 0. \tag{22}$$

Here ω is the forcing frequency, which is not removed by scaling and stretching of the spatial coordinates in order to find velocity fields dependent on ω. In the following problems the time t is scaled such that no tidal conversion takes place for $\omega = 1$.

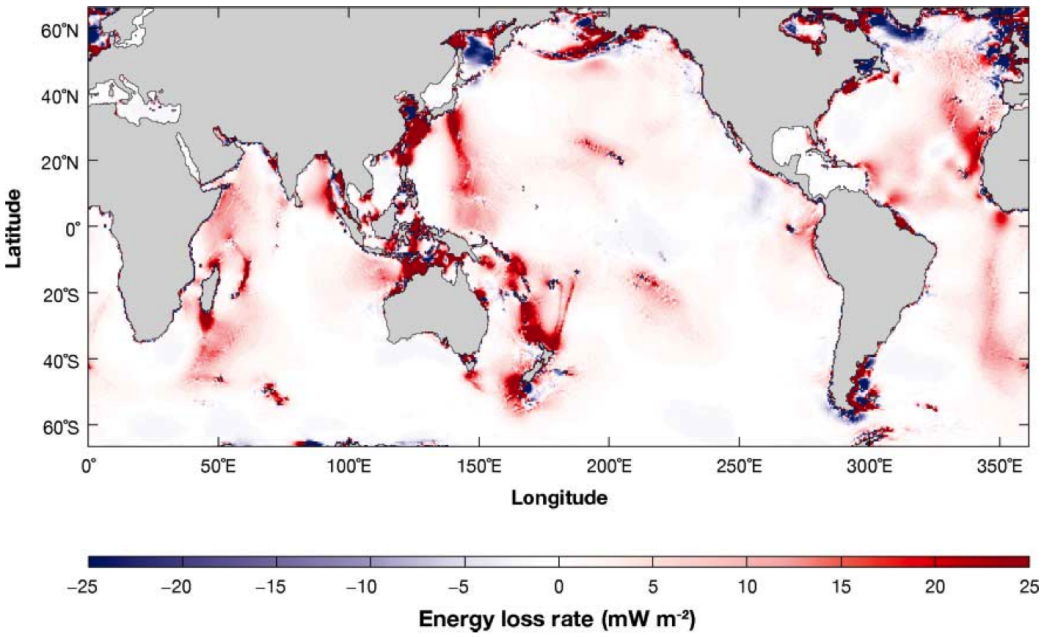

Figure 9: *This figure shows the estimated rate of energy loss from the barotropic M_2 tide, from [5].*

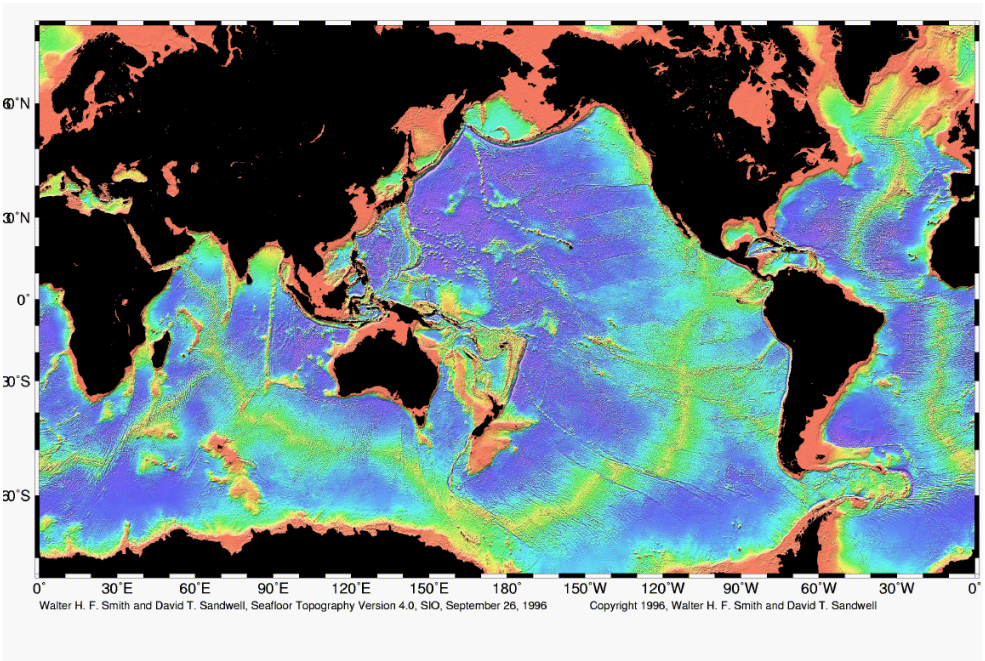

Figure 10: *This figure shows the bottom topography of the oceans, from [18]. Changes in the color indicate the ridges and shelfs in the bottom of the oceans.*

It is useful to split the streamfunction

$$\Psi = \hat{\Psi} + \Psi'$$

into its barotropic part[3] $\hat{\Psi}$ and its baroclinic part Ψ'. The barotropic flow is prescribed to be $\hat{\Psi}(x,z) = \frac{-z}{h(x)}$, where $h(x)$ now denotes the bottom topography $z = -h(x)$. This gives the velocity field $u = -\frac{1}{h(x)}$ and $w = -z\frac{h'(x)}{h(x)^2} = z\frac{\partial u}{\partial x}$, which is barotropic because its horizontal component u is independent of z and thereby independent of the vertical stratification. The barotropic flow is along the bottom $z = -h(x)$ because $\hat{\Psi}(x, -h(x)) = 1$ is a streamline. The surface $z = 0$ is also a streamline of the barotropic flow: $\hat{\Psi}(x, 0) = 0$. The baroclinic (internal wave) part Ψ' has to be constant on the boundaries $z = 0$ and $z = -h(x)$ and it is chosen to be zero. The boundary condition for Ψ is therefore given by

$$\Psi(x, 0) = 0 \quad \text{and} \quad \Psi(x, -h(x)) = 1.$$

A general solution to (22) is given by $\Psi(x,z) = a(x + z/\omega) + g(x - z/\omega)$ for arbitrary functions a and g. The boundary condition at $z = 0$ gives that $a = -g$

[3]The barotropic streamfunction $\hat{\Psi}$ used in this section has nothing to do with the time-dependent streamfunction, denoted by the same symbol, in section (1.1).

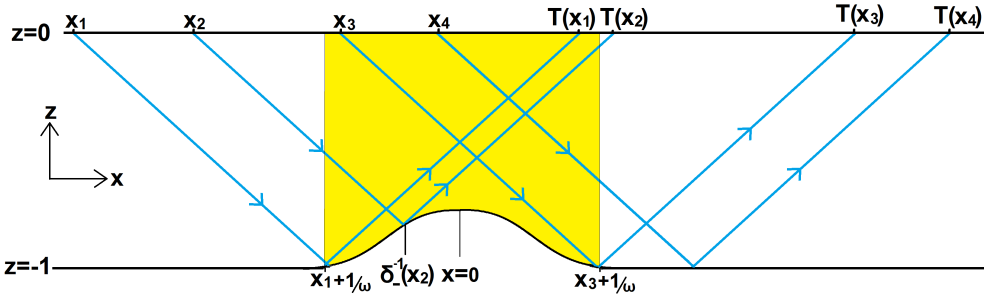

Figure 11: *This sketch shows a bottom topography with finite support irregularity under a rigid lid surface (both black lines). The part of the two-dimensional domain above the irregularity of the bottom is in yellow. Four characteristics oriented towards the right for some (unspecified) ω are shown in blue. The bottom topography is subcritical for this ω because the slope ω of the characteristics with respect to the vertical is larger than the largest slope of the bottom. The map $T_\omega = \delta_{+_\omega} \circ \delta_{-_\omega}^{-1}$ depends on ω and takes one intersection of such a (rightward-oriented) characteristic to its next intersection (x-coordinate) with the surface. For those characteristics which do not reflect a the irregular part of the bottom the map T_ω takes the form $T_\omega(x) = x + 2/\omega$. Notice that $T_\omega(x_1)$ and $T_\omega)(x_2)$ are much closer together than x_1 and x_2, because the bottom is focusing for rightward characteristics between $x_1 + 1/\omega$ and $x = 0$. The bottom is defocusing for rightward characteristics between $x = 0$ and $x_3 + 1/\omega$. As an illustration also the action of δ_-^{-1} is shown for x_2. The map δ_-^{-1} determines the x-coordinate of the reflection point of a characteristic with the bottom, given the characteristics previous intersection (to the left) with the surface.*

and from $\Psi(x, -h(x)) = 1$ follows that

$$a(x - h(x)/\omega) - a(x + h(x)/\omega) = 1. \tag{23}$$

The bottom topography being subcritical means that $|h'(x)/\omega| < 1$ where the prime denotes the derivative. This means that the arguments $\delta_\pm := x \pm h(x)/\omega$ in (23) are both strictly increasing and therefore invertible, so (23) can be rewritten as the functional equation

$$a(T(x)) = a(x) + 1 \tag{24}$$

with $T = \delta_+ \circ \delta_-^{-1}$ and $\delta_\pm(x) = x \pm h(x)/\omega$. This equation (24) is known as Abel's functional equation. See [7] for a general discussion of this functional equation and [1] for its application to internal wave problems. The map T takes a surface reflection point $(x, 0)$ of some characteristic to its next reflection point $(x', 0) = (T(x), 0)$ at the surface, which is to the right of x. This is illustrated in the sketch shown in figure (11).
Notice that if a is a solution to (24), then so is $a+P(a)$ for arbitrary periodic function P with period 1. This can be seen as taking an inhomogeneous solution a and a homogeneous solution $f = P \circ a$ with f satisfying the Schröder functional equation (18). Physically, the homogeneous part f is an internal mode of the domain, which is not dependent on a due to the freedom of choice for P.
If a is linear, then the streamfunction constructed from this function a is purely barotropic (see next section), which means that there are not internal waves (so also no internal mode). In general a solution a to (24) is not purely barotropic, meaning that it includes internal modes which are excited by the barotropic mode. Superimposed onto the internal modes excited by the barotropic mode there can be other internal modes. Due to the linearity of the problem there is no interaction between the internal modes. For the study of tidal conversion the focus lies on the internal modes generated by the barotropic mode, so in the following only $\Psi(x, z) = a(x + z/\omega) - a(x - z/\omega)$ with a linear on some suitable fundamental interval is considered. In this context a suitable fundamental interval is an interval which corresponds to a flat part of the bottom.

3.2 Tidal conversion in solution to Abel's functional equation

Scale the time such that $\omega = 1$[4] and let the domain of the fluid be horizontally infinitely wide with the bottom $z = -h(x)$ being flat in the limit: $h(x) \to 1$ as $x \to \pm\infty$. The stratified fluid lacks tidal conversion if the baroclinic part $\Psi' = \Psi(x, z) - \hat{\Psi}(x, z) = a(x+z) - a(x-z) - \frac{z}{h(x)}$ vanishes for $x \to \pm\infty$, which is equivalent to saying that the streamfunction becomes purely barotropic for $x \to \pm\infty$. Since $\lim_{x\to\pm\infty} h(x) = 1$ it follows that

$$\lim_{x\to\pm\infty} \Psi = \lim_{x\to\pm\infty} \hat{\Psi} = -z.$$

The solution a to Abel's functional equation must satisfy $a(x+z) - a(x-z) = -z$ in the limits, which means that $a(x)$ must approach the linear function $x/2 + c$ for arbitrary constant c. Things simplify if the irregularity is over an interval of finite length.

[4] Alternatively one can stretch the vertical or horizontal axis in order to get $\omega = 1$.

Finite support bottom irregularity

Lets assume that the irregularity in the bottom topography $z = -h(x)$ is over a finite interval $I \subset \mathbb{R}$ and $h(x) = 1$ for all $x \notin I$. For all $x > \sup(I) - 1$ and $x < \inf(I) - 1$ it then follows that $T(x) = x + 2$. See figure (11) for an illustration of why $x > \sup(I) - 1$ and $x < \inf(I) - 1$ are the appropriate bounds for the rightward map T for $\omega = 1$. It's inverse (leftward) map, T^{-1} takes the form $T^{-1}(x) = x - 2$ for $x \notin [\inf(I) + 1, \sup(I) + 1]$. The fluid lacks tidal conversion (for $\omega = 1$) if

$$T^N(x) = x + 2N + c \tag{25}$$

for all $x \in (T^{-1}(\inf(I)), \inf(I)]$ (a fundamental interval), c an arbitrary constant and $N \in \mathbb{N}$ equal or larger than the minimum number of reflections of a characteristic at the irregular part of the bottom. An upper bound N^* for the number of reflections of a characteristic at the irregular part of the bottom can be found by taking

$$N^* = \frac{(\lceil \sup(I) - \inf(I) \rceil)}{\min\limits_{x \in I}(h(x))},$$

where $\lceil ... \rceil$ denotes the ceiling. If $T(x) = x + 2$, then $a(x) = x/2 + c$ for arbitrary constant c is a solution to $a(T(x)) = a(x) + 1$.

Conjecture: Let $\mathbf{H}$ be the space of all continuous bottom functions $h : \mathbb{R} \to \mathbb{R}^+$ with the properties $h(x) = 1$ for all $|x| > L > 0$ for some constant L and such that $x \pm h(x)$ are invertible. It is conjectured that the Lebesque measure of the subset $\mathbf{H}_0 \subset \mathbf{H}$ of functions h which lead to a map T with property (25) is zero.

If this conjecture holds, then this means that it is unlikely (with probability zero) to encounter a bottom topography which lacks tidal conversion, assuming that bottom topographies that one can encounter in a two-dimensional ocean are arbitrarily distributed and belong to $\mathbf{H}$.

One can construct bottom functions $h(x)$ such that the corresponding map T fulfils (25) for some $N \in \mathbb{N}$. This is done in subsection (3.4). Alternatively one can start with a function a which becomes linear with slope $1/2$ in the limits $x \to \pm\infty$. This leads to bottom topographies which are a priori not known. It is possible that $a(x + h(x)) = a(x - h(x)) + 1$ for given function a cannot be solved analytically. In that case it is not possible to determine the bottom topography $z = -h(x)$ which lacks tidal conversion.
In order to end up with a finite support bottom topography lacking tidal conversion one has to start with a function $a(x)$ which becomes linear with slope $1/2$ for all values above and below some maximum and minimum x-value.
In the following section (3.3.1) a known exact solution a to $a(x + h(x)) = a(x - h(x)) + 1$ for given $h(x)$ is analysed and put into context with tidal conversion.

3.3 Tidal conversion in Law's exact solution

In [8], Law presents an exact solution to the functional equation

$$R(x + h(x)) = R(x - h(x)) + 2 \tag{26}$$

for

$$\begin{aligned} h(x) &= L_0 \qquad \text{for } x \leq 0 \\ h(x) &= L_0 + \frac{L_0}{2\pi}\left(\sin^{-1}\left[\sin\theta\cos\frac{2\pi x}{L_0}\right] - \theta\right) \qquad \text{for } x > 0. \end{aligned} \tag{27}$$

Law's continuous exact solution[5]

$$\begin{aligned} R(x) &= \frac{x}{L_0} \qquad \text{for } x \leq L_0 \quad \text{and for all } n \in \mathbb{N} \\ R(x) &= -\frac{1}{\pi}\tan^{-1}\left(\cot\left(\frac{\pi}{L_0}x\right) - 2n\tan\theta\right) + 2n + \frac{1}{2} \quad \text{for } x \in (2nL_0 - L_0, 2nL_0] \\ R(x) &= -\frac{1}{\pi}\tan^{-1}\left(\cot\left(\frac{\pi}{L_0}x\right) - 2n\tan\theta\right) + 2n + \frac{3}{2} \quad \text{for } x \in (2nL_0, 2nL_0 + L_0] \end{aligned} \tag{28}$$

is not derived, but merely presented in [8]. A detailed derivation of the exact solution to (26), presented in the following subsection, gives insight into possible adjustments on $h(x)$ for which exact solutions can be constructed as well. This allows the construction of exact baroclinic (internal wave) streamfunctions Ψ' due to barotropic tidal forcing $\hat{\Psi} = -z/h(x)$ for infinitely many different near-harmonic bottom topographies $z = -h(x)$ lacking tidal conversion (section (3.3.2)).

3.3.1 Construction of Law's exact solution

Here a detailed derivation of the exact solution (28) is presented. Lets start with the trivial relation

$$2\frac{\sin\theta}{\cos\theta} = 2\tan\theta.$$

Multiplying the numerator and the denominator of the left hand side by $\cos\theta\cos\frac{2\pi x}{L_0} - \cos\left(\sin^{-1}(\sin\theta\cos\frac{2\pi x}{L_0})\right)$ gives

$$2\frac{\sin\theta\cos\theta\cos\frac{2\pi x}{L_0} - \sin\theta\cos\left(\sin^{-1}(\sin\theta\cos\frac{2\pi x}{L_0})\right)}{\cos^2\theta\cos\frac{2\pi x}{L_0} - \cos\theta\cos\left(\sin^{-1}(\sin\theta\cos\frac{2\pi x}{L_0})\right)} = 2\tan\theta.$$

Using $\cos^2\theta = 1 - \sin^2\theta$ in the denominator, structuring the expression by introducing $a := \sin^{-1}(\sin\theta\cos\frac{2\pi x}{L_0})$ and applying $\sin\theta\cos\frac{2\pi x}{L_0} = \sin a$ twice gives

$$2\frac{\cos\theta\sin a - \sin\theta\cos a}{\cos\frac{2\pi x}{L_0} - \cos\theta\cos a - \sin\theta\sin a} = 2\tan\theta.$$

The purpose of the restructuring is to make use of $\sin a\cos\theta - \cos a\sin\theta = \sin(a-\theta)$ and $\cos a\cos\theta + \sin a\sin\theta = \cos(a-\theta)$ to get

$$\frac{-2\sin(\theta - a)}{\cos\frac{2\pi x}{L_0} - \cos(\theta - a)} = 2\tan\theta. \tag{29}$$

[5]Notice that the solution presented here differs from the solution presented in [8] by a constant factor 1 if $x \in (2nL_0, 2nL_0 + L_0]$. This is to make the resulting solution $R(x)$ continuous.

A known trigonometric identity (see derivation in appendix E, section (5.5)) is

$$\cot\left(\frac{\alpha-\beta}{2}\right)-\cot\left(\frac{\alpha+\beta}{2}\right)=\frac{-2\sin\beta}{\cos\alpha-\cos\beta}. \tag{30}$$

Applying this relation to (29) with $\alpha=\frac{2\pi x}{L_0}$ and $\beta=\theta-a$ gives

$$\cot\left(\frac{\frac{2\pi x}{L_0}-(\theta-a)}{2}\right)-\cot\left(\frac{\frac{2\pi x}{L_0}+\theta-a}{2}\right)=2\tan\theta. \tag{31}$$

Notice that from (27) for $x>0$ and the definition of a it follows that $h(x)=L_0\left(1+\frac{1}{2\pi}(a-\theta)\right)=L_0\left(1-\frac{\beta}{2\pi}\right)$ and cot is π-periodic. Using this gives

$$\cot\left(\frac{\frac{2\pi x}{L_0}\pm(\theta-a)}{2}\right)=\cot\left(\frac{\pi}{L_0}(x\pm(L_0-h(x)))\right)=\cot\left(\frac{\pi}{L_0}(x\mp h(x))\right).$$

So from (31) follows

$$\cot\left(\frac{\pi}{L_0}(x+h(x))\right)-\cot\left(\frac{\pi}{L_0}(x-h(x))\right)=2\tan\theta. \tag{32}$$

Adding $\cot\left(\frac{\pi}{L_0}(x-h(x))\right)-(2n+2)\tan\theta$ to (32) and taking $\tan^{-1}$ gives

$$\tan^{-1}\left(\cot\left(\frac{\pi}{L_0}(x+h(x))\right)-2(n+1)\tan\theta\right)=\tan^{-1}\left(\cot\left(\frac{\pi}{L_0}(x-h(x))\right)-2n\tan\theta\right). \tag{33}$$

In the following the equation (33) is used to derive $R(x)$ for $x>L_0$, given that $R(x)=\frac{x}{L_0}$ for $x\le L_0$. This is done by induction on n.
Lets start with the induction basis. Take $x^*\in(0,2L_0]$ and notice that by definition (27) h is strictly increasing and $h(nL_0)=L_0$ for all $n\in\mathbb{N}$. So the function $\delta_+(x^*)=x^*+h(x^*)$ maps the interval $(0,2L_0]$ bijectively onto $(L_0,3L_0]$ while $\delta_-(x^*)=x^*-h(x^*)$ maps it bijectively onto $(-L_0,L_0]$, an interval for which R is prescribed. Here the new variable x^* is used only if $\delta_\pm$ is involved. In the following it is related to x either by $x=\delta_+(x^*)$ or $x=\delta_-(x^*)$, both of which are bijective transformation.
By (26) it must hold that $R(\delta_+(x^*))-2=R(\delta_-(x^*))$ for all $x^*\in\mathbb{R}$, so

$$R(\delta_+(x^*))-2=R(\delta_-(x^*))=\frac{x^*-h(x^*)}{L_0}\quad\text{for } x^*\in(0,2L_0]. \tag{34}$$

Upon multiplying (33) with $-\frac{1}{\pi}$ and then adding $\frac{1}{2}$ it coincides with the right hand side of (34). To see this be reminded that $-\tan^{-1}(x)+\frac{\pi}{2}=\cot^{-1}(x)$ for $x>0$. So for $n=0$ and $x^*\in(0,2L_0]$ the left hand side of (34) times $-\pi$ times must equal the left hand side of (33) minus $\frac{1}{2}$:

$$-\pi(R(\delta_+(x^*))-2)=\tan^{-1}\left(\cot\left(\frac{\pi}{L_0}\delta_+(x^*)\right)-2\tan\theta\right)-\frac{\pi}{2}\quad\text{for } x^*\in(0,2L_0].$$

Replacing $\delta_+(x^*)$ for $x^*\in(0,2L_0]$ by $x\in(L_0,3L_0]$, dividing by $-\pi$ and adding 2 gives

$$R(x) = 2 + \frac{1}{2} + c - \frac{1}{\pi}\tan^{-1}\left(\cot\left(\frac{\pi}{L_0}x\right) - 2\tan\theta\right) \text{ for } x \in (L_0, 3L_0].$$

The undetermined constant term $c \in \mathbb{R}$ appears because the functional equation $R(\delta_+(x^*)) = R(\delta_-(x^*)) + 2$ prescribes $R(x)$ for $x \in (L_0, 3L_0]$ only up to a constant. Requiring R to be continuous (which gives a unique solution once prescribed on some fundamental interval) gives $c = 0$ for $x \in (L_0, 2L_0]$ and $c = 1$ for $x \in (2L_0, 3L_0]$.

Lets now assume that $R(x)$ is known for $x \in (2nL_0 - L_0, 2nL_0 + L_0]$ as given in (28) for arbitrary $n \in \mathbb{N}$ and derive $R(x)$ for $x \in (2(n+1)L_0 - L_0, 2(n+1)L_0 + L_0]$ (induction step). For simplicity only the derivation of R on the first half of the interval is worked out, as the second part is similar.
On $(2nL_0 - L_0, 2nL_0]$ the function R is given by

$$R(x) = 2n + \frac{1}{2} - \frac{1}{\pi}\tan^{-1}\left(\cot\left(\frac{\pi}{L_0}x\right) - 2n\tan\theta\right). \tag{35}$$

Replacing $x \in (2nL_0 - L_0, 2nL_0]$ by $\delta_-(x^*)$ for $x^* \in (2nL_0, 2nL_0 + L_0]$ gives

$$R(\delta_-(x^*)) = 2n + \frac{1}{2} - \frac{1}{\pi}\tan^{-1}\left(\cot\left(\frac{\pi}{L_0}\delta_-(x^*)\right) - 2n\tan\theta\right).$$

By equation (33) (multiplying it with $-\frac{1}{\pi}$ and adding $2n + \frac{1}{2}$) the right hand side is equal to

$$R((\delta_-(x^*)) = 2n + \frac{1}{2} - \frac{1}{\pi}\tan^{-1}\left(\cot\left(\frac{\pi}{L_0}\delta_+(x^*)\right) - 2(n+1)\tan\theta\right)$$

and by the functional equation $R(\delta_+(x^*)) = R(\delta_-(x^*)) + 2$ it follows that

$$R(\delta_+(x^*)) = 2 + 2n + \frac{1}{2} - \frac{1}{\pi}\tan^{-1}\left(\cot\left(\frac{\pi}{L_0}\delta_+(x^*)\right) - 2(n+1)\tan\theta\right).$$

When substituting $x \in (2nL_0 + L_0, 2(n+1)L_0]$ for $\delta_+(x^*)$ with $x^* \in (2nL_0, 2nL_0 + L_0]$ one gets

$$R(x) = 2(n+1) + \frac{1}{2} + c - \frac{1}{\pi}\tan^{-1}\left(\cot\left(\frac{\pi}{L_0}x\right) - 2(n+1)\tan\theta\right) \tag{36}$$

where the arbitrary constant c must be zero to have continuity at $x = 2L_0 + L_0$.
This shows that $R(x)$ as defined in (28) is the unique continuous solution satisfying the functional equation (26) for $h(x)$ as defined in (27).
In the following section (3.3.2) adjustments to h are suggested, such that one can also solve for R easily by a similar iterative prescription. In order to understand the solution procedure in the following section it is worth noticing the two differences between $R(x)$ and $R(x + 2L_0)$ for $x \in (2nL_0 - L_0, 2nL_0]$ and any $n \in \mathbb{N}$. The first difference is the constant term, which is a magnitude 2 larger in $R(x+2L_0)$, see (36), compared to $R(x)$, shown in (35). Secondly the factor of $\tan\theta$ inside the $\tan^{-1}$-term is increased by 2. These are the only two differences between $R(x + 2L_0)$ and $R(x)$.

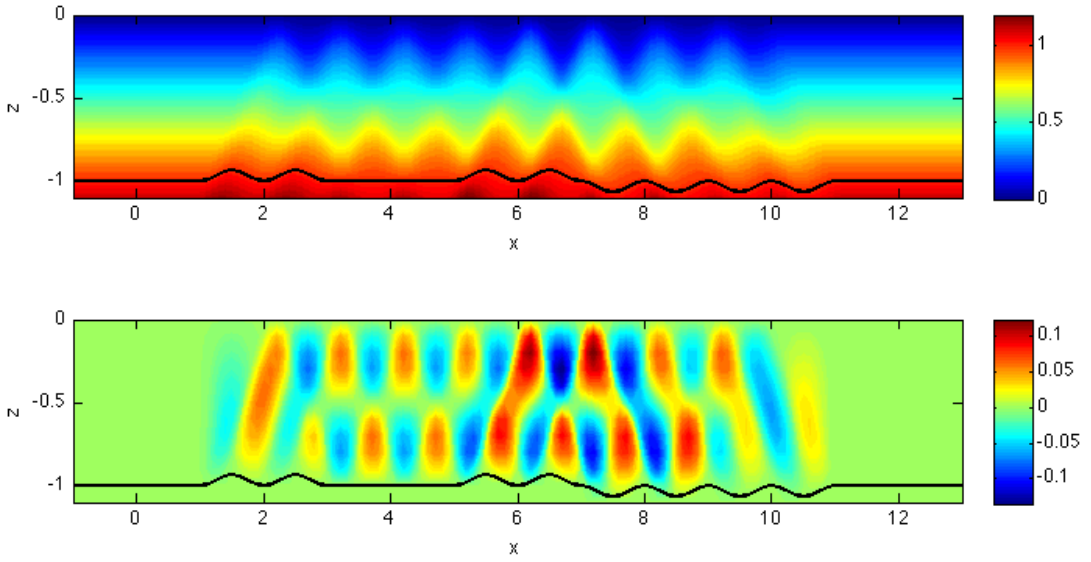

Figure 12: *The upper plot shows the streamfunction* $\Psi(x,z) = \frac{1}{2}(R(x-z) - R(x+z))$ *with* R *as given in (38), for* $S_+ = \{0,2\}$, $S_- = \{3,4\}$, $\theta = 0.2$ *and* $L_0 = 1$. *Its baroclinic component* $\Psi'(x,z) = \Psi(x,z) - (-z/h(x))$ *is shown in the bottom plot. It is clear that there are no internal waves (= baroclinic part is constant) outside the irregular part of the bottom domain. Notice also that the baroclinic part is zero on the bottom* $z = -h(x)$ *(black line), with* $h(x)$ *is defined by (37) for* $S_+ = \{0,2\}$, $S_- = \{3,4\}$ *and* $\theta = 0.2$. *Values below the bottom are set to zero.*

3.3.2 Solutions for different bottom topographies

The aim is to construct baroclinic streamfunction $\Psi'(x,z)$ for infinitely many bottom topographies which lack tidal conversion. The solution procedure from the previous part is adapted to find solutions R to (26) for all bottom topographies

$$
\begin{aligned}
h(x) &= L_0 \qquad \text{for } x \le 0 \text{ and for } x \in ((n+1)L_0, (n+3)L_0] \text{ if } n \in S_0 \\
h(x) &= L_0 + \frac{L_0}{2\pi}\left(\sin^{-1}\left[\sin\theta\cos\frac{2\pi x}{L_0}\right] - \theta\right) \qquad \text{for } x \in ((n+1)L_0, (n+3)L_0] \text{ if } n \in S_+ \\
h(x) &= L_0 - \frac{L_0}{2\pi}\left(\sin^{-1}\left[\sin\theta\cos\frac{2\pi x}{L_0}\right] - \theta\right) \qquad \text{for } x \in ((n+1)L_0, (n+3)L_0] \text{ if } n \in S_-
\end{aligned}
\tag{37}
$$

where the index sets S_+, S_- and S_0 are disjunct subsets of $\mathbb{N}_0$ with $S_+ \cup S_- \cup S_0 = \mathbb{N}_0$, e.g. every index $n \in \mathbb{N}_0$ is in precisely one of the three index sets. Topologically one can interpret S_+ as the collection of ridges (each integer corresponds to a pair of ridges) and S_- as the collection of troughs. See figure (12) for the topography with $S_+ = \{0,2\}$, $S_- = \{3,4\}$.

For any $h(x)$ as given in (37) one can construct $R(x)$ satisfying the functional equation (26) iteratively, similar to the procedure followed in the previous part. This

means that we assume R to be known on some interval $((2n-2)L_0,(2n-1)L_0]$ for any $n \in \mathbb{N}$ and use this to calculate R on $(2nL_0,(2n+1)L_0]$ (induction step). Again we do not consider the intermediate intervals $((2n-1)L_0,(2n)L_0]$ because the calculation is almost identical. The induction basis is left to the reader, as it is the same as in the previous part when $1 \in S_+$, similar when $1 \in S_-$ and trivial when $1 \in S_0$.
Lets assume that

$$R(x) = -\frac{1}{\pi}\tan^{-1}\left(\cot\left(\frac{\pi}{L_0}x\right) - 2k\tan\theta\right) + m + \frac{1}{2} \quad \text{for } x \in ((2n-2)L_0,(2n-1)L_0], \tag{38}$$

for some $m,k \in \mathbb{Z}$. At this point it is not clear that R has to be of this form for some k and m. After the calculation of R on $(2nL_0,(2n+1)L_0]$ it will be justified that R must be of the form (38).
There are three cases:
Case 1: if $n \in S_0$, then R on $(2nL_0,(2n+1)L_0]$ is identical (upon adding a constant to guarantee continuity) to R on $((2n-2)L_0,(2n-1)L_0]$.
Case 2: if $n \in S_+$, then R on $(2nL_0,(2n+1)L_0]$ is defined from R on $((2n-2)L_0,(2n-1)L_0]$ as described above in section (3.3.1). This means that m becomes $m+2$ and $2k$ is replaces by $2k+2$.
Case 3: if $n \in S_-$ then one can use (33) to find that

$$R(x) = -\frac{1}{\pi}\tan^{-1}\left(\cot\left(\frac{\pi}{L_0}x\right) - 2(k-1)\tan\theta\right) + m + 2 + \frac{1}{2} \quad \text{for } x \in (2nL_0,(2n+1)L_0].$$

To summarize the three cases: In all cases m becomes $m+2$. This is to make the resulting function R continuous. If $n \in S_0$, corresponding to a flat bottom $h(x)$ for $x \in ((2n-1)L_0,2nL_0]$, then k stays constant. A ridge, corresponding to $n \in S_+$, leads to an increase of k by 2 and a trough, $n \in S_-$, transforms k to $k-2$.

It remains to be shown that R is of the form (38). Starting out with $R(x) = \frac{x}{L_0}$ for $x < L_0$ one gets

$$R(x) = -\frac{1}{\pi}\tan^{-1}\left(\cot\left(\frac{\pi}{L_0}x\right) - 2n\tan\theta\right) + 2 + \frac{1}{2} \quad \text{for } x \in (2L_0,3L_0].$$

In each iterative step for the prescription of R the constant 2 is added to the expression for R, meaning that $m = n$ in (38). The factor of $\tan\theta$ is increased by 2 during each iterative step when $n \in S_+$ and decreased by 2 when $n \in S_-$. This means that in (38) $2k$ takes any even integer value between $-2n$ and $2n$. This justifies the assumption that R takes the form (38) on $((2n-2)L_0,(2n-1)L_0]$.
If the factor of $\tan\theta$ is zero on some interval, then the expression for R becomes $R(x) = \frac{x}{L_0}$ on this interval. Be reminded that a topography lacks tidal conversion if the solution to the Abel functional equation becomes linear for $x \to \pm\infty$ (see section (3.1)). Be also reminded that the Abel functional equation is derived from a functional equation of the form (26), so the result from subsection (3.1) also applies the solution R satisfying (26). It is easy to check that if

$$|S_+| = |S_-| < \infty, \tag{39}$$

then there exists some N (largest element in $S_+ \cup S_-$) such that $R(x) = \frac{x}{L_0}$ for all $x > (N+1)L_0$. This means that if (39) is satisfied, then the topography generated

by S_+ and S_- according to (37) lacks tidal conversion.
It is easy to see that there are countable infinite many sets $S_+, S_- \subset \mathbb{N}$ which lead to a bottom topography $z = -h(x)$ lacking tidal conversion. This means that the presented method allows to explicitly construct countably infinitly many exact velocity fields for tides over near-harmonic bottom topographies which lack tidal conversion.
Baroclinic streamfunctions $\Psi'(x,z)$ lacking tidal conversion due to barotropic forcing $\hat{\Psi}(x,z) = -z/h(x)$ are given by $\Psi'(x,z) = \Psi(x,z) - \hat{\Psi}(x,z) = \frac{1}{2}(R(x-z) - R(x+z)) + z/h(x)$. In figure (12) the streamfunction $\Psi(x,z) = \frac{1}{2}(R(x-z) - R(x+z))$ and its baroclinic part $\Psi'(x,z)$ are shown for $\theta = 0.2$ and $L_0 = 1$.
The construction of the topographies lacking tidal conversion relies on the observation that the internal wave field generated by barotropic flow over a pair of ridges, defined by (37) for $n \in S_+$, is exactly opposed by the internal wave field generated by barotropic flow over a pair of troughs, defined by (37) for $n \in S_-$ (provided their distance is a multiple of $2L_0$). The linearity of the considered internal wave problem and the absence of diffusion make it possible that the cancellation of these two internal wave fields works over arbitrary distances and independent of the present of other non-trivial velocity fields.
The method for the construction of infinitely many topographies lacking tidal conversion works for any two subcritical bottom topography features with finite support (e.g. a ridge and a trough) such that the internal wave fields generated by these two topographies cancel out. It is of course also possible to combine different types of bottom topographies, provided each bottom topography has a counterpart which cancels its internal wave velocity field.
Instead of taking pairs of ridges and troughs as done for the topographies in (37) one could combined single ridges and troughs (rather than pairs) to generate topographies lacking tidal conversion.

3.4 A ridge which can lack tidal conversion

The ridge bottom topography h_s introduced in the following section lacks tidal conversion for a specific forcing frequency in the hydrostatic limit. This means that the forcing frequency ω is assumed to be much smaller than the Brunt-Väisälä frequency N. Time is scaled such that the specific forcing frequency for which no tidal conversion takes place has the value 1. The parameter s is a scale height for the irregular part of the bottom.
The goal is to determine the energy dissipation of the barotropic tide as a function of forcing frequency ω and bottom scale height s (subsection (3.4.6)).
The bottom topography $z = -h_s$, which lacks tidal conversion for $\omega = 1$, is introduced and constructed in the following subsection. For this bottom topography the map T in Abel's functional equation (24) is computed explicitly in subsection (3.4.2). This makes it possible to solve Abel's functional equation (24) explicitly for general ω, including $\omega = 1$. The resulting exact real-valued baroclinic streamfunction is used in subsection (3.4.6) to determine the energy dissipation of the barotropic tide. To justify the steps made in subsection (3.4.6) it is necessary to compute the full time-dependent streamfunction, which requires a complex-valued streamfunction which propagates energy away from the irregular part of the bottom topography. The complex extension of the streamfunction above the flat bottom is presented in subsection (3.4.4) and for the entire two-dimensional domain this is done numerically in subsection (3.4.5).

3.4.1 Construction of topography lacking tidal conversion

For $|x| > L_s$ where $L_s = \frac{3-s}{2}$ and $0 \leq s < 0.5$ the bottom function $h_s(x) = 1$ is assumed to be flat. For $|x| < l_s$ where $l_s = \frac{1-s}{2}$ the bottom is chosen to be flat as well, but with a different constant: $h_s(x) = 1 - s$. This leaves the two ranges $-L_s < x < -l_s$ and $l_s < x < L_s$ unspecified. Assuming subcritical conditions and $\omega = 1$ means that the wave beam (characteristic) which reflects at the bottom in $x = -L_s$ (where $z = -h_s(-L_s) = -1$) also reflects at the bottom at $x = l_s$, where $z = -h_s(l_s) = 1 - s$. Due to symmetry it follows that there is also a characteristic that reflects at both bottom points at $x = -l_s$ and $x = L_s$. So any wave beam which reflects at the bottom for some $x \in [-L_s, -l_s]$ also reflects at the bottom for some $x \in [l_s, L_s]$ (illustrated in figure (13)). To have no tidal conversion, focusing (defocusing) of characteristics taking place upon one of these two reflections has to be compensated by the other reflection. The goal is to find an easily invertible function h_s which is continuously differentiable everywhere when connected to the h_s as defined above for $|x| < l_s$ and $|x| > L_s$ and which lacks tidal conversion.
The simplest function which satisfies the above criteria is a piecewise quadratic function, denoted by $n_s(x)$ for $x \in [(L_s+l_s)/2, L_s]$ and $m_s(x)$ for $x \in [l_s, (L_s+l_s)/2]$ below. This leads to the bottom topography $z = -h_s(x)$ given by

$$\begin{aligned} h_s(x) &= 1 && \text{for } |x| > L_s \\ h_s(x) &= n_s(|x|) && \text{for } L_s > |x| > \frac{L_s + l_s}{2} \\ h_s(x) &= m_s(|x|) && \text{for } \frac{L_s + l_s}{2} > |x| > l \\ h_s(x) &= 1 - s && \text{for } l_s > |x| \end{aligned} \tag{40}$$

where $L_s = \frac{3-s}{2}$ and $l_s = \frac{1-s}{2}$ and

$$\begin{aligned} n_s(x) &= -2s(x - L_s)^2 + 1 \text{ and} \\ m_s(x) &= 2s(x - l_s)^2 + 1 - s \end{aligned} \tag{41}$$

Verify that $n(L) = 1$, $n'(L) = 0$, $n(\frac{L+l}{2}) = 1 - s/2 = m(\frac{L+l}{2})$, $m(l) = 1 - s$, $m'(l) = 0$ and $m'(\frac{L+l}{2}) = n'(\frac{L+l}{2})$, where the subscript s of n, m, l and L is dropped for notational convenience. So the bottom topography function h_s defined in (40) with n and m as in (41) is continuously differentiable. If the bottom topography is only continuous (but not continuously differentiable), then the corresponding stream-function is only continuous, giving rise to discontinuities in the velocity vectors. It is legitimate to have a discontinuous velocities because the fluid is assumed to be inviscid. However a discontinuous velocity field cannot be a good representation of a weakly viscous fluid and it therefore desirable to start with continuously differentiable bottom topographies.

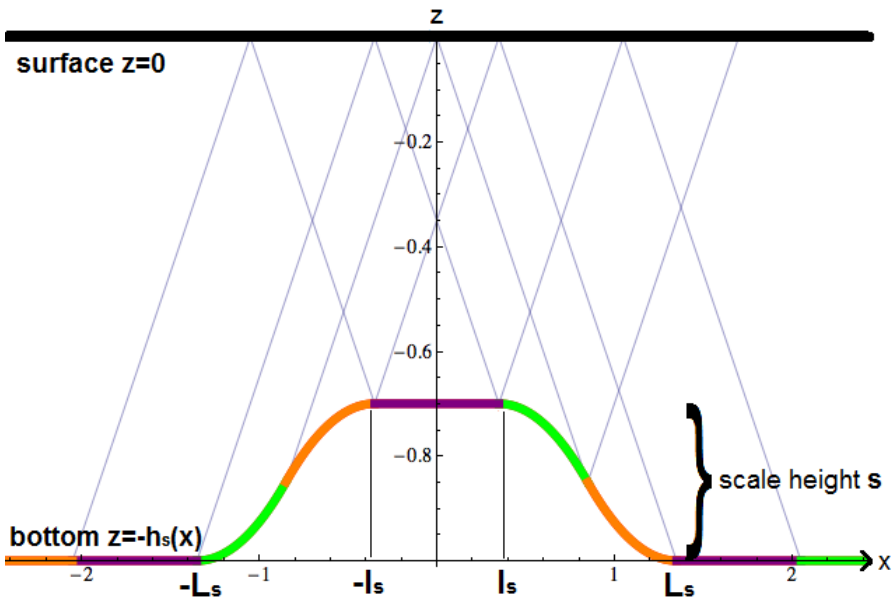

Figure 13: *This figure shows the bottom topography $z = -h_s(x)$ for s=0.3, (green, purple and orange), the surface $z = 0$ (black) and some characteristics (thin blue lines) for $\omega = 1$. Characteristics that are reflected at the green upward slope, $x \in [-L_s, -\frac{L_s+l_s}{2}]$, also reflect on the green downward sloping part, $x \in [l_s, \frac{L_s+l_s}{2}]$. If one reflection at the irregular part of the topography takes place on the orange part, $x \in [-\frac{L_s+l_s}{2}, -l_s]$, then the only other reflection is on the orange part $x \in [\frac{L_s+l_s}{2}, L_s]$. Focusing upon one of these two reflections on the irregular part of the bottom is exactly cancelled by defocusing upon the other reflection. Characteristics that are reflected on the purple parts of the bottom are nowhere focused or defocused, as they passed the irregular part of the bottom by only one reflection on $x \in [-l_s, l_s]$ (purple), where the bottom is flat.*

The function h_s cannot be piecewise linear because this does not lead to a continuously differentiable streamfunction.
The bottom topography defined by this function h_s is subcritical for $\omega = 1$ if $0 \leq s < \frac{1}{2}$. The figure (13) shows the bottom topography $z = -h_{0.3}(x)$ and some characteristics with $\omega = 1$. Notice that for $\omega < 1$ the bottom topography h_s is subcritical only if $0 < s < \frac{\omega}{2} < \frac{1}{2}$.

3.4.2 Forward map T

The map $T_{s,\omega} = \delta_{+_{s,\omega}} \circ \delta^{-1}_{-_{s,\omega}}$ and its inverse $T^{-1}_{s,\omega} = \delta_{-_{s,\omega}} \circ \delta^{-1}_{+_{s,\omega}}$, where $\delta_{\pm_{s,\omega}} = x \pm h_s(x)/\omega$, can now be constructed from the given bottom function h_s defined in (40). See section (3.1) for the purpose of why the construction of T is essential. Due to its extend the expressions for the inverses of $\delta_{\pm_{s,\omega}}$ are presented in the appendix G, section (5.7). The forward map T is defined by

$$\begin{aligned}
T_{s,\omega}(x) &= x + 2/\omega \qquad \text{for } |x + 1/\omega| > L \\
T_{s,\omega}(x) &= n_s(|\delta^{-1}_{-_{s,\omega}}(x)|)/\omega + \delta^{-1}_{-_{s,\omega}}(x) \\
&\qquad \text{for } L - 1/\omega \geq x > (L+l)/2 - (1-s/2)/\omega \\
&\qquad \text{and for } -(L+l)/2 - (1-s/2)/\omega \geq x > -L - 1/\omega \\
T_{s,\omega}(x) &= m_s(|\delta^{-1}_{-_{s,\omega}}(x)|)/\omega + \delta^{-1}_{-_{s,\omega}}(x) \\
&\qquad \text{for } -l - (1-s)/\omega > x \geq -(L+l)/2 - (1-s/2)/\omega \\
&\qquad \text{and for } (L+l)/2 - (1-s/2)/\omega \geq x > l - (1-s)\omega \\
T_{s,\omega}(x) &= x + 2(1-s)/\omega \qquad \text{for } -l - (1-s)/\omega \geq x \geq l - (1-s)/\omega.
\end{aligned} \tag{42}$$

Similarly the inverse $T^{-1}_{s,\omega}$ is given by

$$\begin{aligned}
T^{-1}_{s,\omega}(x) &= x - 2/\omega \qquad \text{for } |x - 1/\omega| > L \\
T^{-1}_{s,\omega}(x) &= n_s(|\delta^{-1}_{+_{s,\omega}}(x)|)/\omega + \delta^{-1}_{+_{s,\omega}}(x) \\
&\qquad \text{for } L + 1/\omega \geq x > (L+l)/2 + (1-s/2)/ \\
&\qquad \text{and for } -(L+l)/2 + (1-s/2)/\omega \geq x > -L + 1/\omega \\
T^{-1}_{s,\omega}(x) &= m_s(|\delta^{-1}_{+_{s,\omega}}(x)|)/\omega + \delta^{-1}_{+_{s,\omega}}(x) \\
&\qquad \text{for } -l + (1-s)/\omega > x \geq -(L+l)/2 + (1-s/2)/\omega \\
&\qquad \text{and for } (L+l)/2 + (1-s/2)/\omega \geq x > l + (1-s)\omega \\
T^{-1}_{s,\omega}(x) &= x - 2(1-s)/\omega \qquad \text{for } -l + (1-s)/\omega \geq x \geq l + (1-s)/\omega.
\end{aligned} \tag{43}$$

3.4.3 Construction of solution to Abel's functional equation

In this subsection a continuous solution to Abel's functional equation (23) for $T_{s,\omega}$ as given in (42) is constructed. The aim is to construct an odd solution $a_{s,\omega}$ such that the streamfunction $\Psi_{s,\omega}(x,z) = a_{s,\omega}(x - z/\omega) - a_{s,\omega}(x + z/\omega)$ is even in x. The streamfunction $\Psi_{s,\omega}(x,z)$ has to be even in x due to the symmetry of $h_s(x)$ in $x = 0$.
Notice that if $a_{s,\omega}(x)$ is a solution to $a_{s,\omega}(x - h_s(x)/\omega) - a_{s,\omega}(x + h_s(x)/\omega) = 1$ for all $x \in \mathbb{R}$, then $-a_{s,\omega}(-x)$ is a solution as well because $h_s(x)$ is an even function. So once a solution $a_{s,\omega}$ to (24) is found (which is not odd), one can easily construct an odd solution $b_{s,\omega}(x) = \frac{1}{2}(a_{s,\omega}(x) - a_{s,\omega}(-x))$.

Solution to Abel's functional equation for $\omega = 1$

The function $a_{s,1}(x)$ is assumed to be linear to the right of the irregular bottom topography. So without loss of generality one can assume $a_{s,1}(x) = (x+s)/2$ for $x > L-1$ because $T_{s,1}(x) = x+2$ for all $x > L-1 = l$ (the constant $s/2$ is added in order to make the resulting solution $a_{s,1}$ odd). Use is made of the algorithm presented in theorem 6 of Beckebanze and Keady, (2014): the function $T_{s,1}$ takes the interval $[-l, l)$ onto $[l, l+2)$, where $a_{s,1}$ is assumed to be linear. So for $x \in [-l, l)$, taking equation (23), one gets

$$\begin{aligned} a_{s,1}(x)+1 &= a_{s,1}(T_{s,1}(x)) = T_{s,1}(x)/2 + s/2 \\ &= \begin{cases} n_s(\delta^{-1}_{-_{s,1}}(x))/2 + \delta^{-1}_{-}(x)/2 + s/2 & \text{for } l \geq x \geq 0 \\ m_s(\delta^{-1}_{-_{s,1}}(x))/2 + \delta^{-1}_{-_{s,1}}(x)/2 + s/2 & \text{for } 0 \geq x \geq -l. \end{cases} \end{aligned}$$

The interval $[-l-2, -l)$ is mapped onto $[l, l+2)$ by $T^2_{s,1} = T_{s,1} \circ T_{s,1}$. The bottom function $h_s(x)$ is constructed such that for the specific forcing frequency $\omega = 1$ it holds that $T^2_{s,1}(x) = x + 2(1-s)$ for $x \in [-l-2, l)$. So for $-2-L \leq x < -l$ the solution $a_{s,1}$ to (24) is linear. It directly follows that then $a_{s,1}(x)$ is linear for all $x < -l$. Working out $n_s(\delta^{-1}_{-_{s,1}}(x))/2 + \delta^{-1}_{-_{s,1}}(x)/2 - 1 + s/2$ and $m_s(\delta^{-1}_{-_{s,1}}(x))/2 + \delta^{-1}_{-_{s,1}}(x)/2 - 1 + s/2$ gives

$$a_{s,1}(x) = \begin{cases} x/2 + s/2 & \text{for } x > l \\ \frac{-1+2s-2sx+\sqrt{1-4s+4s^2+8sx}}{4s} & \text{for } l \geq x \geq 0 \\ \frac{+1-2s-2sx-\sqrt{1-4s+4s^2-8sx}}{4s} & \text{for } 0 \geq x \geq -l \\ x/2 - s/2 & \text{for } x < -l. \end{cases} \tag{44}$$

From this solution $a_{s,1}$ (which is already odd) to Abel's functional equation the streamfunction $\Psi_1(x,z) = a_{s,1}(x-z) - a_{s,1}(x+z)$ is constructed. The bottom plot in figure (15) shows this streamfunction for $s = 0.2$. Its baroclinic part $\Psi'_{s,1}(x,z) = \Psi_{s,1}(x,z) - (-z/h_s(x))$ is shown in figure (16).

Solution to Abel's function equation for general ω

Lets now assume that $a_{s,\omega}(x) = (\omega/2)(x+s)$ is linear for all $x \geq L - 1/\omega$, which is the natural extension from $a_{s,1}(x) = (x+s)/2$ from the previous part. The function $T_{s,\omega}$ takes the interval $I_1 = [T^{-1}_{s,\omega}(L-1/\omega), L-1/\omega)$ onto $I_0 = [L-1/\omega, L+1/\omega)$, so for $x \in I_1$

$$a_{s,\omega}(x) = a_{s,\omega}(T_{s,\omega}(x)) - 1 = (\omega/2)(T_{s,\omega}(x)+s) - 1.$$

This is the first step of the algorithm presented in theorem 6 of Beckebanze and Keady, (2014), which can be used to define the solution $a_{s,\omega}$ iteratively for all $x < L - 1/\omega$: for some $x \in I_n = [T^{-n}(L-1/\omega), T^{-(n-1)}(L-1/\omega))$ the solution $a_{s,\omega}(x)$ is defined by

$$a_{s,\omega}(x) = (\omega/2)(T^n_{s,\omega}(x)+s) - n. \tag{45}$$

Be reminded that the function $T_{s,\omega}$ is linear with slope 1 for $x < -L - 1/\omega$ and $x > L - 1/\omega$. So one has to count the iterations N which are necessary to send

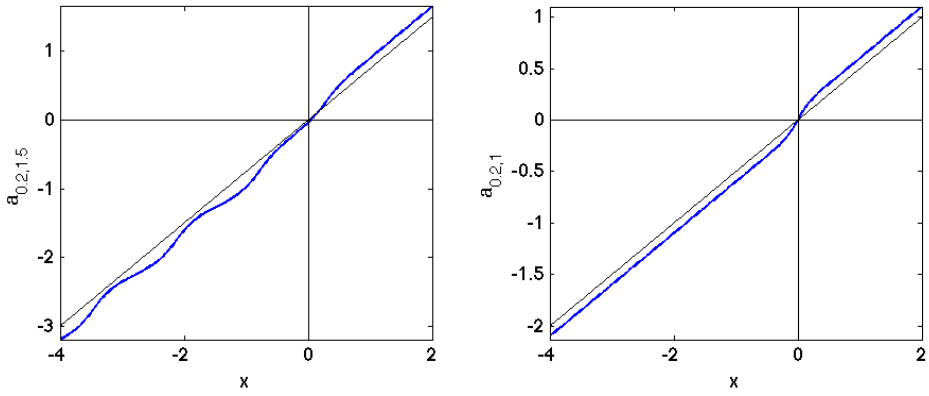

Figure 14: *The left plot shows a solution $a_{s,\omega}$ to Abel's functional equation (23) for $s = 0.2$, $\omega = 1.5$ and where $a(x) = (\omega/2)(x + s)$ is prescribed for $x \geq L - 1/\omega$. Upon subtracting the linear trend $\omega/2$ this solution $a_{s,\omega}(x)$ is periodic with period $2/\omega$ for all $x \leq -L-1/\omega$. The right plot shows the solution $a_{s,1}$, as expressed in (44). The diagonal black lines have slope $\omega/2$ and $1/2$ respectively.*

$L - 1/\omega$ with $T_{s,\omega}^{-1}$ to some value below $-L - 1/\omega$. For $\omega < 1$ this is $N = 2$. All values of $\omega > 1$ considered in the following subsections are such that $N \leq 4$. On the interval $[T_{s,\omega}^{-N}(L - 1/\omega), L - 1/\omega) = I_N \bigcup ... \bigcup I_1$ the solution $a_{s,\omega}$ is defined as in (45).
For $x < T_{s,\omega}^{-N}(L - 1/\omega) = min(I_N)$ the prescription of $a_{s,\omega}$ is simple:

$$a_{s,\omega}(x) = a_{s,\omega}(y) - m = (\omega/2)(T_{s,\omega}^{N}(y) + s) - n - m$$

where $y = x - (2/\omega)m$ for some $m \in \mathbb{N}$ such that $y \in I_N$. For all $x < T_{s,\omega}^{-(N-1)}(L - 1/\omega)$ the solution $a_{s,\omega}$ is periodic with period $2/\omega$ upon subtracting the linear trend $\omega/2$. This can be seen in the left plot of figure (14). In this plot one can also see that $a_{s,\omega}$ is clearly not odd for $\omega = 1.5$. This means that one has to construct an odd solution $b_{s,\omega}(x) = \frac{1}{2}(a_{s,\omega}(x) - a_{s,\omega}(-x))$ to (23) from $a_{s,\omega}$ as suggested in the beginning of the section. With this odd solution $b_{s,\omega}$ one can then compute the streamfunction $\Psi_{s,\omega}(x, z) = b_{s,\omega}(x - z/\omega) - b_{s,\omega}(x + z/\omega)$. This streamfunction $\Psi_{s,\omega}$ is shown in figure (15) for $\omega = 1.5$, 1.1 and 1 and $s = 0.2$. Its baroclinic component $\Psi'_{s,\omega} = \Psi_{s,\omega} - \bar{\Psi}$ for these parameter values is shown in figure (16). For $|x| > L$ the streamfunction $\Psi_{s,\omega}(x, z)$ as well as its baroclinic part $\Psi'_{s,\omega}(x, z)$ are periodic in its x-coordinate with period $2/\omega$.

3.4.4 Complex streamfunction above flat bottom topography

The goal is to construct a streamfunction $\bar{\Psi}_{s,\omega}$ such that its baroclinic part has an energy flux propagating away from the irregular bottom topography. Here the bar on $\Psi_{s,\omega}$ indicates that the streamfunction is complex-valued. This means that the real-valued streamfunction $\Psi_{s,\omega}(x, z) = b_{s,\omega}(x + z/\omega) - b_{s,\omega}(x - z/\omega)$, constructed as before, has to be extended with an imaginary part to facilitate propagation of

the internal wave.
In order to study the dissipation of energy from the barotropic mode $\hat{\Psi}_{s,\omega}$ to the baroclinic internal wave mode $\Psi'_{s,\omega}$ it makes sense to require tidal conversion to be the only energy source for internal waves. This means that there cannot be internal waves (transporting kinetic energy) travelling towards the irregularity of the bottom. So for $x > L$ the baroclinic streamfunction Ψ must facilitate propagation towards the right (away from the irregular part of the bottom), which can be expressed as

$$\bar{\Psi}'_{s,\omega}(x,z) = \sum_{n=1}^{\infty} \psi_n \sin(\pi n z) \exp(i\pi n \omega x) \qquad \text{for } x > L \tag{46}$$

for complex coefficients ψ_n. For notational convenience the dependency of ψ_n on s and ω is not expressed in a subscript. Notice that (46) satisfies the partial differential equation (22). Similarly for $x < -L$ the radiation condition requires the energy to propagate in opposite direction, so the sign of the argument of the x-dependent

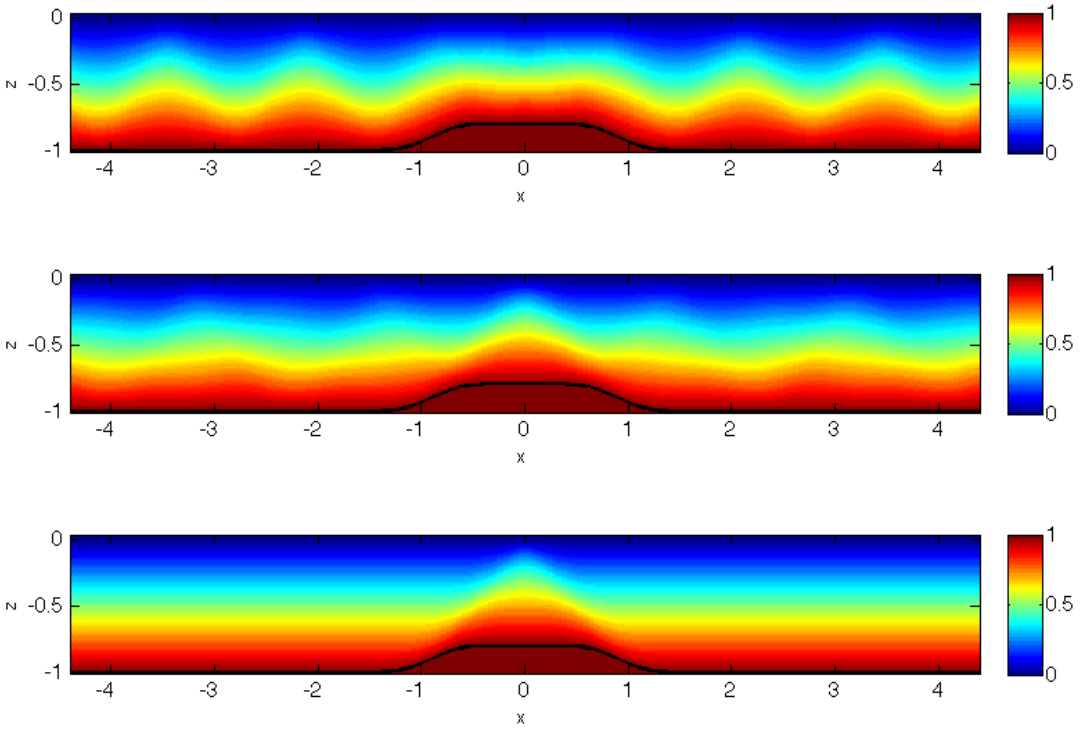

Figure 15: *This figure shows the analytical streamfunction solutions* $\Psi_{s,\omega}(x,z) = b_{s,\omega}(x + z/\omega) - b_{s,\omega}(x - z/\omega)$ *where* $b_{s,\omega}(x) = \frac{1}{2}(a_{s,\omega}(x) - a_{s,\omega}(-x))$ *and* $a_{s,\omega}$ *constructed in the previous subsection, satisfies the boundary conditions* $\Psi_{s,\omega}(x,0) = 0$ *and* $\Psi_{s,\omega}(x,-h_s(x)) = 1$. *The top plot shows* $\Psi_{s,\omega}$ *for* $s = 0.2$ *and* $\omega = 1.5$ *(with* $a_{0.2,1.5}$ *also shown in figure (14)), the middle plots presents* $\Psi_{s,\omega}$ *for* $s = 0.2$ *and* $\omega = 1.1$ *and the bottom plot shows the streamfunction* $\Psi_{s,\omega}$ *for* $s = 0.2$ *and the specific forcing frequency* $\omega = 1$, *which lacks tidal conversion.*

exponential changes. See [2] and [4] for a detailed discussion of why this condition corresponds to energy transportation away from the irregular bottom topography. Only the energy propagation for $x > L$ is considered in the following.
Be reminded that above the flat bottom $z = -1$ the real-valued baroclinic streamfunction

$$\Psi'_{s,\omega}(x,z) = b_{s,\omega}(x + z/\omega) - b_{s,\omega}(x - z/\omega) - \frac{z}{h_s(x)} \tag{47}$$

vanishes at $z = 0$ and $z = -1$ for all $x \in [L, \infty)$ and has $2/\omega$-periodicity in the x-coordinate. This means that for $(x, z) \in [L, \infty] \times [-1, 0]$ one can project $\Psi'_{s,\omega}(x, z)$

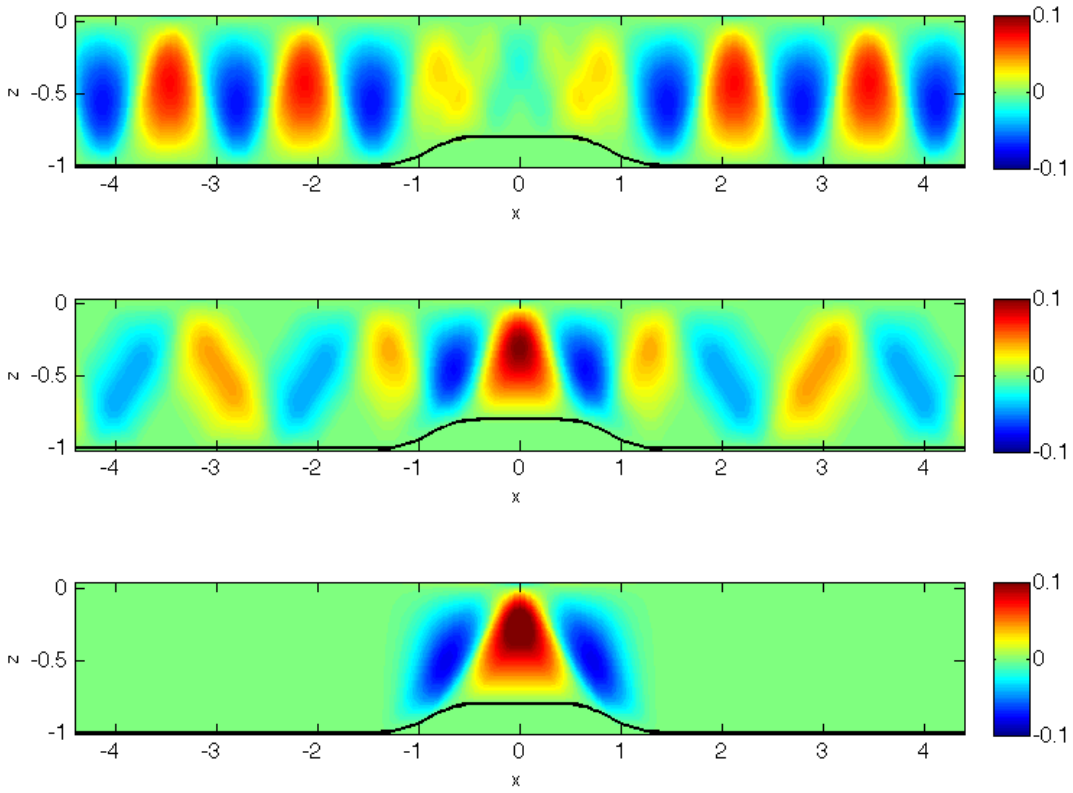

Figure 16: *This figure shows the baroclinic mode* $\Psi'_{0.2,\omega}(x,z) = \Psi_{0.2,\omega}(x,z) - z/h_s(x)$ *where* $\Psi_{0.2,\omega}(x,z) = b_{0.2,\omega}(x + z/\omega) - b_{0.2,\omega}(x - z/\omega)$ *and* $b_{0.2,\omega}(q) = (a_{0.2,\omega}(q) - a_{0.2,\omega}(-q))/2$ *for* $\omega = 1.5$ *(top),* $\omega = 1.1$ *(middle) and* $\omega = 1$*. The bottom* $z = -h_s(x)$ *and the surface* $z = 0$ *are indicated by the black lines. Notice that for* $\omega = 1$ *the baroclinic mode is constant to the right and left of the irregular bottom topography, indicating that there are no internal waves propagating away from the irregular part of the bottom (no tidal conversion). Notice also that the color scale goes from -0.1 to 0.1 only. This shows that the baroclinic part in the streamfunction* $\Psi_{s,\omega}(x,z)$*, which itself takes values between 0 and 1, is small.*

onto the modes $\sin(\pi nz)\cos(\pi nx\omega)$ and $\sin(\pi nz)\sin(\pi nx\omega)$:

$$\Psi'_{s,\omega}(x,z) = \sum_{n=1}^{\infty} \left(\psi_{1,n}\sin(\pi nz)\cos(\pi nx/\omega) + \psi_{2,n}\sin(\pi nz)\sin(\pi nx/\omega)\right).$$

The Fourier coefficients $\psi_{1,n}$ and $\psi_{2,n}$ for $n \in \mathbb{N}$ can be calculated by inverse Fourier transformation from $\Psi'_{s,\omega}(x,z)$ as given on $[L, L+2/\omega] \times [-1,0]$ according to (47). Notice that this can be done exact as (47) is analytic[6]. Using the complex-valued coefficients defined by

$$\psi_n := \psi_{1,n} - i\psi_{2,n} \quad \text{for all } n \in \mathbb{N}$$

[6]In practice it turns out to be more efficient to calculate $\psi_{1,n}$ and $\psi_{2,n}$ numerically as the integrals for the coefficients have to be split over many different subintervals, making the analytical work extremely time-consuming.

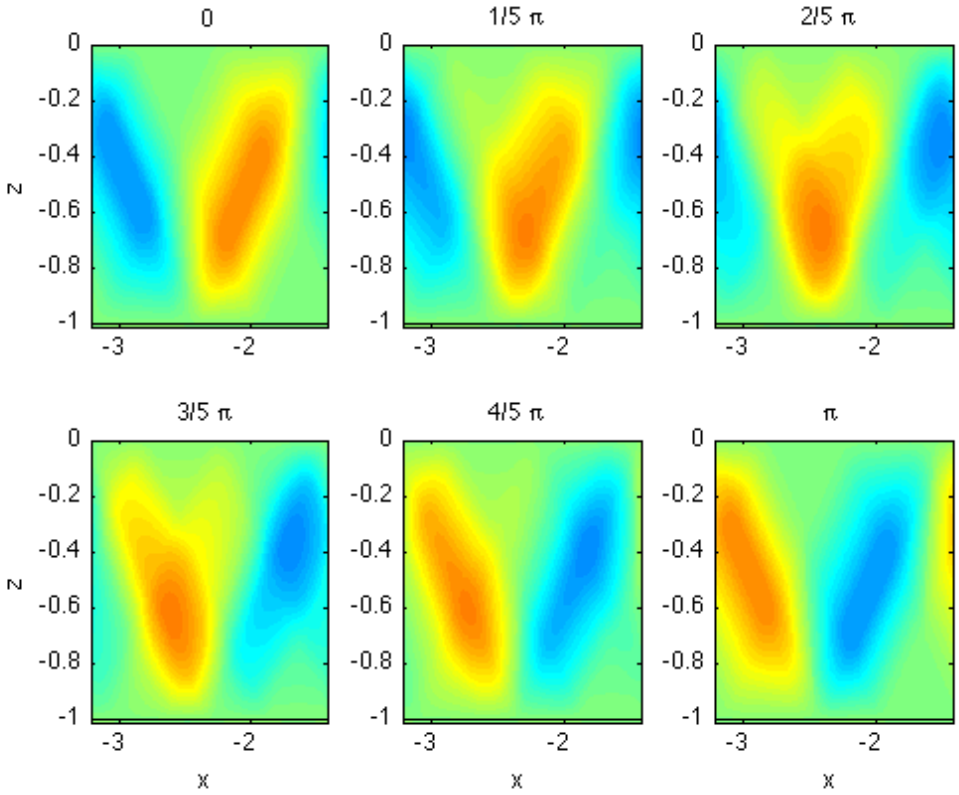

Figure 17: *This figure shows the same six snapshots as in figure (18), but focused on the region to the left of the irregular bottom topography. One can see that over time the internal waves propagate to the left, thereby transporting kinetic energy away from the region of irregular part of the bottom topography. The color bar is the same as in figure (16), which ranges from -0.1 to 0.1.*

in equations (46) makes $\bar{\Psi}'_{s,\omega}(x,z)$ a natural extension of $\Psi'_{s,\omega}(x,z)$ because

$$\Re(\bar{\Psi}'_{s,\omega}(x,z)) = \Re\left(\sum_{n=1}^{\infty}(\psi_{1,n} - i\psi_{2,n})\sin(\pi n\omega z)\exp(i\pi nx)\right) = \Psi'_{s,\omega}(x,z).$$

By construction the complex baroclinic streamfunction $\bar{\Psi}'_{s,\omega}(x,z)$ satisfies the radiation condition. By changing the sign in the x-dependent argument in (46) the real-valued baroclinic streamfunction $\Psi'_{s,\omega}(x,z)$ can also be extended to $(x,z) \in (-\infty,-L]\times[-1,0]$.
A time-series of the real part of the time-dependent baroclinic streamfunction[7]

$$\Psi'_{s,\omega}(x,z,t) = \bar{\Psi}'_{s,\omega}(x,z)e^{-i\omega t} \tag{48}$$

to the left of the irregular bottom ($x < -L_{0.2} = -1.4$) is show in figure (17). The six snapshots over half a period π/ω show that the internal wave perturbation is moving to the left, away from the irregular bottom, transporting kinetic energy with it.
In subsection (3.4.6) the kinetic energy radiated away from the irregular bottom part is calculated and its dependence on the forcing frequency ω and scale height s is analysed.
Above the irregular bottom topography the extension of the real streamfunction to the complex streamfunction as prescribed above does not work. The reason is that the modes $\sin(\pi nz)\cos(\pi nx)$ and $\sin(\pi nz)\sin(\pi nx)$ for $n \in \mathbb{N}$ do not form a basis of $\Psi'(x,z)$ any more, as $\Psi'(x,-1) \neq 0$ for x in the range of the irregular bottom topography.

It is desirable to have a time-dependent streamfunction on the entire spatial domain. To this end an unpublished method by Maas and Harlander, which gives exact expressions for the streamfunction on a chosen grid, is implemented. This is described in the following subsection.

3.4.5 Complex streamfunction above irregular bottom topography

In order to extend the streamfunction to an imaginary part, such that its real part after multiplication with $e^{-i\omega t}$ is time-dependent, a method by Maas and Harlander ([12], unpublished) is used. This method is described in the following.

The method by Maas and Harlander requires a topography which lacks tidal conversion. Here this topography is given by h_{s_0} for some $s_0 \in (0, 0.5)$ (which is not known a priori) with h_{s_0} given by (40). By construction h_{s_0} lacks tidal conversion for $\omega = 1$ and all $s_0 \in (0, 0.5)$. The goal is the determine the complex-valued streamfunction $\bar{\Psi}_{s,\omega}(x,z,t)$ above the bottom topography h_s for some chosen parameter values $\omega \neq 1$ and $s \in (0, \omega/2)$.
The crux of the method is to start with the exact streamfunction $\Psi_{s_0,1}(x,z) = a_{s_0,1}(x-z) - a_{s_0,1}(x+z)$ for $\omega = 1$ with topography $z = -h_{s_0}(x)$, lacking tidal

[7] All time-dependent streamfunctions in this and the following section are complex-valued. The bar on top of the streamfunction is therefore dropped if time-dependency is explicitly expressed

conversion for $\omega = 1$ and to find some residual streamfunction

$$\tilde{\Psi}_{s,\omega} = \bar{\Psi}_{s,\omega} - \Psi_{s_0,1}$$

such that $\Re(\bar{\Psi}_{s,\omega}(x,0)) = 0$ and $\Re(\bar{\Psi}_{s,\omega}(x,-h_s(x))) = 1$. Once complex-valued $\tilde{\Psi}_{s,\omega}$ is calculated, one can determine $\bar{\Psi}_{s,\omega}$. The task is to find a suitable $s_0 \in (0, 0.5)$, which depends on s and ω, such that $\tilde{\Psi}_{s,\omega}$ can be calculated.
Notice that the residual streamfunction $\tilde{\Psi}_{s,\omega}$ also satisfies the partial differential equation (22) and from $\tilde{\Psi}_{s,\omega}(x,0) = \bar{\Psi}_{s,\omega}(x,0) - \Psi_{s_0,1}(x,0) = 0 - 0 = 0$ for all $x \in \mathbb{R}$ it follows that

$$\tilde{\Psi}_{s,\omega}(x,z) = f(x - z/\omega) - f^*(x + z/\omega) \tag{49}$$

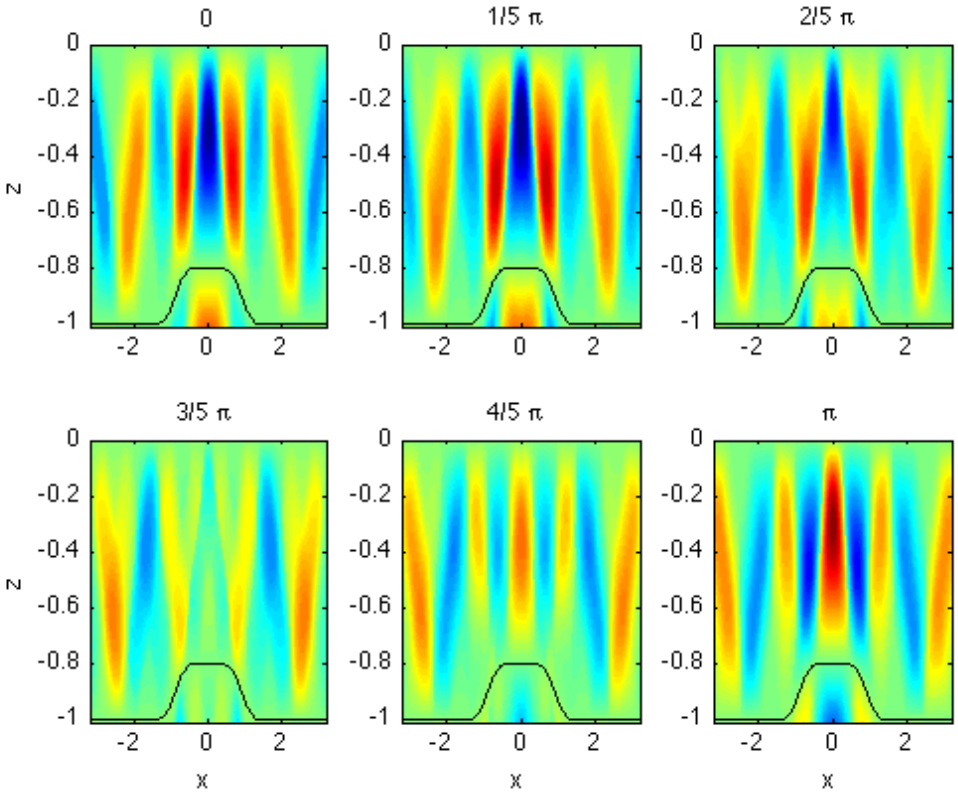

Figure 18: *This figure shows six snapshots of the real part of real part of the time-dependent baroclinic streamfunction* $\Psi'_{s,\omega}(x,z,t) = \bar{\Psi}'_{s,\omega}(x,z)e^{-i\omega t}$ *with* $s = 0.2$ *and* $\omega = 1.1$*, calculated with the method described in section (3.4.5). The parameter values* s_0 *used in this numerical calculation, which guarantees that (51) is satisfied, is* $s_0 = 0.20694432$*. The numbers above the plots indicate the time, scaled with frequency* ω*. The number* π *therefore represents the baroclinic streamfunction* $\Psi'_{s,\omega}(x,z,0)$ *after half a period. Notice that* $\Re(\Psi'_{s,\omega}(x,z,0)) = -\Re(\Psi'_{s,\omega}(x,z,\omega\pi))$*. The color bar is the same as in figure (16), which ranges from -0.1 to 0.1.*

where $*$ denotes the complex conjugate and $f : \mathbb{R} \to \mathbb{C}$ is arbitrary. For $|x| > L$, with $L = \max(L_s, L_{s_0})$, the bottom $z = -h_s(x) = -h_{s_0}(x) = -1$ is flat, which means that $\Re(\tilde{\Psi}_{s,\omega}(x, -h_s(x))) = \Re\left(\bar{\Psi}_{s,\omega}(x, -h_s(x)) - \Psi_{s_0,1}(x, -h_s(x))\right) = 1 - 1 = 0$. This means that

$$\Re(f(x+1) - f^*(x-1)) = 0 \quad \text{for } |x| > L.$$

For $|x| \leq L$ the real part of $\tilde{\Psi}_{s,\omega}(x, -h_s(x))$ does not vanish as

$$\begin{aligned} \Re(\tilde{\Psi}_{s,\omega}(x, -h_s(x))) &= \Re(\bar{\Psi}_{s,\omega}(x, -h_s(x))) - \Psi_{s_0,1}(x, -h_s(x)) \\ &= 1 - a_{s_0,1}(x - h_s(x)) + a_{s_0,1}(x + h_s(x)) \neq 0. \end{aligned} \tag{50}$$

Physically there cannot be any net flux (which radiates kinetic energy) through the bottom $z = -h_s(x)$ because the barotropic tide with frequency $\omega \neq 1$ is assumed to be the only source of energy for the baroclinic internal wave modes. So one has to assume that

$$\Re\left(\int_{-\infty}^{\infty} \tilde{\Psi}_{s,\omega}(x, -h_s(x))dx\right) = \int_{-L}^{L} (1 - a_{s_0,1}(x - h_s(x)) + a_{s_0,1}(x + h_s(x)))dx = 0, \tag{51}$$

which expresses that there is no net flow through the boundary $z = -h_s(x)$. It is this constraint which prescribes s_0. It is possible to evaluate the integral in (51) analytically, which is necessary to be able to solve for s_0 as a function of s. However the integral has to be subdivided into many integrals over different intervals due to the piecewise description of $a_{s_0,1}$, with s_0 part of the integral bounds. For the analysis in this report the value of s_0 is determined numerically.
Condition (51) together with $h_s(x)$ being an even function means that one can write the residual streamfunction at the boundary $z = -h_s(x)$ as a Fourier expansion:

$$\tilde{\Psi}_{s,\omega}(x, -h_s(x)) = \sum_{n=1}^{\infty} \psi_n \cos(\pi n x / L) \quad \text{for } |x| \leq L. \tag{52}$$

For given function $a_{s_0,1}$, where s_0 is determined by (51), one can solve for the real-valued Fourier coefficients ψ_n by inverse Fourier transform. The constraint (50) allows to add any imaginary part to $\tilde{\Psi}_{s,\omega}(x, -h_s(x))$, so one can prescribe

$$\tilde{\Psi}_{s,\omega}(x, -h_s(x)) = \Gamma_{s,\omega}(x) \quad \text{for } |x| \leq L \tag{53}$$

where

$$\Gamma_{s,\omega}(x) = \sum_{n=1}^{\infty} \psi_n e^{-i\pi n x / L}.$$

The constraint for f is then

$$f(x + h_s(x)) - f^*(x - h_s(x)) = \Gamma_{s,\omega}(x) \quad \text{for } |x| \leq L. \tag{54}$$

By construction the residual streamfunction $\tilde{\Psi}_{s,\omega}(x, z) = f(x - z/\omega) - f^*(x + z/\omega)$ satisfies the boundary condition (50).

Numerical solution algorithm

Equation (54) is solved by a numerical algorithm. In the first step this algorithm, which is implemented in MATLAB, determines the reflection points (x-coordinates) at the irregular part of the bottom of four characteristics that start at some given point (x, z) for given forcing frequency ω.
To illustrate this assume (x_0, z_0) to be given and consider the characteristic passing through this point in the direction $\swarrow$ (in (x, z)-coordinates). This characteristic $\swarrow$ is parametrized by $x - z = c_0$ with constant $c_0 = x_0 - z_0$. It intersects with the bottom $z = -h_s(x)$ at $x_1^{\swarrow}$ which satisfies $\delta_+(x_1^{\swarrow}) = x_1^{\swarrow} + h_s(x_1^{\swarrow}) = c_0$. The point $x_1^{\swarrow}$ can be calculated analytically with the expression for δ_+^{-1}, presented in the appendix G (5.7). Continuing along the characteristic (which reflects at the subcritical bottom at $x_1^{\swarrow}$ upward to the left) it next reflects at the surface at $x = x_1^{\swarrow} - 1/\omega$. The next reflection $x_2^{\swarrow}$ at the bottom is then determined by evaluating $\delta_+^{-1}(x_1 - 1/\omega)$. This procedure is repeated until the irregular part of the bottom has been passed (which is the case if $x_i^{\swarrow} < L_s$).
Doing the same also for the other three possible characteristics starting at (x_0, z_0) results in at most four non-empty sets

$$\begin{aligned} S^{\swarrow} &= \{x_i^{\swarrow} | i = 1, ...N^{\swarrow}\}, \\ S^{\searrow} &= \{x_i^{\searrow} | i = 1, ...N^{\searrow}\}, \\ S^{\nwarrow} &= \{x_i^{\nwarrow} | i = 1, ...N^{\nwarrow}\}, \\ S^{\nearrow} &= \{x_i^{\nearrow} | i = 1, ...N^{\nearrow}\}. \end{aligned} \tag{55}$$

If $|x_0| > L_s$, then exactly two of the four sets are non-empty.
The value of the residual streamfunction $\tilde{\Psi}_{s,\omega}$ at the point (x_0, z_0) is then determined by adding up $\Gamma_{s,\omega}(x_i)$ for all $x_i \in S^{\swarrow} \bigcup S^{\searrow}$ and subtracting it for all $x_i \in S^{\nwarrow} \bigcup S^{\nearrow}$:

$$\tilde{\Psi}(x_0, z_0) = \sum_{n=1}^{N^{\swarrow}} \Gamma_{s,\omega}(x_i^{\swarrow}) + \sum_{n=1}^{N^{\searrow}} \Gamma_{s,\omega}(x_i^{\searrow}) - \sum_{n=1}^{N^{\nwarrow}} \Gamma_{s,\omega}(x_i^{\nwarrow}) - \sum_{n=1}^{N^{\nearrow}} \Gamma_{s,\omega}(x_i^{\nearrow}).$$

By construction the function $\tilde{\Psi}(x, z)$ has the form (49) and satisfies (54).
The barotropic part $\hat{\Psi}_{s,\omega}(x, z) = -z/h_s(x)$ can now be subtracted from the numerically calculated streamfunction $\bar{\Psi}_{s,\omega}(x, z) = \tilde{\Psi}_{s,\omega}(x, z) + \Psi_{s_0,1}(x, z)$ to get the baroclinic time-dependent part

$$\Psi'_{s,\omega}(x, z, t) = \left(\tilde{\Psi}_{s,\omega}(x, z) + \Psi_{s_0,1}(x, z) + z/h_s(x)\right) e^{-i\omega t}. \tag{56}$$

This baroclinic time-dependent part is identical to the $\Psi'_{s,\omega}(x, z, t)$ as calculated by (48) above the flat bottom within reasonable numerical errors. For a grid of $\Delta x = \Delta z = 0.01$ the relative error was found to be less than 1% everywhere and below 10^{-5} at most grid points.
The snapshots of the real part of the time-dependent baroclinic streamfunction in figure (18) are produced with this numerical algorithm. It verifies that the time-dependent baroclinic streamfunction as calculated in subsection (3.4.4) is correct. The analytical expression for the baroclinic streamfunction, expression (47), is therefore used in the following part to determine the kinetic energy which is radiated away from the irregular part of the bottom and to compare this with the trapped kinetic energy.

3.4.6 Radiated and trapped energy

The interest lies in the energy dissipation in the barotropic tide due to the generation of internal waves. The kinetic energy is proportional to the square of the absolute velocity $u^2 + w^2$ of the velocity field (u, w). As the proportionality can be scaled it is assumed that the kinetic internal wave energy E in some domain $\Omega \subset \mathbb{R}^2$ is

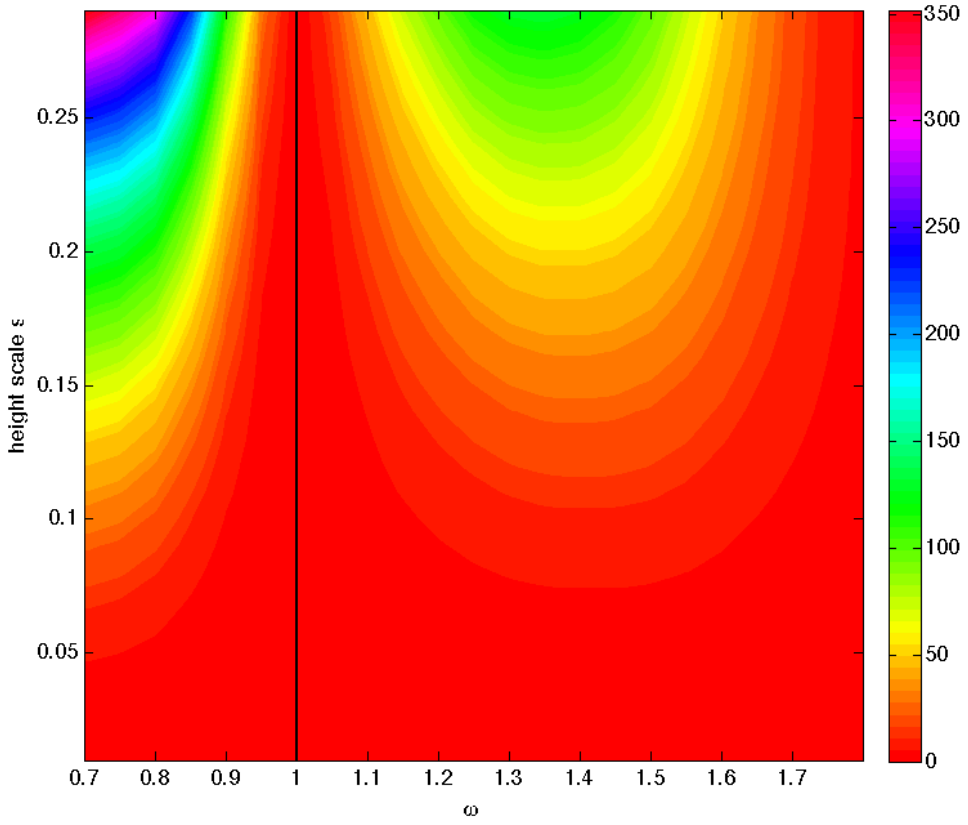

Figure 19: *This figure shows the radiated energy* $E_{\leftrightarrow} = 2E_{\leftarrow}$ *of the barotropic mode integrated over one tidal period* $2\pi/\omega$*, as a function of forcing frequency* ω *(horizontal axis) and scale height* s *(vertical axis). The lower bound for* ω *is chosen such that the bottom topography* $z = -h_s(x)$ *is subcritical for all plotted values of* s*. The case of no tidal conversion,* $\omega = 1$*, is marked by the black line. The grid size in* s *is* 0.01 *and in* ω *it is* 0.05*. The smallest value for* s *is* 10^{-5}*. For each pair* (s, ω) *the radiated energy* $E_{\leftarrow}$ *is numerically determined from the exact baroclinic streamfunction (47), integrated over* $[-L_s - 2/\omega, -L_s] \times [-1, 0]$*.*

defined as

$$E(\Omega,t) = \int_\Omega u^2(x,z,t)+w^2(x,z,t)\,dxdz = \int_\Omega \left(\frac{\partial\Psi'(x,z,t)}{\partial z}\right)^2+\left(\frac{\partial\Psi'(x,z,t)}{\partial x}\right)^2 dxdz.$$

The energy loss rate $\partial_t E$ of the barotropic mode can be determined by calculating the kinetic energy flux of the baroclinic (internal wave) mode along some path from $z=-1$ to $z=0$ to the right or left the irregular part of the bottom. The entire barotropic energy dissipation rate is then twice this baroclinic energy flux, as the baroclinic energy flux away from the irregular bottom part must be the same in both directions due to symmetry. The energy loss rate $\partial_t E$ integrated over one tidal period $2\pi/\omega$ is referred to as the radiated kinetic energy and denoted by $E_{\leftarrow}$, where the arrow indicates the direction of radiation. The radiated kinetic energy $E_{\leftrightarrow} = 2E_{\leftarrow}$ is shown in figure (19) as a function of ω and s.

One can determine $E_{\leftrightarrow}$ by integrating $\Psi'_{s,\omega}(x,z,t)$ over the domain $[-L_s-2/\omega, -L_s]\times$

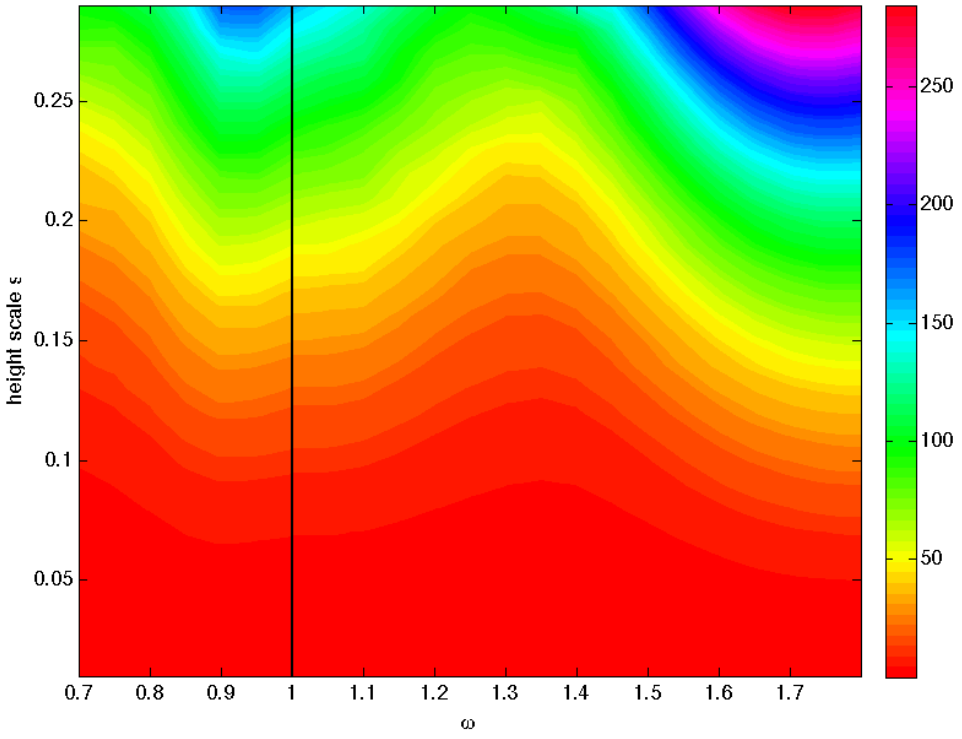

Figure 20: *This figure shows the trapped energy E_0 as a function of forcing frequency ω (horizontal axis) and scale height s (vertical axis). Notice that it is only weakly dependent on the forcing frequency ω around $\omega = 1$, but that it strongly increases in magnitude as ω increases towards $\omega = 1.8$.*

$[-1, 0]$. So the radiated energy $E_{\leftarrow}$ is the kinetic energy of the baroclinic streamfunction integrated over the plotted domain in figure (17) (at any time t). Computationally this is convenient because $\Psi'_{s,\omega}(x, z, t)$ for $t = 0$ is given by the exact expression (47). Due to time limitation of the project the radiated energy $E_{\leftarrow}$ presented in figure (19) is calculated by determining the baroclinic velocity field $(u(x, z), w(x, z))$ from the exact baroclinic streamfunction $\Psi'_{s,\omega}(x, z)$ with central difference in space numerical approximations and then numerically integrating the square of the components on a grid with grid sizes $\Delta x = \Delta z = 0.05$. The smallest value for s is 10^{-5}. It is possible to calculate the kinetic energy analytically. It requires differentiation of (47) with respect to x and z, taking the square of these derivatives and integrating them over the domain $[-L_s - 2/\omega, -L_s] \times [-1, 0]$. The main difficulty lies in the tracing of domains and ranges of $b_{s,\omega}$ and h_s, as these two functions are defined by several functions on subsequent intervals.

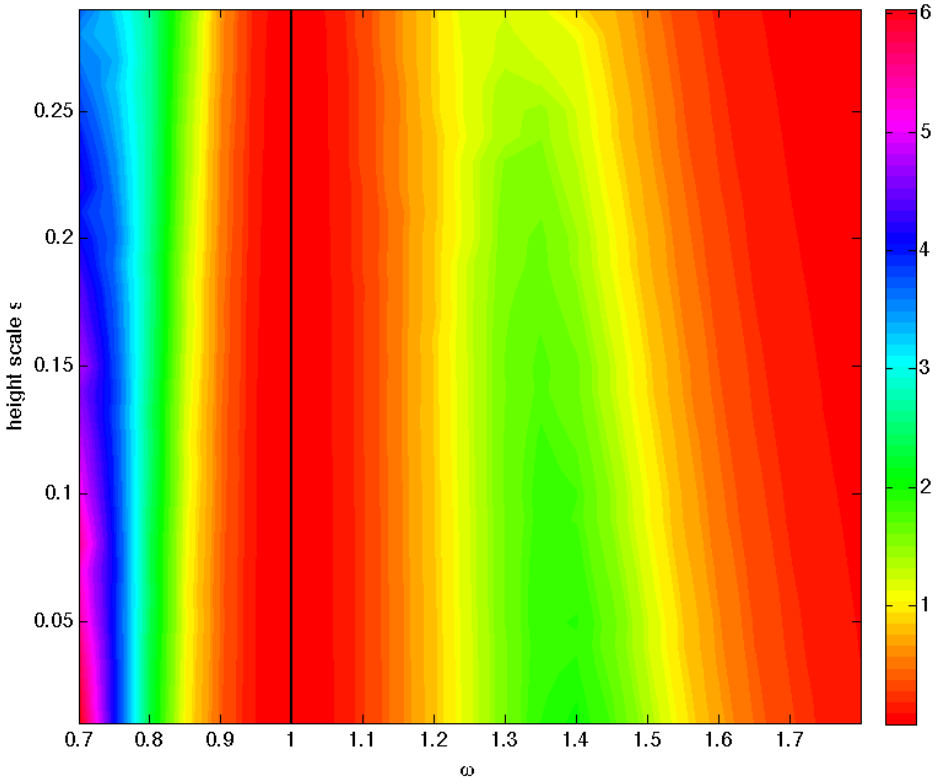

Figure 21: *This figure the ratio of the radiated energy $E_{\leftrightarrow}$ with the trapped energy E_0 s a function of forcing frequency ω (horizontal axis) and scale height s (vertical axis). Notice that the colours on the color scale are periodic. A ratio above 5 (also red) can only be found in the bottom left corner.*

It has been found that there are internal waves above the irregular bottom topography, also in the case of no tidal conversion (see figure (16)). The kinetic energy of these trapped internal waves is referred to as the trapped energy E_0. For the cases of no tidal conversion the trapped energy E_0 is well-defined, as it is simply the kinetic energy of the entire baroclinic velocity field (with baroclinic streamfunction given by (47) for $\omega = 1$). For the cases of tidal conversion one has to distinguish between propagating and trapped (standing) waves. This is done by defining the trapped energy E_0 to be the kinetic energy of the baroclinic wave field given by the streamfunction $\Psi'(x, z, 0) = \Psi'(x, z)$ as given in equation (47) integrated from $x = -L_s$ to $x = L_s$ and $z \in [-h_s(x), 0]$. This is a natural extension of the trapped energy definition from the case of no tidal conversion and is shown in figure (20).
The ratio of the radiated energy $E_{\leftrightarrow}$ with the trapped energy E_0 is shown in figure (21).
Notice that the radiated energy $E_{\leftarrow}$ depends strongly on both parameters s and ω (see figure (19)). This shows that the height of the ridge as well as the barotropic tidal frequency are important parameters in determining the barotropic energy dissipation to internal waves.
In figure (21) one can see that the ratio $E_{\leftrightarrow}/E_0$ of the radiated and trapped kinetic energies depends only weakly on the height of the ridge (parameter s). This is a remarkable result, which is discussed in the following.

3.5 Discussion

The weak dependence of the ratio of the radiated and trapped kinetic energies on the height of the ridge is interesting because it gives a connection between the infinitesimal small bottom topography and finite size bottom perturbation.
Many studies on tidal conversion consider an ocean if infinitely depth, see for example [2] and references in [6]. Upon scaling the ocean to finite size this means that the height of the irregular bottom topography, which can lead to tidal conversion, is infinitesimal small. If the ratio of the radiated and trapped kinetic energies turns out to be approximately independent of the scale height in general, then one can easily relate results for infinitesimal small bottom topographies to finite size bottom irregularities of the same shape.

An interesting question to ask is whether the method used here to construct two-dimensional exact baroclinic streamfunctions by solving Abel's functional equation can be generalized to three-dimensional tidal conversion problems. One of the main ingredients that made the construction of the exact internal wave solutions possible is the fixed angle of the propagation direction of internal waves in a uniformly-stratified fluid with respect to vertical direction and the abnormal "rule of reflection" associated with it. The map T makes implicitly use of it.
In contrast to the two-dimensional case discussed in this thesis, the fixed angle with respect to the vertical does not uniquely describe the propagation direction in three dimensions upon reflection. The reflection in the horizontal plane is described by the "normal" rule of reflection: the angle of the outgoing wave beam (projected into the horizontal plane) is the same angle of the incident angle with respect to the normal of the bottom topography (also projected into the horizontal place).
A generalization of the map T therefore requires to define a map $T : \mathbb{R}^2 \to \mathbb{R}^2$ which takes the two horizontal coordinates (x, y) onto $T(x, y) = (T_1(x, y), T_2(x, y))$ such

that this extended rule of reflection of a characteristic in three dimension is satisfied. Topographies lacking tidal conversion can be constructed from maps which become linear upon (finite) composition of itself. No true three-dimensional topographies lacking tidal conversion (which cannot be mapped into one horizontal dimension) for barotropic modes oscillating in one (horizontal) direction is known. As barotropic modes usually form elliptic orbits due to the rotation of the earth it is also interesting to ask whether topographies lacking tidal conversion for such elliptic tidal forcing exist.

We expect that it is much more unlikely to encounter three dimensional topographies lacking tidal conversion in the space of topographies (for a given frequency and uniform stratification) because a map $T : \mathbb{R}^2 \to \mathbb{R}^2$ associated with such a three-dimensional topography must become linear in both T_1 and T_2.

4 Conclusions

In section 2 analytical solutions to small-amplitude standing internal wave in a uniformly stratified fluid confined to trapezoidal domains and exhibiting (1,1) attractors are constructed. The exact streamfunctions are constructed by two different methods, of which one is new. The new method derives the streamfunction solution from solutions to Abel's functional equation, which turns out to be useful for a large class of internal wave problems, including the tidal conversion problem in section 3 and other subcritical topographies treated in Beckebanze and Keady, 2014. It also gives new insight into the fractal structure of the internal waves in a trapezoid: the self-similarity of the velocity field is exact as one zooms in onto the attractor.
The baroclinic (internal wave) field in a uniformly stratified ocean caused by barotropic flow over a ridge is constructed for different barotropic tidal frequencies and for a variable relative height of the ridge. The parameter range for the barotropic tidal frequency includes a frequency for which no internal wave propagate away from the ridge. This makes it possible to study the energy dissipation of the barotropic tide as a function of relative height of the ridge and forcing frequency. For all parameter values internal waves are trapped to the region of the ridge. It is found that the ratio of the kinetic energy of these trapped internal waves and the kinetic energy radiated away from the ridge is only weakly dependent on the relative height of the ridge, but strongly depends on the forcing frequency.

Acknowledgement

I would like to express my gratitude to my supervisors Leo Maas and Gerard Sleijpen for useful comments, remarks and inspiration. I highly appreciate the fact that Leo Maas came a long way to Utrecht every other week for discussion of the progress of my research. I also want to thank my supervisors for the openness to let me direct the research towards topics which were originally not planned. This includes the collaboration with Grant Keady, with whom I have written an article, [1]. I want to thank Grant Keady for the successful collaboration, which has taught me many new aspects of writing and publishing an article, as well as for the many inspiring Skype talks. I thank my family and friends for support and my parents also for financial support. Last but not least I am thankful to the Institute for Marine and Atmospheric research Utrecht (IMAU) for providing a suitable workspace and to my fellow students for creating a comfortable working atmosphere in the IMAU student room.

5 Appendices

5.1 Appendix A: $\log_5$-periodicity of energy E_n for $\tau = \frac{3}{2}$

The kinetic energy of a wave field $(u(x,z), w(x,z))$ at some point (x,z) is proportional to $u(x,z)^2 + v(x,z)^2$. It is interesting to analyse the kinetic energy of the Fourier modes of the velocity field, as it gives insight on spatial scale and variance of the kinetic energy distribution. In section (**??**) the streamfunction Ψ is determined by deriving exact expressions of its Fourier coefficients a_n. The kinetic energy of the n^{th} Fourier mode of the velocity field $(u(x,z), w(x,z)) = (\partial_z \Psi(x,z), -\partial_x \Psi(x,z))$ integrated over the entire trapezoidal domain D_τ is proportional to $n^2 a_n^2$.
In the following $E_n := n^2 a_n^2$ as a function of $n \in \mathbb{N}$ is analysed. In [11], where the Fourier coefficients a_n are calculated exactly for $\tau = \frac{3}{2}$, E_n is plotted as a function of $\log_5(n)$ in figure 1. This plot indicates that the values of E_n for $n \in \mathbb{N}$ sample along some curve with period 1, suggesting that E_n as $\log_5$-periodicity. Here it shown that

$$\lim_{n\to\infty} E_{5n} = E_n$$

for $\tau = \frac{3}{2}$. For this parameter value the coefficients a_n are given by

$$a_n = \frac{2n}{\pi} \sum_{k=0}^{\infty} \sin\left(\frac{n\pi}{3\cdot 5^k}\right) \left(\frac{1}{n^2 - (3/2)^2 \cdot 5^{2k}} - \frac{1}{n^2 - (3/2)^2 \cdot 5^{2k+2}}\right)$$

in equation (10) in [11]. This leads to

$$\begin{aligned} E_n &= n^2 \left(\frac{2n}{\pi} \sum_{k=0}^{\infty} \sin\left(\frac{n\pi}{3\cdot 5^k}\right) \left(\frac{1}{n^2 - (3/2)^2 \cdot 5^{2k}} - \frac{1}{n^2 - (3/2)^2 \cdot 5^{2k+2}}\right)\right)^2 \\ &= \frac{4n^4}{\pi^2} \left(\sum_{k=0}^{\infty} \sin\left(\frac{n\pi}{3\cdot 5^k}\right) \left(\frac{(3/2)^2(5^{2k} - 5^{2k+2})}{n^4 - n^2(3/2)^2(5^{2k} + 5^{2k+2}) + (3/2)^4 5^{4k+2}}\right)\right)^2. \end{aligned}$$

Similarly we can calculate E_{5n}:

$$\begin{aligned} E_{5n} &= 5^4 \frac{4n^4}{\pi^2} \left(\sum_{k=0}^{\infty} \sin\left(\frac{n\pi}{3\cdot 5^{k-1}}\right) \left(\frac{5^2 \cdot (3/2)^2(5^{2k-2} - 5^{2k})}{5^4 \cdot (n^4 - n^2(3/2)^2(5^{2k-2} + 5^{2k}) + (3/2)^4 5^{4k-2})}\right)\right)^2 \\ &= \frac{4n^4}{\pi^2} \left(\sum_{k=-1}^{\infty} \sin\left(\frac{n\pi}{3\cdot 5^k}\right) \left(\frac{(3/2)^2(5^{2k} - 5^{2k+2})}{n^4 - n^2(3/2)^2(5^{2k} + 5^{2k+2}) + (3/2)^4 5^{4k+2}}\right)\right)^2 \\ &= \frac{4n^4}{\pi^2} \left(\sin\left(\frac{5n\pi}{3}\right) \left(\frac{(3/2)^2(5^{-2} - 1)}{n^4 - n^2(3/2)^2(26/25) + (3/2)^4 5^{-2}}\right)\right)^2 \\ &+ \frac{4n^4}{\pi^2} \sin\left(\frac{5n\pi}{3}\right) \left(\frac{(3/2)^2(5^{-2} - 1)}{n^4 - n^2(3/2)^2(26/25) + (3/2)^4 5^2}\right) \\ &\cdot \left(\sum_{k=0}^{\infty} \sin\left(\frac{n\pi}{3\cdot 5^k}\right) \left(\frac{(3/2)^2(5^{2k} - 5^{2k+2})}{n^4 - n^2(3/2)^2(5^{2k} + 5^{2k+2}) + (3/2)^4 5^{4k+2}}\right)\right) \\ &+ \frac{4n^4}{\pi^2} \left(\sum_{k=0}^{\infty} \sin\left(\frac{n\pi}{3\cdot 5^k}\right) \left(\frac{(3/2)^2(5^{2k} - 5^{2k+2})}{n^4 - n^2(3/2)^2(5^{2k} + 5^{2k+2}) + (3/2)^4 5^{4k+2}}\right)\right)^2 \\ &= s_n(s_n + n \cdot a_n) + E_n \end{aligned}$$

where $s_n := \frac{2n^2}{\pi}\left(\sin\left(\frac{5n\pi}{3}\right)\left(\frac{(3/2)^2(5^{-2}-1)}{n^4-n^2(3/2)^2(26/25)+(3/2)^4 5^{-2}}\right)\right)$.
Now it will be shown that $s_n(s_n + na_n)$ converges to zero for $n \to \infty$. It is clear that s_n^2 converges to zero because $|s_n^2| \leq \frac{4n^4}{\pi^2}|\frac{(3/2)^4(5^{-2}-1)^2}{(n^4-n^2(3/2)^2(26/25)+(3/2)^4 5^2)^2}| \leq \frac{c}{n^4}$ for some sufficiently large $c \in \mathbb{R}^+$.
Similarly we can observe that $|s_n \cdot n \cdot a_n| \leq c' \sum_{k=0}^{\infty} \frac{(3/2)^2(5^{2k}-5^{2k+2})}{n^4-n^2(3/2)^2(5^{2k}+5^{2k+2})}$ for some constant $c' > 0$, so also $s_n \cdot n \cdot a_n$ converges to zero for $n \to \infty$. This concludes the prove that E_n is $\log_5$-periodic for $n \to \infty$.
From section (2.3) it is known that for $\tau = \frac{3}{2}$ the analytical streamfunction solution contracts with a factor $p = \frac{\tau+1}{\tau-1} = 5$ towards the attractor, leading to an exact $\log_5$ periodicity as the attractor is approached. This is an indication that the approximate $\log_5$-periodicity in the Fourier energy terms E_n results from the exact $\log_5$-periodicity in part of the streamfunction Ψ. The streamfunction Ψ is not entirely $\log_5$-periodic because the self-similarity only holds as one zooms in onto the attractor, but not zooming out. Analysis of numerical results suggests that for general $\tau \in (1, 2)$ the energy E_n has $\log_p$-periodicity with $p = \frac{\tau+1}{\tau-1}$ as $n \to \infty$. It is speculated that this can be proven as above for general τ.

5.2 Appendix B: Γ-equation reviewed

In [11] it is argued that the Fourier coefficients which prescribe the exact internal wave streamfunction are a solution of a set of countable infinite linear equations. The linear equations are prescribed by a countable infinite matrix, referred to as Γ, and the Fourier coefficients of any function which guarantees the vanishing of the streamfunction on the boundary of the domain.
Here it is shown that the countable infinite matrix Γ is not invertible. This implies that it is not possible to generate unique Fourier coefficients of the streamfunction solution if a function F, which guarantees the vanishing of the streamfunction on the boundary of the domain, is prescribed. It turns out that the system of countable infinite linear equations is in fact under-determined. This ill-posedness results from the fact that the domain of the function F, which should guarantee the vanishing of the streamfunction on the boundary, is not sufficiently large (shown in section (2.1)).
Extending the domain of F leads to a well-posed set of constraints which result in a streamfunction solution for a trapezoidal domain which does vanish on its boundaries.

The two following subsections show how the countable infinite matrix Γ is derived and that it defines an operator on the Hilbert space of square-summable sequences. In subsection (5.2.3) it is argued that Γ is under-determined.

5.2.1 Derivation of Γ

In [11] a countable infinite matrix Γ' is introduced (in [11] it is denoted by Γ) which satisfies

$$\cos(k\pi\frac{\xi}{3}) = \sum_{n=0}^{\infty}(-1)^k \Gamma'_{n,k} \cos(n\pi\xi). \tag{57}$$

for $\xi \in [-1,1]$ and $k \in \mathbb{N}$. It is stated that the countable infinite matrix which satisfies (57) is given by

$$\Gamma'_{n,k} \equiv -\frac{3k}{\pi} \sin\left(\frac{k\pi}{3}\right) \frac{(-1)^n \epsilon_n}{k^2 - 9n^2} \tag{58}$$

for $n \in \mathbb{N} \bigcup \{0\}$, $k \in \mathbb{N}$ and $\epsilon_n = 2$ if $n \neq 0$ and $\epsilon_0 = 1$.
Notice that it is unclear which values the countable infinite matrix takes if $k = 3n$ because one cannot divide by zero.
In the following a slightly different countable infinite matrix Γ is derived, namely $\Gamma_{n,k}$ which satisfies

$$\cos(k\pi\frac{\xi}{3}) = \sum_{n=0}^{\infty} \Gamma_{n,k} \cos(n\pi\xi). \tag{59}$$

It will turn out that $\Gamma_{n,k} = -\Gamma'_{n,k}$ for $k \neq 3n$ and $\Gamma_{n,3n} = 1$.
Notice that the entry $\Gamma_{n,k}$ of the countable infinity matrix Γ is the n^{th} Fourier coefficient of the function $\cos(\frac{k\pi x}{3})$ over the interval $x \in [-1,1]$ for some given $k \in \mathbb{N}$. So from (59) one can conclude that

$$\Gamma_{n,k} = \frac{1}{L_n} \int_{-1}^{1} \cos(\frac{k\pi x}{3}) \cos(n\pi x) dx.$$

where $L_n := \int_{-1}^{1} \cos(n\pi x)^2 dx$. Lets make a case distinguishing in order to evaluate this integral:

Case 1: $n, k \in \mathbb{N}$, $k \neq 3n$
Evaluating the integral now gives

$$\Gamma_{n,k} = \frac{(-1)^n 6k \sin(\frac{k\pi}{3})}{\pi(k^2 - 9n^2)}.$$

This expression corresponds exactly to $-\Gamma'_{n,k}$ as defined in (58).

Case 2: $n = 0$, $k \in \mathbb{N}$
The second cosines term under the integral becomes 1 for $n = 0$ and $L_0 = 2$, so evaluating $\frac{1}{L_0} \int_{-1}^{1} \cos(\frac{k\pi x}{3}) dx$ gives $\Gamma_{0,k} = \frac{3\sin(\frac{k\pi}{3})}{\pi k} = -\Gamma'_{0,k}$.

Case 3: $n \in \mathbb{N}$, $k = 3n$
If $k = 3n$, then both cosine terms under the integral are equal and the integral becomes $\Gamma_{n,3n} = \int_{-1}^{1} \cos(n\pi x)^2 dx = 1$. Notice that this expression for $k = 3n$ corresponds with the limit $\lim_{k \to 3n} \left(-\Gamma'_{n,k}\right) = 1$.

It can be concluded that Γ is the extension of $-\Gamma'$. In fact Γ' can only be derived from (57) if $(-1)^k$ is replaced by -1.

5.2.2 Γ is an operator on ℓ^2

The countable infinite matrix Γ works on countably infinite vectors, in other words: on sequences. An interesting question is therefore whether Γ defines an operator on

the Hilbert space $\ell^2 := \{(a_n)_{n\in\mathbb{N}} : \sum_{k=1}^{\infty} a_n^2 < \infty\}$ of square-summable sequences. The space ℓ^2 is clearly a suitable domain for Γ, so one has to check whether Γ maps ℓ^2 into itself. This is checked by showing that $s \in \ell^2$ implies $\|\Gamma \cdot s\|_2 < \infty$.
Lets split Γ into three parts: $\Gamma^{(j)}_{n,k} = \Gamma_{n,3k-j}$ for $j = 0, 1, 2$. If $\|\Gamma^{(j)} \cdot s\|_2 < \infty$ for $j = 0$, 1 and 2 for any $s \in \ell^2$, then also $\|\Gamma \cdot s\|_2 < \infty$. By definition $\Gamma^{(0)}$ is the countable infinite identity matrix, so clearly $\|\Gamma^{(0)} \cdot s\|_2 = \|s\|_2 < \infty$.
By equation (59) we have that

$$\cos(\pi \left(k\xi + \frac{2}{3} \right)) = \sum_{n=0}^{\infty} \Gamma^{(1)}_{n,k} \cos(n\pi\xi). \tag{60}$$

Define the function $f(\xi) := \sum_{k=1}^{\infty} s_k \cos(\pi(k\xi + \frac{2}{3}))$ for $\xi \in [-\pi, \pi]$. By definition $f \in L^2([-\pi, \pi])$, the function space defined by the 2-norm because $s \in \ell^2$. Substituting (60) into the Fourier expansion of f gives

$$f(\xi) = \sum_{k=1}^{\infty} s_k \sum_{n=0}^{\infty} \Gamma^{(1)}_{n,k} \cos(n\pi\xi) = \sum_{n=0}^{\infty} \left(\sum_{k=1}^{\infty} \Gamma^{(1)}_{n,k} s_k \right) \cos(n\pi\xi).$$

Parseval's Theorem states that

$$\|f\|_2 := \left(\int_{-\pi}^{\pi} |f(x)|^2 dx \right)^{1/2} = \| \sum_{k=1}^{\infty} \Gamma^{(1)}_{n,k} s_k \|_2,$$

where $\|f\|_2$ denotes the 2-norm of $f \in L^2([-\pi, \pi])$. Next it will be shown that $\|f\|_2 < \infty$, which implies the desired result $\| \sum_{k=1}^{\infty} \Gamma^{(1)}_{n,k} s_k \|_2 = \|\Gamma^{(1)} \cdot s\|_2 < \infty$.
Using $\cos(a + b) = \cos a \cos b - \sin a \sin b$ with $a = \pi k\xi$ and $b = 2\pi/3$ gives

$$\|f\|_2 = \| \sum_{k=1}^{\infty} s_k \cos(\pi \left(k\xi + \frac{2}{3} \right)) \|_2 = \| \sum_{k=1}^{\infty} s_k \left(\cos(\pi k\xi) \cos\left(\frac{2\pi}{3} \right) - \sin(\pi k\xi) \sin\left(\frac{2\pi}{3} \right) \right) \|_2.$$

This norm can be bounded by

$$\| \cos\left(\frac{2\pi}{3} \right) \sum_{k=1}^{\infty} s_k (\cos(\pi k\xi) \|_2 + \| \sin\left(\frac{2\pi}{3} \right) \sum_{k=1}^{\infty} s_k \sin(\pi k\xi) \|_2.$$

Since $\cos(\frac{2\pi}{3}) \leq 1$ and $\sin(\frac{2\pi}{3}) \leq 1$ we get

$$\|f\|_2 \leq \| \sum_{k=1}^{\infty} s_k (\cos(\pi k\xi) \|_2 + \| \sum_{k=1}^{\infty} s_k \sin(\pi k\xi) \|_2 = 2 \sum_{k=1}^{\infty} |s_k|^2 = 2\|s\|_2 < \infty$$

because $s \in \ell^2$. This completes the proof that $\|\Gamma^{(1)} \cdot s\|_2 < \infty$. The proof for $\|\Gamma^{(2)} \cdot s\|_2 < \infty$ is similar. Thereby it is verified that Γ is a well-defined operator on ℓ^2.

5.2.3 Underdetermination of Γ

In the following it is shown that the linear system $\Gamma \cdot a = F$ for $F \in \ell^2$, from now on also referred to as Γ-equation, is under-determined. This implies that Γ is not

invertible and that a solution a is not unique.
Be reminded that a function is invertible if and only if it is a bijection. A counterexample will be provided to show that Γ is not injective and therefore not bijective. Let us first study the structure of Γ as defined above in more detail. The first components of Γ are

$$\Gamma = \begin{pmatrix} \frac{3\sqrt{3}}{2\pi} & \frac{3\sqrt{3}}{4\pi} & 0 & -\frac{3\sqrt{3}}{8\pi} & -\frac{3\sqrt{3}}{10\pi} & 0 & \frac{3\sqrt{3}}{14\pi} & \frac{3\sqrt{3}}{16\pi} & 0 & \dots \\ \frac{3\sqrt{3}}{8\pi} & \frac{6\sqrt{3}}{5\pi} & 1 & \frac{12\sqrt{3}}{7\pi} & \frac{15\sqrt{3}}{16\pi} & 0 & -\frac{21\sqrt{3}}{40\pi} & -\frac{24\sqrt{3}}{55\pi} & 0 & \dots \\ -\frac{3\sqrt{3}}{35\pi} & -\frac{3\sqrt{3}}{16\pi} & 0 & \frac{3\sqrt{3}}{5\pi} & \frac{15\sqrt{3}}{11\pi} & 1 & \frac{21\sqrt{3}}{13\pi} & \frac{6\sqrt{3}}{7\pi} & 0 & \dots \\ \frac{3\sqrt{3}}{80\pi} & \frac{6\sqrt{3}}{77\pi} & 0 & -\frac{12\sqrt{3}}{65\pi} & -\frac{15\sqrt{3}}{56\pi} & 0 & \frac{21\sqrt{3}}{32\pi} & \frac{24\sqrt{3}}{17\pi} & 1 & \dots \\ -\frac{3\sqrt{3}}{143\pi} & -\frac{3\sqrt{3}}{70\pi} & 0 & \frac{3\sqrt{3}}{32\pi} & \frac{15\sqrt{3}}{119\pi} & 0 & -\frac{21\sqrt{3}}{95\pi} & -\frac{3\sqrt{3}}{10\pi} & 0 & \dots \\ \frac{3\sqrt{3}}{224\pi} & \frac{6\sqrt{3}}{221\pi} & 0 & -\frac{12\sqrt{3}}{209\pi} & -\frac{3\sqrt{3}}{40\pi} & 0 & \frac{21\sqrt{3}}{176\pi} & \frac{24\sqrt{3}}{161\pi} & 0 & \dots \\ -\frac{3\sqrt{3}}{323\pi} & -\frac{3\sqrt{3}}{160\pi} & 0 & \frac{3\sqrt{3}}{77\pi} & \frac{15\sqrt{3}}{299\pi} & 0 & -\frac{21\sqrt{3}}{275\pi} & -\frac{6\sqrt{3}}{65\pi} & 0 & \dots \\ \vdots & \vdots & \vdots & \vdots & \vdots & \vdots & \vdots & \vdots & \vdots & \ddots \end{pmatrix}$$

The fact that $\Gamma_{n,3l} = \delta_{n,l}$ for all $l \in \mathbb{N}$ leads to the nice structure that every third column represents a unit sequence.

Define a sequence β by:
$\beta_1 = 1$
$\beta_2 = -2$
$\beta_{3n} = -\Gamma_{n,1} + 2\Gamma_{n,2}$ for $n \in \mathbb{N}$
$\beta_l = 0$ else wise

This sequence $\beta = \{\beta_n\}_{n\in\mathbb{N}}$ is an element of ℓ^2. To see this notice that $\|\beta\|_2^2 = 1 + 2^2 + c_1^2 - 4 < c_1, c_2 > +4c_2^2$ where $c_1 = \{\Gamma_{1,n}\}_{n\in\mathbb{N}\bigcup\{0\}}$ and $c_2 = \{\Gamma_{2,n}\}_{n\in\mathbb{N}\bigcup\{0\}}$. Both c_1 and c_2 are elements of ℓ^2, so $< c_1, c_2 >$ and $c_2^2 = | < c_2, c_2 > |$ are finite. This means that $\|\beta\|_2^2$ is also finite, so $\beta \in \ell^2$.
Now it will be shown that $\Gamma \cdot \beta = 0$. For the first element of $\Gamma \cdot \beta$ it is clear that it is zero because $\Gamma_{0,1} \cdot \beta_1 + \Gamma_{0,2} \cdot \beta_2 = \frac{\sqrt{3}}{\pi} - 2 \cdot \frac{\sqrt{3}}{2\pi} = 0$. The i^{th} element of the sequence $\Gamma \cdot \beta$ is the sum $\Gamma_{i,1} \cdot 1 + \Gamma_{i,2} \cdot (-2) + \Gamma_{i,3i} \cdot \beta_i = 0$ because all other components $\Gamma_{i,3l} \cdot \beta_l$ for $l \in \mathbb{N}$,$l \neq 3i$ vanish since $\Gamma_{n,3l} = 0$ for $l \neq 3n$. This shows that Γ is not injective because β is a non-trivial element in the kernel of Γ. This completes the proof that Γ cannot be inverted.

5.3 Appendix C: Constraints on F

5.3.1 Periodicity of $F_\tau(\xi)$

In this section it is analysed for which values of τ the function $F(\xi)$ is periodic.
The function $F(\xi)$ satisfies the functional equation (12) which is equivalent to $\Psi(x, \tau(x-1)) = 0$. So $F(\xi)$ is periodic if and only if the constraint $\Psi(x, \tau(x-1)) = 0$ is periodic for $x \in \mathbb{R}$ because ξ is linearly related to x.
The Fourier series solution Ψ given in (15) is periodic in x and z coordinates with period 2τ. This means that

$$\Psi(x, z) = \Psi(x + 2\tau k, z + 2\tau l)$$

for all $k, l \in \mathbb{Z}$. So $\Psi(x, \tau(x-1)) = 0$ is periodically satisfied for $x \in \mathbb{R}$ with period T_τ if $\Psi(x, \tau(x-1)) = 0 \Leftrightarrow \Psi(x + T_\tau, \tau(x + T_\tau - 1)) = 0$. This means that $T_\tau = 2\tau k$

and $\tau T_\tau = 2\tau l \Leftrightarrow T_\tau = 2l$ for some $k, l \in \mathbb{Z}$.

If $\tau \in \mathbb{Q} \bigcap (1,2)$, then $\tau = \frac{a}{b}$ for some $a, b \in \mathbb{N}$, $b \geq 2$, $a \geq 3$. So $T_\tau = 2\frac{a}{b}k = 2l$ and we find the (smallest) period $T = 2a$ (for $k = b$ and $l = a$).

If $\tau \in \mathbb{I} \bigcap (1,2)$, then it is impossible to satisfy both $T = 2\tau k$ and $T = 2l$ because if it was possible, then one could write $\tau = \frac{k}{l}$ which contradicts the assumption that $\tau \in \mathbb{I} := \mathbb{R} - \mathbb{Q}$.

From $a \geq 3$ (which is necessary to satisfy $1 < \tau < 2$) it follows that $T_{\frac{3}{2}} = 6$ is the smallest possible period for $\tau \in (1,2)$, which is the case $\tau = \frac{3}{2}$ discussed in [11]. More on the specific case $\tau = \frac{3}{2}$ can be found in in the following subsection.

5.3.2 Domain of $F_\tau(\xi)$ for $\tau = \frac{3}{2}$

Here it is shown for $\tau = \frac{3}{2}$ that $F(\xi) = \sum_{n=1}^{\infty} a_n \cos(n\pi(\frac{1}{6}\xi + \frac{1}{2}))$ is in fact defined for $\xi \in \mathbb{R}$ once F is defined for $x \in [\frac{3}{5}, 1]$ and assumed to be symmetric or antisymmetric.
Notice that the streamfunction Ψ is periodic with period $2\tau = 3$ in x and z coordinates. The coordinate transformation $x = \frac{1+\xi}{2}$ therefore leads to a periodicity with period $4\tau = 6$ in ξ. This means that any choice for the function $F(\xi)$ must be periodic with period 6.
It is clear that if $F(\xi)$ is known for $\xi \in (\frac{1}{5}, 1]$ and $\xi \in [-1, -\frac{1}{5})$, then one can iteratively specify $F(\xi)$ for all $\xi \in [-\frac{1}{5}, \frac{1}{5}]$ thanks to the relation $F(\xi) = F(5\xi)$.
In [11] it is pointed out that if one uses the coordinate transformation $\xi = \frac{2s+3}{5}$, which identifies $s \in [-1, 1]$ to $\xi \in [\frac{1}{5}, 1]$, one gets $F(\xi) = F(5\xi) = \sum_{n=1}^{\infty} a_n \cos(n\pi(\frac{5}{6}\xi + \frac{1}{2})) = \sum_{n=1}^{\infty} (-1)^n a_n \cos(n\pi\frac{s}{3})$. It is argued that from this relation it can be concluded that both the symmetric part $F^s(\xi)$ and antisymmetric part $F^a(\xi)$ of $F(\xi)$ must be symmetric around $\frac{3}{5}$ on $\xi \in [\frac{1}{5}, 1]$. However this argument is not correct and the statement happens to be true for $F^s(\xi)$ only; the antisymmetric part $F^a(\xi)$ must be antisymmetric around $\frac{3}{5}$ on $\xi \in [\frac{1}{5}, 1]$. This can be derived from the periodicity with period 6 together with the condition that $F(5\xi) = F(\xi)$. Lets discuss the symmetric and antisymmetric cases separately.
If the symmetric part $F^s(\xi)$ is prescribed on $\xi \in [\frac{1}{5}, 1]$, then so is it on $\xi \in [1, 5]$ by $F^s(\xi) = F^s(5\xi)$ and on $\xi \in [-5, -1]$ by symmetry around $\xi = 0$. The function value $F^s(\xi)$ for $\xi \in [-5, -1]$ must be equal to $F^s(\xi + 6)$ due to periodicity with period 6. Using $\xi = t + 3$ for $t \in [-2, 2]$ (equivalent to $\xi \in [1, 5]$) we get $F^s(t+3) = F^s(\xi) = F^s(-\xi) = F^s(-\xi + 6) = F^s(-t + 3)$, showing that $F^s(\xi)$ must be symmetric around $\xi = 3$ on $\xi \in [1, 5]$. This is equivalent to saying that $F^s(\xi)$ is symmetric around $\xi = \frac{3}{5}$ on $\xi \in [\frac{1}{5}, 1]$.
For the antisymmetric part $F^a(\xi)$ it follows by the same arguments as for $F^s(\xi)$ that once it is prescribed on $\xi \in [\frac{1}{5}, 1]$, then it is also prescribed on $\xi \in [1, 5]$ and $\xi \in [-5, -1]$. Using again $\xi = t+3$ for $t \in [-2, 2]$ it follows that $F^a(t+3) = F^a(\xi) = -F^a(-\xi) = F^a(-\xi + 6) = -F^a(-t + 3)$, so $F^a(\xi)$ must be antisymmetric around $\xi = 3$ on $[1, 5]$ or equivalently antisymmetric around $\xi = \frac{3}{5}$ on $[\frac{1}{5}, 1]$.
It is trivial that due to periodicity the function F is defined on $\mathbb{R}$ once it is defined on any connected interval of length 6. Notice also that on any connected interval of lengths 6 the integral over the function must vanish because $\cos(n\pi(\frac{1}{6}\xi + \frac{1}{2}))$ vanishes integrated over an interval of length 6 for every $n \in \mathbb{N}$, so also $F(\xi) =$

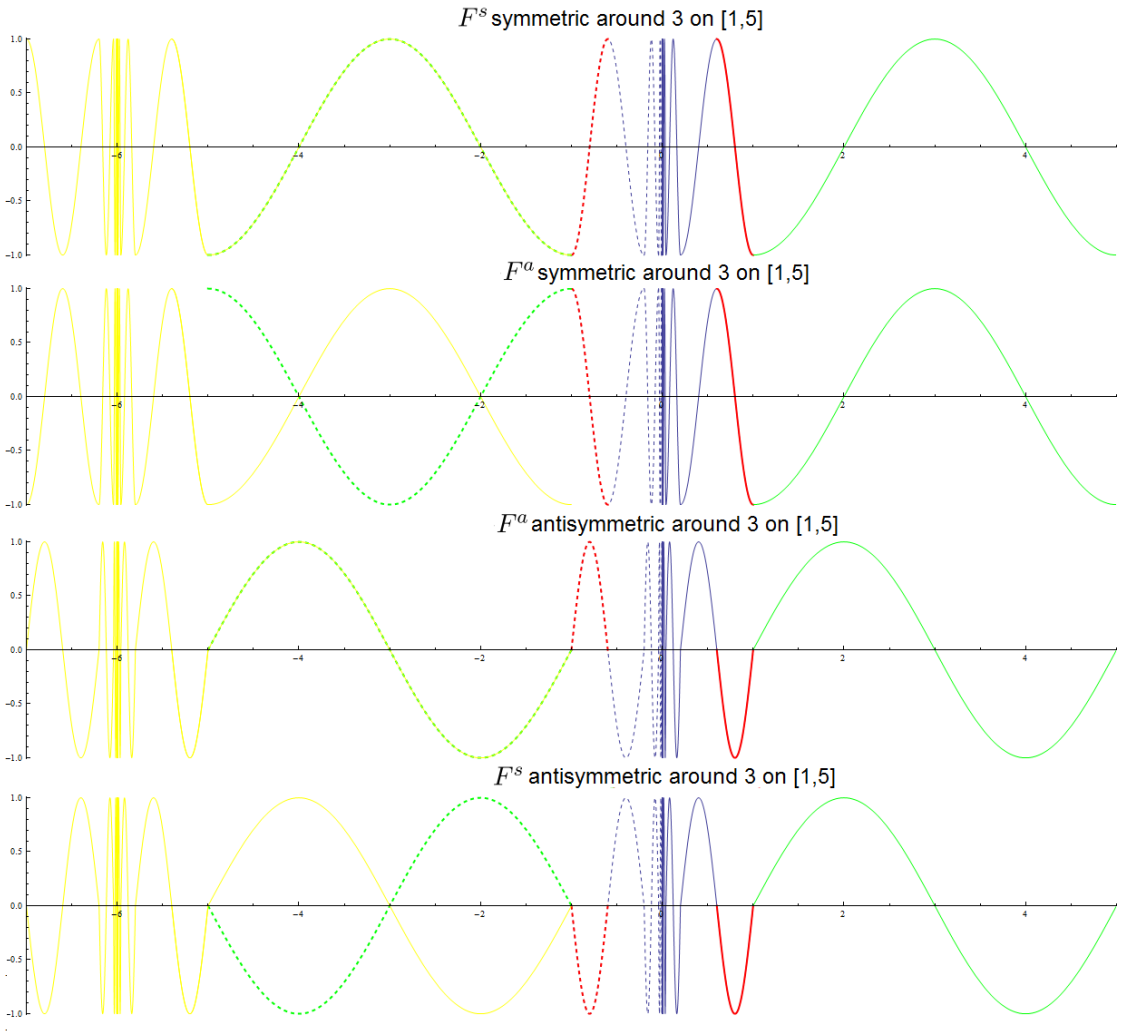

Figure 22: *This figure shows the function $F(\xi)$ on the range $\xi \in [-7, 5]$ for four different choices on the fundamental intervals (part in red). The blue part is the extension onto $[0, \frac{1}{5}]$, the green part the extension onto $[1, 5]$ via $F(\xi) = F(5\xi)$. The dashed part corresponds to (anti)symmetric mirroring around $\xi = 0$ and everything in yellow results from a shift of length 6 to the left (periodicity). On the top the function F is assumed to be symmetric around $\xi = 0$ and chosen such that it is symmetric around $\xi = 3$ on [1,5]. It can be seen that the function value is singular everywhere, meaning that it is well defined. For F symmetric around $\xi = 0$, but antisymmetric around $\xi = 3$ on [1,5] (second from top) this is clearly not the case because the function is not well defined on [-5,-1].Choosing $F(\xi)$ antisymmetric around $\xi = 0$ for all ξ and antisymmetric around $\xi = 3$ on [1,5] (second from bottom) gives a consistent definition of $F(\xi)$ while choosing $F^a(\xi)$ symmetric around $\xi = 3$ on [1,5] (bottom) lead again to a contradiction.*

$\sum_{n=1}^{\infty} a_n \cos(n\pi(\frac{\tau-1}{\tau}\xi + \tau - 1))$ vanishes over such an integral. This means that F^s cannot be a non-zero constant. The symmetric and antisymmetric prescriptions of F^s and F^a are also illustrated in figure (22).

5.4 Appendix D: Weak streamfunction solution

In this subsection it is shown that any function $f : I \subset \mathbb{R} \to \mathbb{R}$ which is continuous and piecewise continuously differentiable leads to a weak streamfunction solution $\Psi(x, z) = f(x - z) - f(x + z)$ to (8) on some open domain $D \subset \mathbb{R}^2$. The interval I must be sufficiently large such that $(x, z) \in D$ implies $(x \pm z) \in I$. In order to satisfy the Dirichlet boundary condition $\Psi = 0$ on ∂D the function f must satisfy $f(x - z) = f(x + z)$ for all $(x, z) \in \partial D$.
A function Ψ is a weak solution of the equation $\frac{\partial^2 \Psi}{\partial x^2} - \frac{\partial^2 \Psi}{\partial z^2} = 0$ on a closed domain $\bar{D}$ if it satisfies

$$\int_D \left(\frac{\partial^2 \Psi}{\partial x^2} - \frac{\partial^2 \Psi}{\partial z^2} \right) \phi \; dxdz = 0 \tag{61}$$

for every smooth function ϕ (with compact support, which is satisfied for any smooth function on a bounded and closed domain D).
Notice that the finitely many points in I on which f is not continuously differentiable lead to finitely many lines (characteristics) in $D \subset \mathbb{R}^2$ on which Ψ is not continuously differentiable. This means that Ψ is continuously differentiable almost everywhere on D in Lebesgue measure. Denote D' the subset of D on which Ψ is continuously differentiable. Notice that Lebesgue measures of D and D' are equal because the finite points in I on which f is not continuously differentiable lead only to finitely many lines (characteristics) in $D \subset \mathbb{R}^2$ on which Ψ is not continuously differentiable. So the integral in (61) can simply be restricted to D'. On D' it is possible to apply integration by parts on (61) because Ψ and ϕ are both continuously differentiable and due to the compact support of ϕ it follows that (61) is equivalent to

$$\int_{D'} \left(\frac{\partial^2 (f(x - z) - f(x + z))}{\partial x^2} - \frac{\partial^2 (f(x - z) - f(x + z))}{\partial z^2} \right) \phi d\mathbf{x} = 0. \tag{62}$$

Clearly we have that $\frac{\partial^2 (f(x-z)-f(x+z))}{\partial x^2} - \frac{\partial^2 (f(x-z)-f(x+z))}{\partial z^2} = 0$, so (62) is true for any smooth function ϕ on D which concludes the prove that Ψ is a weak solution of the (8).
Theorem 3 in Beckebanze and Keady, (2014) states that the only solution to Schröder's functional equation for some map T exhibiting a fixed point is a constant solution. This leads to a constant streamfunction for the internal wave problem associated with the map T, which is not particularly interesting. This means that one has to work with weak solutions or exclude the attractor from the domain in order to study frictionless internal waves.

5.5 Appendix E: Derivation of a trigonometric identity

Here the trigonometric relation

$$\cot\left(\frac{\alpha - \beta}{2}\right) - \cot\left(\frac{\alpha + \beta}{2}\right) = \frac{-2\sin\beta}{\cos\alpha - \cos\beta}$$

is derived. This relation is used in the derivation of the solution R to (26).
Write $\frac{\alpha+\beta}{2} = a$ and $\frac{\alpha-\beta}{2} = b$, then

$$\cot\left(\frac{\alpha-\beta}{2}\right) - \cot\left(\frac{\alpha+\beta}{2}\right) = \frac{\cos b}{\sin b} - \frac{\cos a}{\sin a} = \frac{\cos b \sin a - \cos a \sin b}{\sin a \sin b}.$$

Using $\sin(a-b) = \cos b \sin a - \cos a \sin b$ and $\sin a \sin b = \mp(\cos(a \pm b) - \cos a \cos b)$ gives

$$\frac{\cos b \cos a - \cos a \sin b}{\sin a \sin b} = \frac{\sin(a-b)}{1/2 \sin a \sin b + 1/2 \sin a \sin b} = \frac{\sin(a-b)}{1/2 \cos(a-b) - 1/2 \cos(a+b)}.$$

Substituting $a - b = \beta$ and $a + b = \alpha$ gives

$$\frac{\sin(a-b)}{1/2 \cos(a-b) - 1/2 \cos(b+a)} = \frac{-2 \sin \beta}{\cos \alpha - \cos \beta},$$

which is the desired result.

5.6 Appendix F: Generality of method to construct Law's exact solutions

The aim in studying the construction of the exact solution presented in [8] is to get an idea whether this general method can be recovered and whether it is suitable to construct exact solutions $R(x)$ for other functions $h(x)$ that can be of interest as bottom topography in the context of standing internal gravity waves. In section (3.3.2) the use of relation (33) is modified to find exact streamfunctions $\Psi(x,z) = \frac{1}{2}(R(x-z) - R(x+z))$ lacking tidal conversion for infinitely many bottom topographies h.
Another crucial relation used in the construction of the exact solution R to (26) is the relation (30). Here it is shown that this relation cannot be used to find fundamentally different bottom topography h as given in (27).
Taking

$$\cot(x - h(x)) - \cot(x + d(x)) = \frac{-2 \sin 2h(x)}{\cos 2x - \cos 2h(x)} = c \tag{63}$$

for any constant c one can solve for $h(x)$ to get an idea of the diversity of the function $h(x)$ which solves (63).
Multiplying with $\cos 2x - \cos 2h(x)$, replacing $\sin(2h(x))$ by $\sqrt{1 - \cos^2(2h(x))}$ and taking the square on both sides of (63) gives

$$4(1 - \cos^2(2h(x))) = c^2 \left(\cos^2(2x) - 2\cos(2x)\cos(2h(x)) + \cos^2(2h(x))\right)$$

Treat $\cos(2h(x))$ as a variable y. The two solutions of the quadratic equation

$$(-4 - c^2)y^2 + 2c^2 \cos(2x) y + 4 - c^2 \cos(2x)^2 = 0$$

are given by

$$y_\pm = \frac{c^2 \cos(2x) \pm 2\sqrt{4 + c^2(1 - \cos^2(2x))}}{4 + c^2}.$$

Check that the solutions $y_\pm$ are real for all $c, x \in \mathbb{R}$ and that $|y_\pm| \leq 1$. The solutions for $h(x)$ are given by taking $\frac{1}{2}\cos^{-1}$ of $y_\pm$:

$$h(x) = \frac{1}{2}\cos^{-1}\left(\frac{c^2\cos(2x) \pm 2\sqrt{4 + c^2\sin^2(2x)}}{4 + c^2}\right).$$

Numerically it has been shown that this solution corresponds to $h(x)$ in (27) where c is related to θ via $c = 2\tan\theta$.
In [8] the author does not present the construction of the presented exact solution, but claims that it comes from a "general method which yields a class of near-harmonic trajectories with exactly solvable R(x)". This general method is not published elsewhere [C. K. Law, personal communication]. C. K. Law says that the exact solution R for near-harmonic function $h(x)$ is derived in the following way: For some harmonic $h_0(x)$ an approximate solution $R_0(x)$ is constructed. Then it is examined for which $h(x)$ this R_0 is an exact solution. This general approach might be useful to find exact intern wave solutions to other domains.

5.7 Appendix G: Analytical expressions of $\delta_\pm$

Calculating the inverse of $\delta_-(x) = x - h_s(x)$ where h_s is the bottom function defined in (40) gives

$$\begin{aligned}
\delta^{-1}_{-_{s,\omega}}(x) &= x + 1/\omega \qquad \text{for } x > L - 1/\omega \\
\delta^{-1}_{-_{s,\omega}}(x) &= \frac{-\omega + 6s - 2s^2 + \sqrt{\omega^2 + 8s - 12\omega s + 4\omega s^2 + 8\omega s x}}{4s} \\
&\qquad \text{for } L - 1/\omega \geq x > \frac{L+l}{2} - (1 - s/2)/\omega \\
\delta^{-1}_{-_{s,\omega}}(x) &= \frac{-\omega + 2s - 2s^2 - \sqrt{\omega^2 - 8s + 4\omega s + 8s^2 - 4\omega s^2 - 8\omega s x}}{4s} \\
&\qquad \text{for } \frac{L+l}{2} - (1 - s/2)/\omega \geq x > l - (1 - s)/\omega \\
\delta^{-1}_{-_{s,\omega}}(x) &= x - (1 - s)/\omega \qquad \text{for } l - (1 - s)/\omega \geq x > -l - (1 - s)/\omega \\
\delta^{-1}_{-_{s,\omega}}(x) &= \frac{\omega - 2s + 2s^2 - \sqrt{\omega^2 - 8s - 4\omega s + 8s^2 + 4\omega s^2 - 8\omega s x}}{4s} \\
&\qquad \text{for } -l - (1 - s)/\omega \geq x > -(L + l)/2 - (1 - s/2)/\omega \\
\delta^{-1}_{-_{s,\omega}}(x) &= \frac{-\omega - 6s + 2s^2 + \sqrt{\omega^2 + 8s + 12\omega s - 4\omega s^2 + 8\omega s x}}{4s} \\
&\qquad \text{for } -(L + l)/2 - (1 - s/2)/\omega \geq x > -L - 1/\omega \\
\delta^{-1}_{-_{s,\omega}}(x) &= x + 1/\omega \qquad \text{for } -L - 1 \geq x.
\end{aligned} \tag{64}$$

The inverse of $\delta_+(x) = x + h_s(x)$ is given by

$$
\begin{aligned}
\delta^{-1}_{+_{s,\omega}}(x) &= x - 1/\omega \qquad \text{for } x > L + 1/\omega \\
\delta^{-1}_{+_{s,\omega}}(x) &= \frac{\omega + 6s - 2s^2 - \sqrt{\omega^2 + 8s + 12\omega s - 4\omega s^2 - 8\omega s x}}{4s} \\
&\qquad\qquad \text{for } L + 1/\omega \geq x > \frac{L+l}{2} + (1 - s/2)/\omega \\
\delta^{-1}_{+_{s,\omega}}(x) &= \frac{-\omega + 2s - 2s^2 + \sqrt{\omega^2 - 8s - 4\omega s + 8s^2 + 4\omega s^2 + 8\omega s x}}{4s} \\
&\qquad\qquad \text{for } \frac{L+l}{2} + (1 - s/2)/\omega \geq x > l + (1 - s)/\omega \\
\delta^{-1}_{+_{s,\omega}}(x) &= x + (1 - s)/\omega \qquad \text{for } l + (1 - s)/\omega \geq x > -l + (1 - s)/\omega \\
\delta^{-1}_{+_{s,\omega}}(x) &= \frac{-\omega - 2s + 2s^2 + \sqrt{\omega^2 - 8s + 4\omega s + 8s^2 - 4\omega s^2 + 8\omega s x}}{4s} \\
&\qquad\qquad \text{for } -l + (1 - s)/\omega \geq x > -(L + l)/2 + (1 - s/2)/\omega \\
\delta^{-1}_{+_{s,\omega}}(x) &= \frac{\omega - 6s + 2s^2 - \sqrt{\omega^2 + 8s - 12\omega s + 4\omega s^2 - 8\omega s x}}{4s} \\
&\qquad\qquad \text{for } -(L + l)/2 + (1 - s/2)/\omega \geq x > -L + 1/\omega \\
\delta^{-1}_{+_{s,\omega}}(x) &= x - 1/\omega \qquad \text{for } -L + 1 \geq x.
\end{aligned}
\tag{65}
$$

These expressions for $\delta^{-1}_{\pm}$ have to be substituted into the expression for the map T presented in (42) and its inverse T^{-1} expressed (43). Thereby these expression are part of the exact description of the streamfunction solutions presented in the solution a, equation (45), to Abel's functional equation.

References

[1] F. Beckebanze and G. Keady, 2014, *On functional equations leading to exact solutions for standing internal waves*, submitted to Wave Motion and available via arXiv

[2] O. Bühler and M. Holmes-Cerfon, 2011, *Decay of an internal tide due to random topography in the ocean*, Journal of Fluid Mechanics, **678**, pp. 271- 293

[3] H. A. Dijkstra, 2008, *Dynamical Oceanography*, Springer-Verlag Berlin Heidelberg, e-ISBN: 978-3-540-76376-5

[4] E. Chen, *Degradation of the internal tide over long bumpy topography*, available on Woods Hole Oceanographic Institution file server, year unknown.

[5] G. D. Egbert and R. D. Ray, 2001, *Estimates of M2 tidal energy dissipation from TOPEX/Poseidon altimeter data*, Journal of Geophysical Research, doi: 10.1029/2000JC000699

[6] C. Garrett and E. Kunze, 2007, *Internal Tide Generation in the Deep Ocean*, Annu. Rev. Fluid Mech. **39**, pp. 57-87

[7] M. Kuczma, 1968, *Functional equations in a single variable*, PWN-Polish Scientific Publishers

[8] C. K. Law, 1994, *Resonance Response of the Quantum Vacuum to an Oscillating Boundary*, Physical Review Letters, **73**, no. 14

[9] J. Laitochova, 2007, *Group iteration for Abel's functional equation*, Nonlinear Analysis: Hybrid Systems, **1**, issue 1, pp. 95-102

[10] L. R. M. Maas, 2011, *Topographies lacking tidal conversion*, Journal of Fluid Mechanics, **683**, pp. 5-24, DOI: 10.1017/jfm.2011.245

[11] L. R. M. Maas, 2008, *Exact analytic self-similar solution of a wave attractor field*, Physica D, doi:10.1016/j.physd.2008.11.006

[12] L. R. M. Maas and U. Harlander, unpublished, *Tidal conversion over subcritical topographies using the characteristic method*

[13] L. R. M. Maas and F. Lam, 1995, *Geometric focusing of internal waves*, Journal of Fluid Mechanics, **300**, pp. 1-41.

[14] W. Munk, 1966, *Abyssal recipes*, Deep-Sea Res. **13**, pp. 707-730

[15] W. Munk and C. Wunsch, 1998, *Abyssal recipes II. Energetics of the tides and wind*, Deep-Sea Res. **45**, pp. 1977-2010.

[16] K.L. Polzin et al, 1997, *Spatial Variability of Turbulent Mixing in the Abyssal Ocean*, Science **276**, no. 5309, pp. 93-96, DOI: 10.1126/science.276.5309.93

[17] A.N. Swart, 2007, *Internal Waves and the Poincaré Equation: Numerical Computation and Laboratory Experiments*, Ph.D. thesis, Universiteit Utrecht.

[18] W. Smith and D. Sandwell, 1997, *Measured and Estimated Seafloor Topography*, World Data Service for Geophysics, Boulder Research Publication RP-1, poster, 34" X 53"